Thesis

For the degree of

Doctor of Philosophy

On the topic entitled

Central and Peripheral Nervous System Injuries: Evidence of Demyelination and Remyelination



Ву

Rahul Shankar Rao Rayilla (Enrolment No: 16LTPH14)

Under the Supervision of

Prof. Prakash Babu Phanithi

Neuroscience Laboratory

Department of Biotechnology and Bioinformatics School of Life Sciences, University of Hyderabad Hyderabad – 500 046, T.S., INDIA



Department of Biotechnology and Bioinformatics School of Life Sciences, University of Hyderabad Hyderabad – 500 046, T.S., INDIA

DECLARATION

The research work presented in this thesis entitled "Central and Peripheral Nervous System Injuries: Evidence of Demyelination and Remyelination" has been carried out by me under the guidance of Prof. Prakash Babu Phanithi in the Department of Biotechnology and Bioinformatics, School of Life Sciences, University of Hyderabad, Hyderabad, T.S., India. I hereby declare that this work is original and has not been submitted elsewhere of any other University or Institute.

O Charles

Rahul Shankar Rao Rayilla

Place: Hyderabad

Date: 27/09/2023



Department of Biotechnology and Bioinformatics School of Life Sciences, University of Hyderabad Hyderabad – 500 046, T.S., INDIA

CERTIFICATE

This is to certify that, thesis entitled "Central and Peripheral Nervous System Injuries: Evidence of Demyelination and Remyelination" is a record of bonafide work done by Rahul Shankar Rao Rayilla, Ph.D. research scholar, Department of Biotechnology and Bioinformatics, School of Life Sciences, University of Hyderabad under my guidance and supervision. The thesis has not been submitted elsewhere for the award of any degree or diploma. I recommend his thesis for submission towards the partial fulfilment of "Doctor of Philosophy".

Signatures

Supervisor: \

Prof. Praklash Babu

Department of Biotechnology & Bioinformatics

Department of Biotechnology & Biotechnology &

Head of the Department:

HEAD

Dept. of Biotechnology & Bioinformatics University of Hyderabad Hyderabad.

Dean, School of Life Sciences:

संकाय अध्यक्ष / Dean जीव विज्ञान संकाय / School of Life Sciences हैदराबाद विश्वविद्यालय/University of Hyderabad हैदराबाद / Hyderabad-500 046.



Department of Biotechnology and Bioinformatics School of Life Sciences, University of Hyderabad Hyderabad – 500 046, T.S., INDIA

CERTIFICATE

This is to certify that the thesis entitled "Central and Peripheral Nervous System Injuries: Evidence of Demyelination and Remyelination" submitted by Rahul Shankar Rao Rayilla bearing registration number 16LTPH14 in fulfilment of the requirements for award of Doctor of Philosophy in the Department of Biotechnology and Bioinformatics, School of Life Sciences is a bonafide work carried out by him under my supervision and guidance.

This thesis is free from plagiarism and has not been submitted elsewhere in any other University or Institution for award of any degree or diploma.

Further the student has the following publication (s) before submission of the thesis.

Publications:

- 1. **Rayilla, R. S.,** Naidu, M., & Babu, P. P. (2023). Surgically Induced Demyelination in Rat Sciatic Nerve. Brain Sciences, 13(5), 754. https://doi.org/10.3390/brainsci13050754
- 2. **Rahul Shankar Rao Rayilla** and Prakash Babu Phanithi. Demyelination In The Rat Traumatic Brain: Evidence of Cell Death (*Under communication*)
- 3. Shilpak Bele, Shravan Babu Girada, Aramita Ray, Abhishek Gupta, Srinivas Oruganti, Phanithi Prakash Babu, Rahul SR Rayilla, Shashi Vardhan Kalivendi, Ahamed Ibrahim, Vishwajeet Puri, Venkateswar Adalla, Madhumohan R Katika, Richard Di Marchi, Prasenjit Mitra (2020) MS-275, a class 1 histone deacetylase inhibitor augments glucagon-like peptide-1 receptor agonism to improve glycemic control and reduce obesity in diet-induced obese mice eLife 9:e52212.
- 4. THIAZOLYL-INDOLE derivatives as fluorescent probes. **Indian patent:** E-18(iii)/2050/2020/CHE. **Grant No:** 202041020018. (Filed)

Awards and Achievements

As a supervisor, I confirm Rahul Shankar Rao Rayilla presented his research work in few conferences and meeting organized by Society for Neurochemistry, India (SNCI) held across India during the year 2017-2023.

Rahul Shankar Rao Rayilla demonstrated "Sciatic Nerve Injury Model through a surgical procedure: Neuropathic Pain" in IBRO-APRC-SNCI School which was held in host University-University of Hyderabad during December, 2022.

- 1. **Best oral presentation award** on the topic "Demyelination in the Rat Traumatic Brain: Evidence of Cell Death" BIOANVESHANA, School of Life Sciences, University of Hyderabad, Telanagana State, India.
- 2. First prize for the Best poster presentation on the topic "Surgically Induced Demyelination in Rat Sciatic Nerve", DST-INSPIRE Review Meeting, K. L. University, Vijayawada- Organisers: Dr. K. L. Narayana & Dr. Umesh Kumar Mishra, Scientist E, DST- New Delhi.

This work is dedicated to my Father (Laxman Rao), Mother (Vasantha Rao), Brother (Mayur Rao), and my buddies Alex Senior, Spike, Happy Donald, and Alex Junior. I am nothing without all of them.

Acknowledgments

I am grateful to my guide **Prof. Prakash Babu Phanithi,** who has inspired and encouraged me since the beginning of my Ph.D.

I thank my madam **Dr. Anwita**, for being my shadow power, who has safeguarded me up to this point with her inspiration and stayed with me all the time with her tips, creative thoughts, and ideas on research.

I am grateful to my doctoral committee members **Prof. Ravi Kumar Gutti** and **Dr. Prakash Prabhu,** for their encouragement and support during my Ph.D.

I am grateful to **Prof. Appa Rao**, who has been an inspiration and role model to me since my first day on campus.

I am grateful to the Dean, School of Life Sciences, **Prof. Shiva Kumar, Prof. J.S.S. Prakash,** Head of the Department, Department of Biotechnology and Bioinformatics, and former head, **Prof. Padmasree,** who were always there to assist me when I needed it.

I am grateful to **Prof. Kota Arun Kumar,** Department of Animal Biology, Faculty Incharge, Animal House Facility, University of Hyderabad for his efforts and help on animal experiments throughout my Ph.D. with his team **Dr. Tarun** (Veterinarian), **Yadagiri and Samuel** (Facility assistants).

I thank **Prof. Brahamanandam, Ph.D. course work coordinator, IAEC** for his the animal studies approval and support.

I thank **Prof. Ramaswamy Nanna, Prof. Sadanandam, Dr. A. V. Rao,** and **Dr. Shasthree** for recognizing my talent for science, and **Dr. A. V. Rao** changed my life by taking personal care of me and sending me University of Hyderabad to work under his friend, **Prof. Naresh Babu V. Sepuri** for my masters dissertation. I enjoyed being in his lab, and I am glad to collaborate with **Prof. Rajgopal** during my masters dissertation, who graciously enabled me to utilize his lab facilities.

I am grateful to **Dr. Ranjani Chakravarthy,** MD (Pathology), FRCPath (UK), Managing Director and Consultant Histopathologist, Cpathlabs (India). **Tirumala Chari,** Histopathologists, PathnSitu for their help in neuropathological studies.

I thank Mounica Kannan, Nalini, Raja Laxmi, Rajesh, and Deepthi for their help on proteomics studies and microscopic imaging.

I feel blessed to have **former** and **present labmates** who are always there for me when I need them. **Muthyam** (Lab Assistance), the driving force behind my successful Ph.D. research, Thank you.

I thank my close friends across the world, **Raj**- software (Australia), **Akanaksha**-Ph.D. research scholar (Japan), **Shari**- Professor (USA), **Anita**-Ph.D. Astrobiology (Chile), **Lamha**- Media (Pakistan), **Eli**-Ph.D. research scholar (Iran), **Diana**-Artist (USA), **Lubna Mariam** (Dubai), **Anusha** (Japan).

I thank my friends across India who are waiting for my Ph.D. submission, **Dr. Murugesan** (Chennai), **Sowmya** (Lucknow), **Burman** (BHU), **Tania** (Shillong), **Kate** (Nagaland), **Madhuri** (NIN), Lokesh (NIN), **Sharon & Manajri** (BITS-Pilani, Hyd), **Aditya** (CCMB).

I am grateful to all of my childhood, college, and Ph.D. friends from ILS, Medical Sciences, Social Sciences, S. N. School, Hindi Department, Institute of Life Sciences (DRILLS), and Life Sciences who wished me success in my future endeavors.

Without them my life is incomplete, its all about my family. I thank god for giving Laxman Rao (Father) and Vasantha Rao (Mother) who treat me as of there own body part and gave me the beautiful life. Thanking is a tiny word for my younger brother Mayur Rao who sacrificed many things in his life just to make me happy. I am happy to have Alex Senior, Spike, Happy Donald, Alex junior in my life, without them my life is incomplete.

I acknowledge the funding bodies **Department of Science and Technology (DST), Science and Engineering Research Board (SERB)** grant no: CRG/2020/005021, CRG/2019/002570, **Institute of Eminence (UoH-IoE),** University of Hyderabad –grant no: F11/9/2019-U3 (A), **Department of Bio-technology (DBT)** grant no: BUILDER-DBT-BT/INF/22/SP41176/2020. **Department of Science and Technology (DST) – Inspire Fellowship** under Ref. No: DST/INSPIRE/03/2015/003047.

I am grateful to the **Department of Science and Technology (DST)** for awarding me the **DST-Inspire fellowship** in honour of my academic achievements and for financially supporting me.

S. No	Content	Page. No's	
1	Glossary	1-3	
2	Thesis Title, Abstract, & Keywords	4	
3	Chapter 1: Pro-inflammation, ER-Mitochondrial Mediated Cell Death and Demyelination following Traumatic Brain Injury: Teriflunomide Attenuate Cell Death and Promote Myelin Restoration.		
I	Title, abstract, graphical abstract and keywords		
II	Introduction	7-12	
III	Materials and methods		
IV	Results		
V	Discussion	37-42	
4	Chapter 2: Surgically Induced Demyelination in Rat Sciatic Nerve: Teriflunomide (TF) assisted Remyelination.	43-71	
I	Title, abstract, graphical abstract, and keywords	43-44	
II	Introduction	45-48	
III	Materials and methods	49-56	
IV	Results	57-67	
V	Discussion	68-71	
5	Chapter 3: Applications of the Developed Sciatic Nerve Injury Model (Collaboration with Prof. Nagarajan, School of Chemistry, UOH)	72-88	
I	Title, abstract, and keywords	72-73	
II	Introduction	74-75	
III	Materials and methods	76-80	
IV	Results	81-87	
V	Discussion	88	
6	Altogether Summary	89	
7	Bibliography	90-99	

Glossary

CNS : Central nervous system

p-TBI : Post-traumatic brain injury

PNS: Peripheral nervous system

SNI : Sciatic nerve injury

SD : Sprague Dawley

TF : Teriflunomide

TBI : Traumatic brain injury

p-SNI : Post-sciatic nerve injury

PNIs : Peripheral nervous system injuries

TEM: Transmission electron microscopy

MALDI-MS : Matrix-assisted laser desorption/ionization

Mass spectrometry

ER : Endoplasmic reticulum

UPR : Unfolded protein response

BiP : ER binding protein chaperone

ATF6 : Activating transcription factor 6

MTCH1 : Mitochondrial carrier homolog 1

Bcl-2 : B-cell lymphoma 2

BAX : Bcl-2 associated X protein

BAK : Bcl-2 homologous antagonist/killer

Bcl-xL : B-cell lymphoma-extra large

Apaf-1 : Apoptotic protease activating factor-1

TNFα : Tumour necrosis factor alpha

TNF/3 : Tumour necrosis factor 3

IL-1 : Interleukin-1

IL-6 : Interleukin-6

ROS : Reactive oxygen species

PBS: Phosphate buffer saline

MBP : Myelin basic protein

CNPase : 2, 3-cyclic nucleotide 3- phosphodiesterase

CD68 : Cluster of differentiation 68

DAB : 3, 3`-Diaminobenzidine

DPX : Dibutylphthalate polystyrene xylene

H and **E** : Haematoxylin and eosin

RIPA: Radioimmunoprecipitation assay buffer

BCA : Bicinchoninic acid

BAD : Bcl-2 associated agonist of cell death

GAPDH : Glyceraldehyde-3-phosphate dehydrogenase

BSA : Bovine serum albumin

HEPES: 4-(2-hydroxyethyl)-1-piperazineethanesulfonic acid

IPG: Immobilized pH gradient

IEF : Isoelectric focusing

2D-gel : 2-dimensional gel

pI : Isoelectric point

SDS-PAGE: Sodium dodecyl sulphate-poly acrylamide

Gel electrophoresis

TPCK: N-tosyl-L-phenylalanine chloromethyl ketone

TFA: Trifluoroacetic acid

EC : Eriochrome cyanine r

LFB : Luxol fast blue

H₂SO₄ : Sulphuric acid

 $\mathbf{H_2O_2}$: Hydrogen peroxide

DMSO: Dimethyl sulphoxide

DAPI : 4`,6-diamidino-2-phenylindole

FFPE: Formalin fixed paraffin embedded

CHO cells : Chinese hamster ovary cells

SK-N-SH cells: Human neuroblastoma cell line

Thp-1 cells : Human leukemia monocytic cell line

HEK: Human embryonic kidney cell line

HELA: Henrietta lacks cell line

COX7B : Cytochrome C oxidase subunit 7B

PRDX3 : Thioredoxin-dependent peroxide reductase

SPYA : Serine-pyruvate aminotransferase

ACADL : Long-chain specific acyl-CoA

ACPM: Acyl carrier protein

M20M : Mitochondrial 2-oxoglutarate/malate carrier

protein

MTCH1 : Mitochondrial carrier homolog 1

TTC19 : Tetratricopeptide repeat protein 19

AATM : Aspartate aminotransferase

IPYR2 : Inorganic pyrophosphatase 2

GCSH : Glycine cleavage system H protein

CH10, Hspe 1 : Heat shock protein

AATM : Aspartate aminotransferase

IPYR2 : inorganic pyrophosphatase 2

Thesis title

Central and Peripheral Nervous System Injuries: Evidence of Demyelination and Remyelination

Abstract

Myelin is a fatty insulator that aids in the speeding up of electrical impulses or communication between neurons in the nervous system. However, the processes driving cell death that aggravates demyelination remain elusive. This thesis focuses on understanding cell death mechanisms in the white matter lesions of the central nervous system (CNS) and changes in mitochondrial protein following post-traumatic brain injury (p-TBI) from the early to late stages. We developed a peripheral nervous system (PNS) surgical sciatic nerve injury (SNI) model that can induce demyelination in Sprague Dawley (SD) young male rats using a single partial sciatic nerve suture surgery. Further, Teriflunomide (TF) administration promoted recovery and remyelination in the rats with central and peripheral nervous system injuries. In addition, we showed application of the developed model. For this we used a natural compound analogue, as a fluorophore. This showed promising results in vitro, in vivo and tissue sections by labelling the mitochondria. The fluorescence was observed using Perkin Elmer in vivo imaging by injecting the fluorophore in the rat sciatic nerve model. The weight-drop approach was used to generate traumatic brain injury (TBI) young SD-rats. Immunostaining and immunoblots were used to explore cell death mechanisms and demyelination. To investigate mitochondrial protein changes, proteomic investigations as well as matrix-assisted laser desorption/ionization mass spectrometry (MALDI-MS) was carried out. Histology and immunostaining demonstrate demyelination or myelin loss from early to severe phases after a post-sciatic nerve injury (p-SNI) to the sciatic nerve, with no self-recovery. The rotarod test confirms the nerve-damaged rats' lack of motor function. Transmission electron microscopic (TEM) imaging of nerve-damaged rats reveals axonal atrophy and inter-axonal gaps. However, TF treatment reversed cell death pathways by inhibiting endoplasmic reticulum (ER) stress and promoted remyelination in rats with brain injuries related to CNS. Similarly, our findings in PNS following p-SNI rats noted subsequent remyelination after TF administration. Additionally, to test the efficacy of our PNS surgical model, we used a synthesized compound which showed promising results in vivo, ex vivo, and in vitro mitochondrial dye.

Keywords: Central nervous system · Traumatic brain injury · Peripheral nervous system · Sciatic nerve injury · Pro-inflammation · ER-stress · Mitochondrial apoptotic pathway · Demyelination · Teriflunomide Therapy · Remyelination · Fluorophore.

Chapter 1

Pro-inflammation ER-Mitochondrial Mediated Demyelination following
Traumatic Brain Injury: Teriflunomide Attenuate Cell Death and Promote
Myelin Restoration

I. Abstract

In central nervous system (CNS), researchers tend to concentrate on the grey matter because of the neuronal cell bodies which are extremely difficult to recover following injury. Aside from that, there is a scarcity of anti-inflammation and myelin regeneration therapies for traumatic brain injury (TBI). This study sought to shed light on the relevance of white matter, which are highly composed of axonal fibres that aid in neural transmission. Teriflunomide (TF), repurposed for the first time on TBI rats. Using a TBI rat model, we damage the rat brain white matter. We find the active period of pro-inflammation, ER stress and mitochondrial apoptotic pathway of cell death and demyelination in rat brain white matter lesions following TBI. Further we investigate the changes in mitochondrial protein of rat brain following TBI. Our results uncover pro-inflammation triggers ER stress and activate mitochondrial apoptotic pathway of cell death and promote demyelination in rat brain white matter lesions. We show mitochondrial protein alterations in injured rat brain which may aid in the discovery of new cell death indicators. TF attenuates pro-inflammation and inhibits ER stress and reverses mitochondrial apoptotic mode of cell death with scientific evidences of recovery and myelin restoration.

Keywords: White matter injury, pro-inflammation, mitochondrial dysfunction, demyelination, Teriflunomide, remyelination

Traumatic Brain Injury Teriflunomide (TF) administration following p-TBI Studies Histopathology and western blotting studie **Futhanization** Histopathology and western blotting studies Identification of novel mitochondrial proteins following p-TBI as cell death indicators Pro-inflammation, ER-stress, mitochondrial dysfunction, and demyelination in rat brainfollowing p-TBI TF promoted anti-inflammation, ER associated mitochondrial apoptotic pathway inactivation, and remvelination

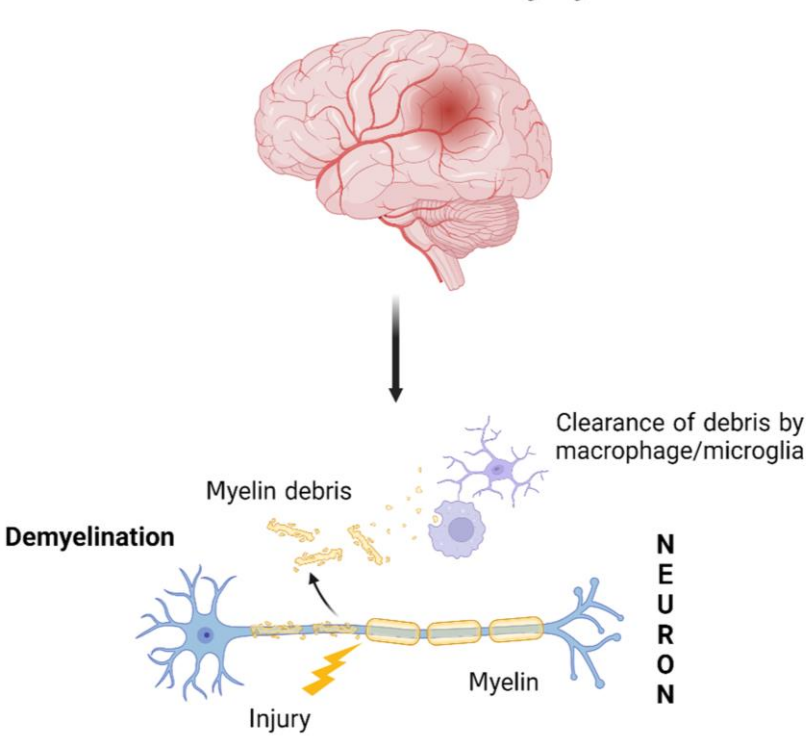
II. Introduction

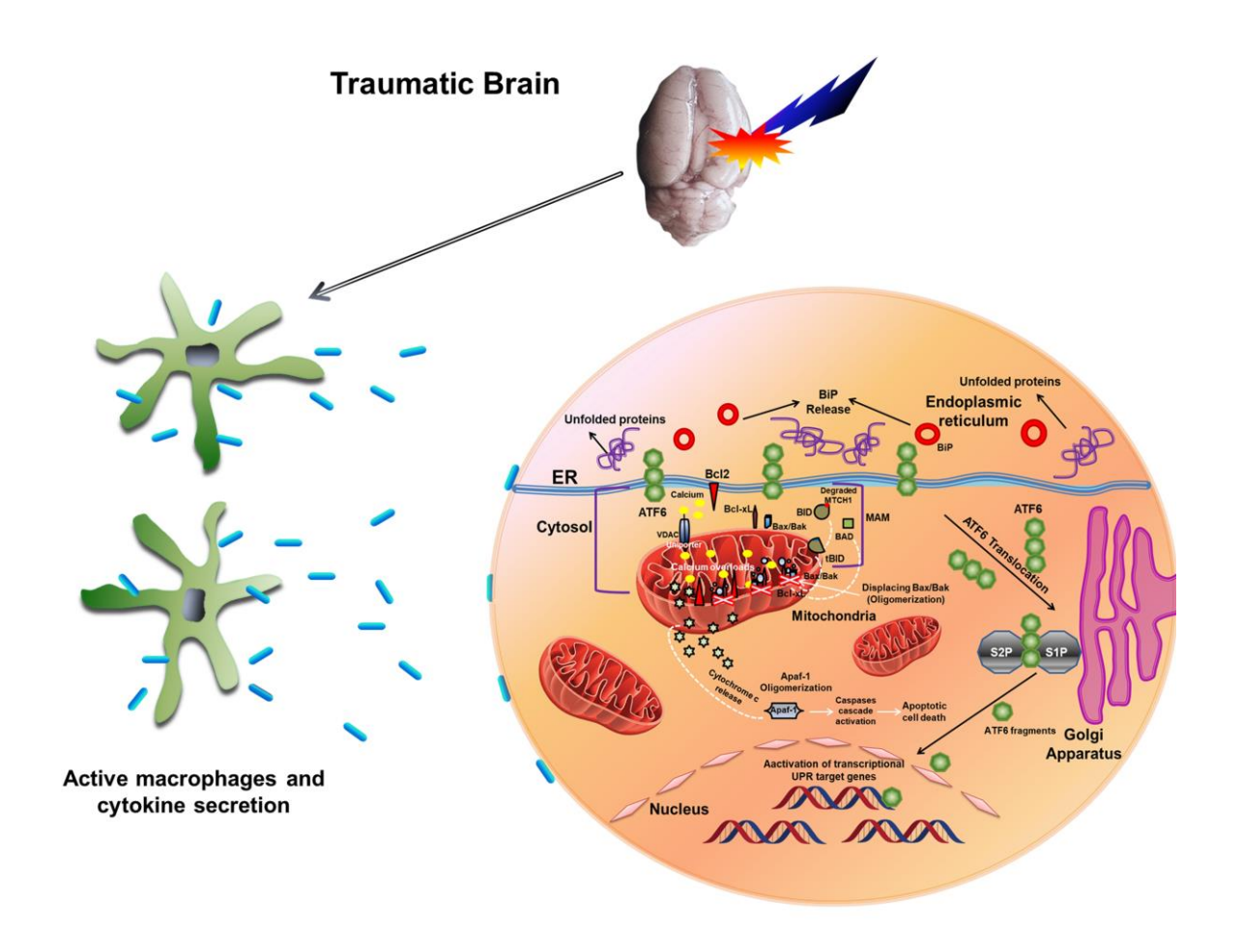
Introduction

Demyelination is the abnormal process in which the myelin sheath, which protects the axons for proper neural transmission or neuronal communication, is lost or damaged. Myelin loss compromises both axon survival and the flow of electrical impulses in local circuits. Clinical disability arises as a result over time [1]. Many neurodegenerative diseases, persistent inflammatory demyelinating polyneuropathy, and nervous system injuries can all result in demyelination.

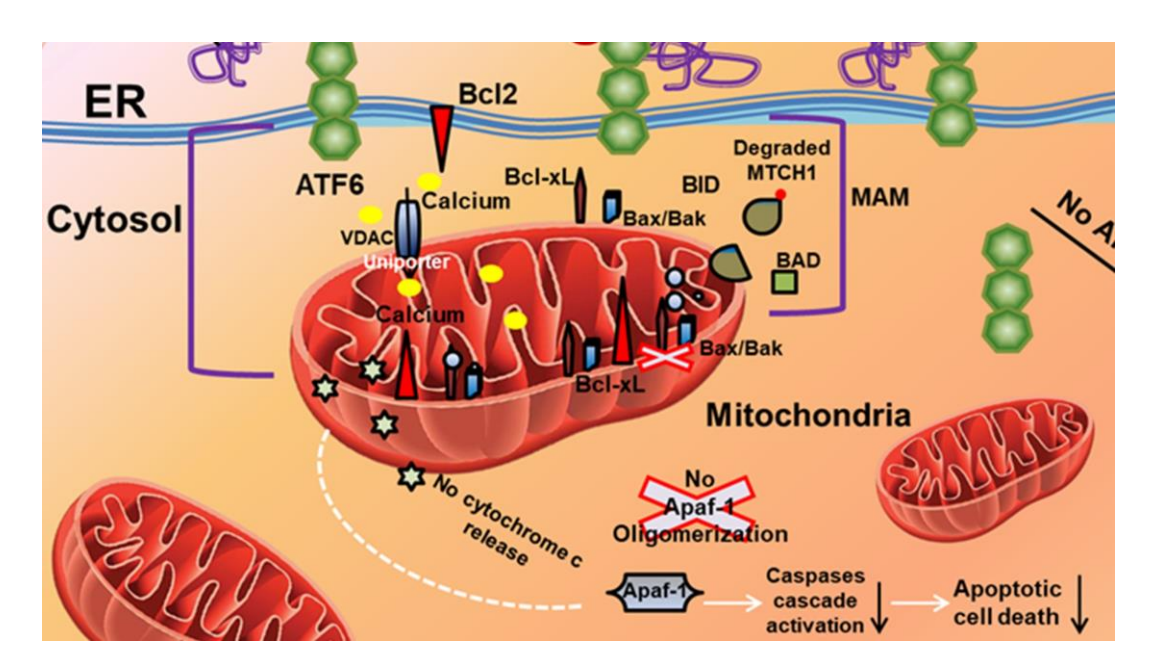
TBI is generally caused by a forceful impact on the head, which results in a concussive head injury or diffuse damage [2, 3]. Recent studies have indicated that pathological alterations are generated by the influence on the brain, stressing the importance of white matter integrity, which includes axons [4, 5]. White matter atrophy has a limited chance of healing due to the loss of neuronal cell bodies [6, 7]. Demyelination is the term used to describe white matter lesions that are characterized by myelin sheath loss and oligodendrocytic cell death.

Traumatic Brain Injury

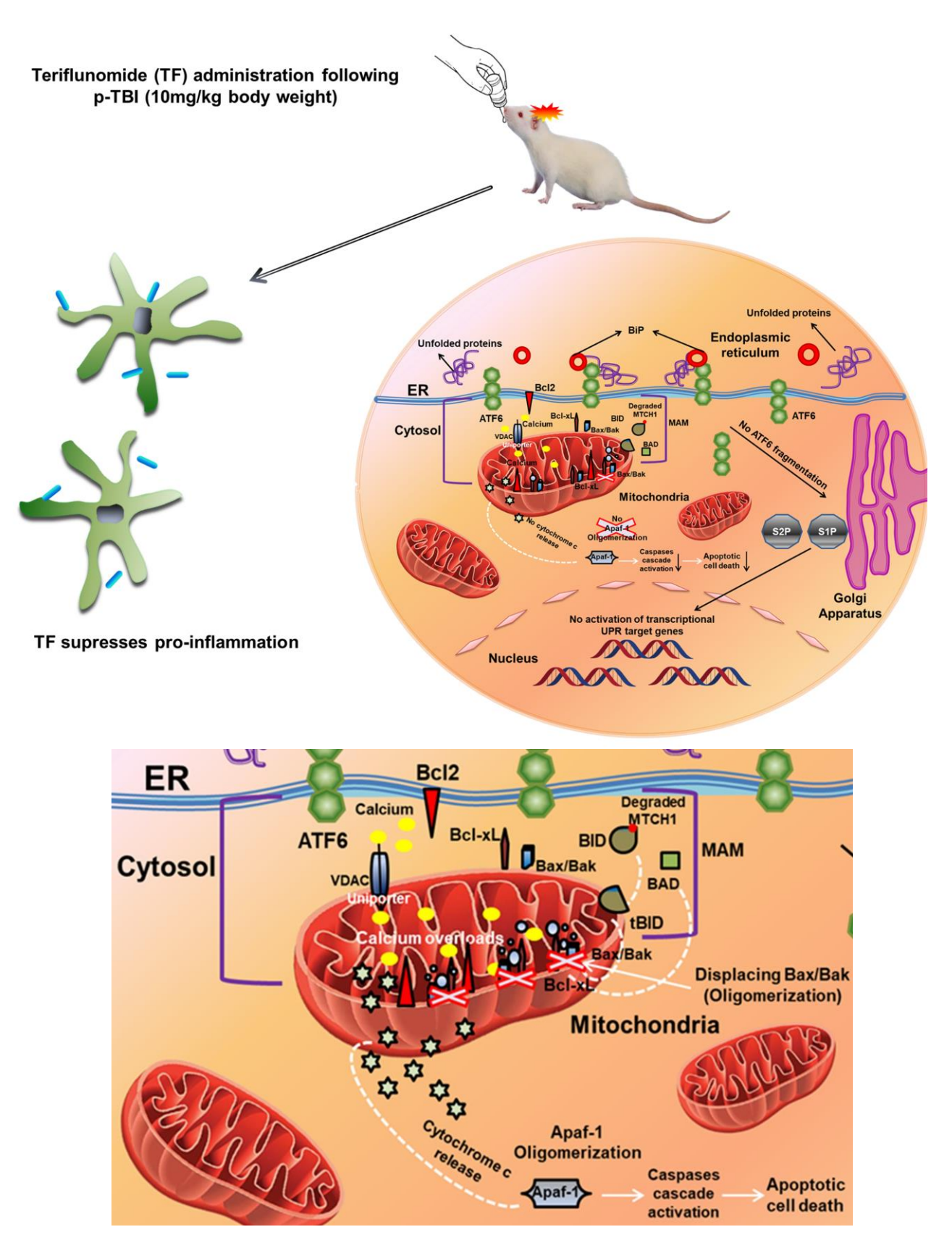




Activated macrophages in the damaged brain secrete cytokines; producing inflammation and promoting ER stress [8]. The aberrant build-up of unfolded proteins response (UPR) under ER stress occurs in the release of a protein chaperone (BiP) from the ER stress sensors and activates activating transcription factor 6 (ATF6), which translocates into the cytoplasm [9]. The Golgi apparatus proteases S1P and S2P break the translocated ATF6 sensors into pieces that migrate into the nucleus and trigger increased inflammation in numerous neurodegenerative diseases [10, 11].



Mitochondrion plays a crucial role in cell survival and death. Mitochondrial carrier homolog 1 (MTCH1) is a pro-apoptotic protein found in the mitochondrial outer membrane that functions as a receptor for truncated BID (tBID) [12, 13]. Under stress conditions, MTCH1 triggers BID to truncated form tBID where it promotes BAK (pro-apoptotic protein) oligomerization and cytochrome C release [14]. Bcl-2 associated death promoter (BAD), on the other hand, displaces BAX/BAK from BCL-xL to induce oligomerization and cytochrome C release [15]. After oligomerization in reaction to cytochrome C release, apoptotic protease activating factor-1 (Apaf-1) forms a massive complex called an apoptosome, further activating the caspase cascade and promoting cell death [16].



Prediction, Teriflunomide (TF) administration supresses pro-inflammation, ER stress inhibition, reverses mitochondrial apoptotic pathway mechanism, and promotes myelin restoration or remyelination by resident oligodendrocyte progenitor cells differentiation and maturation.

TF is an oral immunomodulatory FDA approved drug for the treatment of relapsing-remitting demyelinating illnesses in multiple sclerosis [17, 18]. TF suppresses dihydroorotate dehydrogenase, which inhibits pyrimidine production and promotes oligodendroglial differentiation and myelination. A small dose of TF causes the cell cycle to exit, whereas a larger dose causes a reduction in cell survival [19].

To address the possibilities and active period of this mechanism in white matter lesions of rat-injured brains, we utilized the traditional weight drop method model as an approach to induce TBI in rats and damage the rat white matter. We found the activated macrophage-secreted cytokines under inflammatory stimuli trigger ER stress that lasts for a week. Further, ER stress activated mitochondrial apoptotic pathways to promote cell death resulted in enhanced demyelination for more than three weeks following TBI. We noted mitochondrial protein alterations in one week injured rat brains which are with functional properties such as oxidative phosphorylation, detoxification, respiratory chain, proteins misfolding and refolding, and apoptosis. These altered proteins are appropriate for the development of new cell death indicators. TF administration inactivated the macrophages and reduced the cytokine secretion in injured rat brain white matter lesions. Inhibition of ER stress reversed the mitochondrial apoptotic pathway and stimulated myelin restoration or remyelination. Interestingly, TF treatment restored the altered mitochondrial proteins.

III. Materials and Methods

Ethics Statement: All the animal experiments were carried out after the approval of the institutional animal ethical committee (UH/IAEC/PPB/2023–1/08), University of Hyderabad, India. Species- Sprague Dawley (SD) rats (3 months old, 220–250 g male) were purchased from the National Institute of Nutrition (NIN), Hyderabad. As per the experimental requirement, animals were acclimatized in the animal house facility, University of Hyderabad before 10 days of the experiments (Reg number: 151/1999/CPCSEA). The animals were housed in cages with an ambient temperature of 24 °C, constant and standard air humidity, natural day and night cycles, quality food, and water ad libitum.

Estimation of sample size by Power Analysis approach using G*Power 3.1 software:

Cohen 1998 and Navarro 2015 proposed three categories of effect sizes:

- 1. 0.2 (small effect size), difference is unimportant between the groups
- 2. 0.5 (medium effect size), difference is important between the groups
- 3. 0.8 (larger effect size), difference is highly important between the groups

Effect size was obtained based on the previous studies on demyelination in the animal models and TF treatment to promote anti-inflammation and remyelination [20, 21]. Significant differences between the groups are highly important.

• To determine the sample size, in this study, we employed a larger effect size f (0.8), α-err prob (0.05), power (1 β-err prob) (0.8), number of groups (Experiment 1: 3 groups), as per the Cohen's standard effect size.

In Experiment 1, the sample size is n = 21/3 groups, therefore n = 7/group. Nonetheless, like in previous studies, we utilized n = 6/group.

Experiment 1. Histology and immunostaining elucidates the pro-inflammation that initiates ER-stress which generates the activation of mitochondrial apoptotic pathway and promotes demyelination from early to late phases based on pro-longed time periods after p-TBI to rats.

Animal group	Species, age, weight, and sex	Number of animals per group (n
Sham	SD-male rats, 8-week-old, and weighing 220- 250 g	6
48 h p-TBI	SD-male rats, 8-week-old, and weighing 220- 250 g	6
7 d p-TBI	SD-male rats, 8-week-old, and weighing 220- $$ 250 g $$	6

• To determine the sample size, in this study, we employed a larger effect size f (0.7), α-err prob (0.05), power (1 β-err prob) (0.8), number of groups (**Experiment 2:** 5 groups), as per the Cohen's standard effect size.

In Experiment 2, the sample size is n = 30/5 groups, therefore n = 6/group.

Experiment 2. Histology, immunostaining, and western blotting exhibits the anti-inflammation, ER stress associated mitochondrial apoptotic pathway inactivation, and myelin restoration or remyelination in TF administered rat brains after p-TBI.

Animal group	Species, age, weight, and sex	Number of animals per group (n)
Vehicle	SD-male rats, 8-week-young, and weighing 220-250 g	6
48 h p-TBI	SD-male rats, 8-week-young, and weighing 220-250 g	6
7 d p-TBI	SD-male rats, 8-week-young, and weighing 220-250 g	6
21 d p-TBI	SD-male rats, 8-week-young, and weighing 220-250 g	6
TF administered rats group	SD-male rats, 8-week-young, and weighing 220-250 g	6

Note. For pathology, experiment 2 utilizes 7 d p-TBI group aforementioned in Experiment 1 being compared to Vehicle and TF groups. Experiment 2 utilized n = 6 rats/condition for pathological studies; n = 6 rats/condition for western blotting of vehicle, 48 h, 7 d p-TBI, 21 d p-TBI, and TF administered rats group.

• To determine the sample size, in this study, we employed a larger effect size f (0.8), α-err prob (0.05), power (1 β-err prob) (0.8), number of groups (Experiment 3: 3 groups) as per the Cohen's standard effect size.

In Experiment 3, the sample size is n = 21/3 groups. Nonetheless, we employed n = 6/group as per previous studies to maintain animal numbers consistency across all groups. Experiment 3. 2D-gel electrophoresis and MALDI-MS proteomics studies of rat brain mitochondrial samples (Vehicle, 4 d p-TBI, and TF administered rat group) for the identification of future novel cell death indicators.

Animal group	Species, age, weight, and sex	Number of animals per group (n)
Vehicle	Sprague Dawley (SD) male rats, 8-week- old, and weighing 220-250 g	6
7 d p-SNI	Sprague Dawley (SD) male rats, 8-week- old, and weighing 220-250 g	6
TF administered rats group	Sprague Dawley (SD) male rats, 8-week- old, and weighing 220-250 g	6

We used a sample size of n = 6/condition since the entire experiment was conducted on SD-rats and n = 6 is the typical sample size for rat models.

Animal groups for CNS: Rats were weighed and anaesthetized through intraperitoneal administration. Avertin (2, 2, 2-Tribromoethanol 1.25 g, 2-Methyl-2-Butanol-2.5 ml per 100 ml) Dose: 150 mg/kg of body weight or 12.4 ml/kg of body weight of the animal model. Site: intraperitoneal, Volumes: 3 ml/250 g of selected SD rats. Sham (SH) group (n = 6) animals were placed on the weight drop platform without inducing TBI or dropping weight on the head and this group only used to compare among the experimental injury groups. Vehicle (VEH) treated (n = 6) [carboxymethylcellulose made up to 0.06% (w/v) in water, to which Tween 80 was added to reach a final concentration of 0.5% (v/v)] without compound, administered orally for 2 weeks on alternate days to the control rats to check the adverse effect and this group only used to compare among the injury and treatment groups. 48 hour (48 h) p-TBI experimental animal group (n = 6) represents a separate batch of TBI induced rats which were maintained for 48 h followed by euthanasia to study the pathological alterations at 48 h p-TBI point. 7 days (7 d) p-TBI experimental animal group (n = 6) represents TBI induced rats which were maintained for 7 d followed by euthanasia to study the pathological alterations at 7 d p-TBI point. A separate group of rats (n = 6) were anesthetized, and TBI was induced by the weight-drop method and the animals were maintained for 21 days (21 d) followed by euthanasia to study the pathological alterations at 21 d p-TBI (n = 6). Teriflunomide (TF) treatment group (n = 6) represents the drug administered group which received their first dose of TF 10 mg/kg body weight soon after the recovery from anaesthesia experimental after head injury. Compound formulation dissolved carboxymethylcellulose made up to 0.06% (w/v) in water, to which Tween 80 was added to reach a final concentration of 0.5% (v/v). TF treatment continued for 2 weeks on alternate days, followed by euthanasia, and brains were excised to study the pathological alterations.

TBI test apparatus for rats: Approximately 200 g mill weights, along with an attached metal loop at the top, were used to induce TBI in rats. A fishing line or thread was tied at the loop to allow the weight to pass freely. Care was taken to tape or stick the scored tin aluminium foil to the U-shaped stage made up of clear plastic with a collection of sponge bottoms. A column pipe was set with a fixing stand that can pass the mill weights freely from top to bottom. Holes were drilled on either side of the vertical column pipe at an experimental height of 90 cm with a drilling machine to use the key pin which holds the mill weights in the middle of the column pipe.

Inducing TBI in rats: weight Drop method: Rats were anesthetized and rapidly put on the surface of the tin foil U-shaped stage, facing the open side, and positioned the chest towards the foil's underside. The rat head was positioned exactly below the experimental column pipe by maintaining 10 cm distance. Mill weights were dropped from the top of the fixed column pipe and stopped at a height of 90 cm from the bottom by inserting a key pin in the drilled holes of the column pipe. The key pin was pulled and mill weights were passed from the column pipe and strike the rat head to induce TBI experimentally. Soon after the strike, the rats were made a rapid rotation of 180 °C and landed on the sponge in the supine position. Immediately, 2% lignocaine gel was applied to the rat head with a cotton ball for all the experimental rat groups. Rats are

transferred to the recovery chamber and placed in a supine position. For the sham group, rats were placed on the tin foil without pulling the key pin to avoid the mill weights striking the head. 2% lignocaine gel was applied to the rats' heads, and then the rats were shifted to the recovery chamber in a supine position. Individual experiments were done on each rat to induce TBI by repeating the weight drop method apparatus setup.

Weight Drop Method





TF administration: After 10 d p-SNI, rats were sedated, and the partial ligation or suture was removed, and the rats were given their TF doses after recovery from anaesthesia (TF provided by NATCO Pharma Limited, Hyderabad, T.S., India). TF was administered orally at a dos-age of 10 mg/kg body weight through rat oral gavage for two weeks on alternate days [22]. TF was dissolved in the vehicle: carboxymethylcellulose made up to 0.06% (w/v) in water, to which Tween-80 was added to reach a final concentration of 0.5% (v/v). Rats were euthanized shortly after the therapy

was completed, and sciatic nerves were severed and preserved in 10% formalin for pathological examinations.

Euthanasia: Rats were euthanized by an overdose of sodium pentobarbital (100 mg/kg) injected intraperitoneally at different time points. Rats were then perfused and the brain samples were excised for further studies.

Perfusion fixation: Euthanized animals were placed on the shallow tray filled with crushed ice. Under the rib cage, lateral incisions of 5-6 cm were made through the integument and abdominal wall carefully to separate the liver from the diaphragm, followed by another small incision in the diaphragm using the curved, blunt scissors, which continued to the entire rib cage along with the pleural cavity. Lung displacement was done using curved, blunt scissors, and a cut was made through the rib cage up to the collarbone, followed by a similar cut on the contralateral side. The tip of the sternum was clamped with the hemostat and placed over the head. A small incision to the posterior end of the left ventricle using iris scissors was made and a 15-gauge blunt-or olivetipped perfusion needle was inserted through the cut ventricle into the ascending aorta. The heart was clamped using a hemostat to secure the needle and prevent leakage. Finally, an incision was made in the animal's right atrium using iris scissors to create as large an outlet as possible without damaging the descending aorta. The outlet port perfusion equipment was attached to the needle base by avoiding air bubbles, and the 80 mm Hg pressure of the manometer bulb was maintained throughout the buffer infusion period with a proper needle angle adjustment to achieve the maximum flow rate. Fixation was almost pumped into the animal and the clear running of the fluid was monitored. The clearance of the liver was observed, which is an indicative of proper perfusion. Fixation tremors have been observed within seconds, which can be considered as the true time of fixation indicator. Further, the pressure was gradually increased up to a maximum of 130 mm Hg to maintain a steady flow rate. The outlet valve was closed soon after the completion of the fixation process, followed by the ending time recordings, and the stiffness of the animal was observed.

Paraffin-embedded tissue sections: Freshly collected brain samples were sliced into 3 mm cross slices and fixed with 10% formalin for 48 h at room temperature. After fixation, samples were washed under running tap water for 1 h, followed by dehydration steps using 70%, 80%, and 95% alcohol changes for 30 min each and 3 changes of 100% alcohol for 1 h each. Brain samples were cleared in 1 change of xylene for 5 min and another step of xylene + melted paraffin (1:1 ratio for 5 min), followed by immersing the samples in 3 changes of paraffin (Paraplast®-polyisobutylene mixture, catalog no. P3558–SIGMA–ALDRICH®) for 1 h each and the brain slices were embedded in a paraffin block. Brain slice blocks were fixed to the microtome (LEICA RM2145)

and 10 µm cross sections were cut and floated in a 40 °C maintained water bath containing clear distilled water. Tissue sections were transferred carefully to the glass slides for further neuropathological studies.

Haematoxylin and eosin staining (H & E): Formalin-fixed paraffin-embedded FFPE rat brain corpus callosum cross sections were first deparaffinized by two xylene changes for tissue clearing. Sections were rehydrated accordingly in different alcohol gradients followed by a water wash. The processing section slides were then dipped in nuclear stain (Haematoxylin) for 3-5 min and shifted to the stain (eosin) for extracellular matrix and cytoplasmic staining for 2 min, followed by a water wash. Following staining, the sections were dehydrated in various alcohol gradients before tissue clearing with xylene and DPX mounting.

Immunohistochemistry for CNS: Brain cross sections were deparaffinized using a heating pad and the sections were cleared with xylene. Tissue sections were further rehydrated with alcohol gradients. The sections were then transferred to antigen retrieval buffer (trypsin 0.05% in 100 ml of PBS) for 15 min at 37 °C and permeabilized (Triton X-100 0.2% in PBS) followed by one step of PBS wash. Sections were blocked (BSA 1%, NGS 5% in PBS) and left for 1 h at room temperature. Approximately 100 µl of diluted primary antibodies of myelin basic protein (MBP) (AB clonal, A1664, 1:200), CNPase-2, 3-cyclic nucleotide 3-phosphodiesterase (GenScript, A01308-40, 1:100), S100 Beta EP 32 (PathnSitu, CR070, 1:400), BiP (Santa Cruz Biotechnology, 13539, 1:400), ATF6 (Santa Cruz Biotechnology, 22799, 1:400), CD68 KP 1 (PathnSitu, PM113, 1: 200), and TNFα (Novus Biologicals, NBP1-19532, 1: 200) were applied to the sections and incubated for 30 min at room temperature, followed by a PBS wash. Approximately 100 µl of diluted biotinylated secondary antibody was applied to the sections and incubated for 30 min at room temperature by protecting them from sunlight, followed by PBS washes, and then DAB substrate solution was applied to the sections with repeated PBS washes. Haematoxylin is used for counter-staining the sections followed by the water wash, dehydrated in graded alcohol steps, and then DPX mounted.

Western blotting: Rat brains were dissected and brains are homogenised in Radioimmunoprecipitation assay buffer (RIPA) buffer (Sigma Aldrich, R0278) containing protease inhibitors. Protein concentrations were determined by the BCA Assay (Thermo Fisher Scientific). 30 μg per each sample and an equal volume of protein were loaded on gels and further transferred to nitrocellulose membrane (BIO-RAD) and blocked with 5% skimmed milk and were probed with the following primary antibodies: TNFα (Novus Biologicals, NBP1-19532, 1: 500), BiP (Santa Cruz Biotechnology, 13539, 1:500), p-Perk, (Cell Signalling Technology, #3179, 1:1000), BAD (Cell Signalling Technology, #9291, 1:1000), Bcl-xL (Cell signaling Technology, #2764, 1:1000),

BAX (Cell Signalling Technology, #2772, 1:1000), Caspase-3 (Novus Biologicals, NBP2-25080, 1:2000), Cleaved caspase-7 (Cell Signalling Technology, #8438, 1:1000), MBP (AB clonal, A1664, 1:500), CNPase -2, 3-cyclic nucleotide 3-phosphodiesterase (GenScript, A01308-40,1: 500), GAPDH (Cell Signalling Technology, #2118, 1:1000).

Mitochondria isolation: Rat brains were collected and white matter regions are finely minced by adding around 5 ml of buffer 1: 1.25 ml of 8X mitochondria buffer (10.28 g sucrose for a final concentration of 0.6 M, 400mg BSA for a final concentration of 0.8%, 2.08 g HEPES for a final concentration of 160 mM, pH to 7.4 and made-up to 50 ml with distilled water). The minced brain with the solution was then transferred to the polytron homogenizer. Homogenized tissue samples were collected into pre-chilled micro-centrifuge tubes and centrifuged at 700g for 10 min at 4 °C. The supernatant was transferred to new pre-chilled micro-centrifuge tubes and the pellets were discarded. The supernatant was centrifuged at 10,500g for 10 min at 4 °C and the pellet was resuspended in 500 μl of (buffer 2: Add 60 μl of 500 mM EGTA for a final concentration of 3 mM, 0.392 g of D-mannitol for a final concentration of 215 mM, 1.25 ml of 8X mitochondria buffer, pH to 7.4 and make up to 10 ml with distilled water) and centrifuged at 10,500g for 10 min at 4 °C. The final mitochondrial pellet was suspended in 100 μl of Buffer: 2 followed by a quick spin for the final mitochondrion for a few seconds. Add 1/100 volume of Protease Inhibitor Solution (100X) to Lysis Buffer 1 and Buffer 2 (i.e., if using 2 ml of Disruption Buffer, add 20 μl of Protease Inhibitor Solution). Determine protein concentration using the BCA assay.

2D-gel electrophoresis, Rehydration of IPG strips and First Dimension Separation IEF (Isoelectric focusing):

The first-dimension separation of 2D-gel is IEF. In this, proteins are separated based on differences in their isoelectric point (pI) [23].

Mitochondrial protein samples were added to the rehydration tray and the cover removed from the selected IPG strip pH 4-10, 18 cm, and the gel was allowed to slide down onto the rehydration buffer in the tray. The tray was overlaid with mineral oil to prevent the evaporation and precipitation of urea during rehydration and left for 20 h for complete rehydration. The rehydrated IPG strips were transferred to the IEF tray gel side up using two notches, and the IPG strips were overlaid with mineral oil and run through the IEF according to the protocol (GE Healthcare).

IPG strip equilibration and running of the second dimension by SDS-PAGE: following IEF, the strips were transferred to the new tray gel side up and filled with the recommended volume of equilibration buffer 1, followed by incubation for 10 minutes. Buffer 1 was removed and equilibration buffer 2 was added for 10 min of incubation. After equilibration, IPG strips were

removed and followed by a rinse with SDS-PAGE running buffer, and the strips were placed on the prepared 12% SDS-PAGE gel and sealed with 0.5% of agarose solution, and the electrophoresis unit was run. Comparative studies of the gels for the up-regulation and downregulation for the detection of the protein were analysed by IMR software version 7.0.0.GE Healthcare (all the above experimental protocols and buffers are purchased from GE Healthcare). *In-gel digestion and mass spectrometric analysis of MS:* Automated spot cutter was used to collect the spots of interest. For in-gel digestion, the gel plugs were washed with water twice for 5 min and incubated with 100% acetonitrile for 10 minutes. Then, the gels were dried completely for at least 30 minutes. The protein in the gel was digested by treatment with TPCK—treated trypsin in 50 mM ammonium bicarbonate at 37 °C overnight with gentle agitation. After digestion, peptides were extracted with 50 µl of 50% acetonitrile and 0.1% trifluoroacetic acid (TFA) twice, concentrated, and extensively treated with ZipTip. Then trypsin digests were mixed with an equal volume of matrix solution, comprising saturated dihydroxy benzoic acid in 50% acetonitrile and 0.1% TFA. The samples were spotted on a MALDI target plate and subjected to mass spectrometric analysis. A Q-STAR Pulser-i equipped with a MALDI, source was used for the mass spectrometric analysis of trypsin digestion. Raw data to mzml file conversion was done using Flex analysis 3.2 software and followed by the mascot online search engine tool for protein identification and peptide sequencing.

<u>Statistical analysis:</u> All the immunohistochemistry and western blotting statistical estimations were quantified as the mean percentage of expression by <u>ImageJ software</u>. In Sigma plot 11.0 software, a single group, one sample t-test is used to estimate the Mean \pm SEM from each individual experimental animal groups. <u>GraphPad Prism 8.0.2</u>, column analysis, one-way ANOVA test is used for the multiple comparisons (Tukey test) of the mean and significant *p-value*.

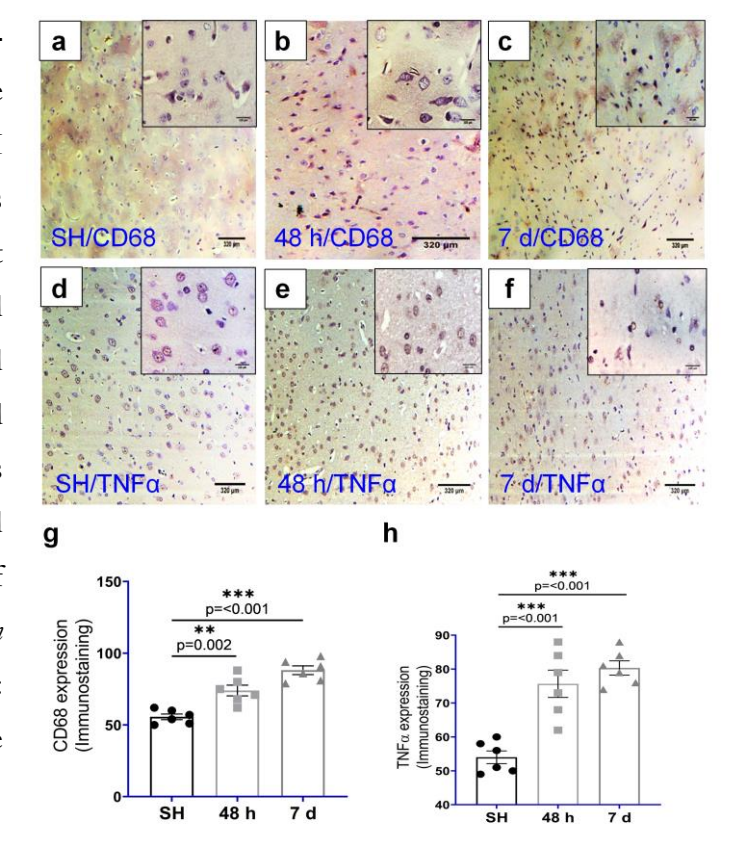
IV. Results

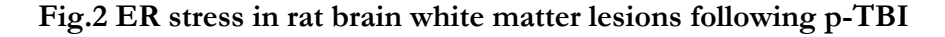
1. Pro-inflammation triggered ER stress and stimulate demyelination in rat brain white matter lesions following TBI (early and mild phases).

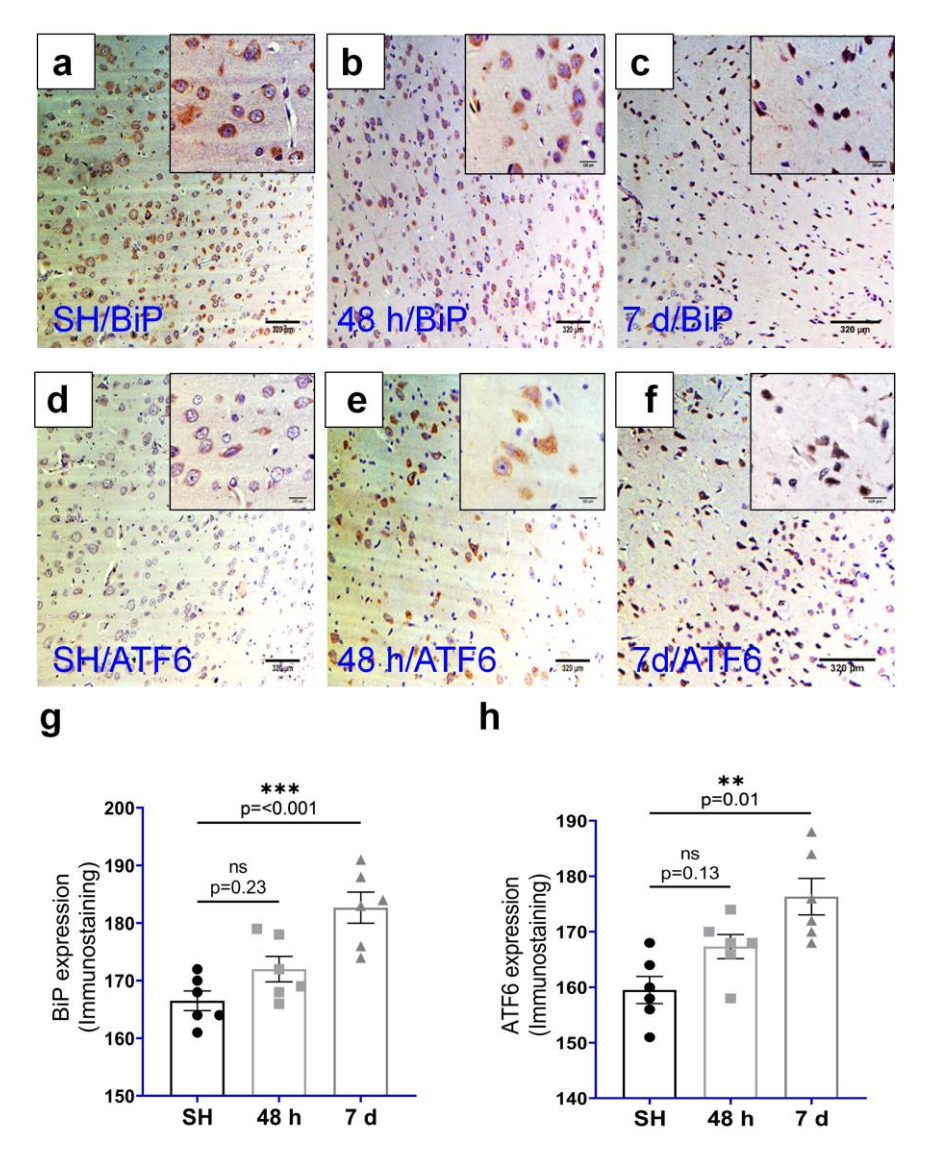
We used a well-established weight drop method to injure the rat brain and damage the white matter. Immunolabeling with CD68 detected macrophages and TNFα detected cytokines in 48 h post-TBI rat brain white matter cross sections, with an enhanced expression noted in 7 d post-TBI samples (Fig. 1a-h). BiP immunostaining for ER chaperone binding protein and ATF6 for ER sensor identified early labelling in 48 h p-TBI rat brain white matter samples, which increased in 7 d p-TBI rat brain white matter samples (Fig. 2a-h). These data describe the role of proinflammation in ER stress at 48 h p-TBI, which was enhanced by 7 d p-TBI.

Fig.1 Pro-inflammation in rat brain white matter lesions following p-TBI

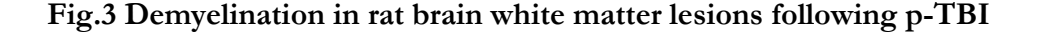
Photomicrographs of macrophages (ac) and cytokines (d-f) in rat brain white matter lesions. Sham (a, d) 48 h p-TBI (b, e) and 7 d p-TBI (c, f). Cross section samples were taken from rat brain white matter and immunostained for CD68 to detect macrophages and TNFα to detect cytokines. Activated macrophages noted in b and cytokines secretion in e which further enhanced **c, f.** Graphical depiction of macrophages in \mathbf{g} and cytokines in \mathbf{h} . n= 6/condition. Statistical significance: **P = 0.002, ***P = < 0.001. Scale bar= $320\mu m$.

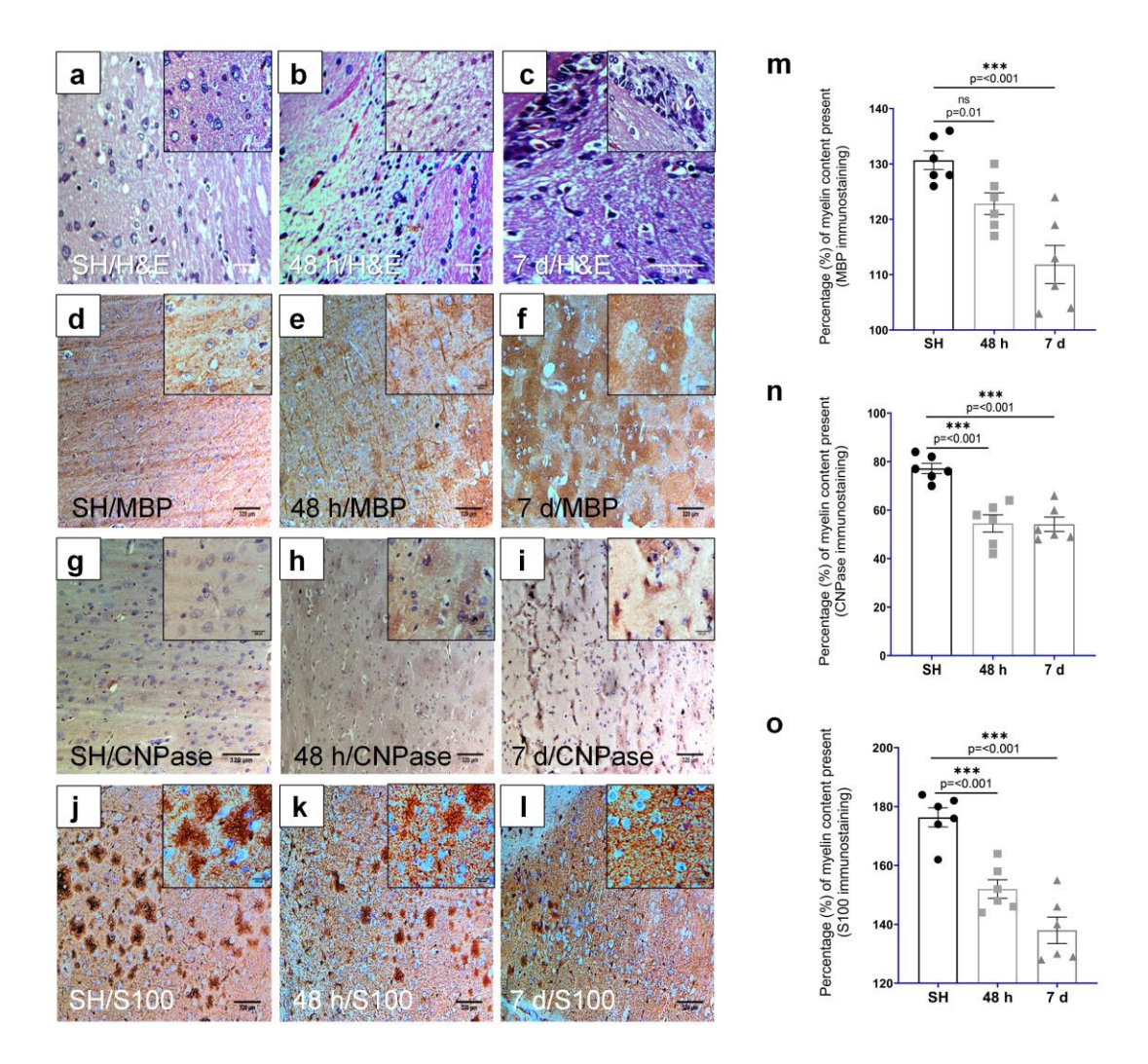






Micrographs of sham (a, d), 48 h p-TBI (b, e) and 7 d p-TBI (c, f) rat brain white matter cross section samples immunostained for BiP to detect ER chaperone binding protein release (a-c) and ATF6 for ATF6 ER sensor activation (d-f). Early BiP expression in b which enhanced in c and ATF6 sensor activation detected in e which enhanced in f. Graphical depiction of ATF6 in g and BiP in h. n = 6/condition. Statistical significance: (ns) P = 0.13, 0.23, **P = 0.01, ***P = 0.001. Scale bar = 320µm.





Photomicrographs of haematoxylin & eosin H & E (**a-c**), myelin basic protein MBP (**d-f**), 2', 3'-cyclic nucleotide 3'-phosphodiesterase CNPase (**g-i**), and S100 (**j-l**) in rat brain white matter lesions. Sham (**a**, **d**, **g**, **j**), 48 h p-TBI (**b**, **e**, **h**, **k**), and 7 d p-TBI (**c**, **f**, **i**, **l**). Cross section samples were taken from white matter and immunostained for MBP, CNPase, and S100 to detect the percentage of myelin content. Noted cell morphological alterations began in **b** which increased in **c**. Immunostain for MBP detected myelin loss in **e** which enhanced in **f**. Immunostain for CNPase detected myelin loss in **h** which enhanced in **i**. Immunostain for S100 detected early myelin loss in **k** whereas increase myelin loss noted in **l**. Graphical illustration of MBP in **m**, CNPase in (**n**), and S100 in **o**. n = 6/condition. Statistical significance: P = 0.01(ns), ***P = < 0.001. Scale bar = 320µm.

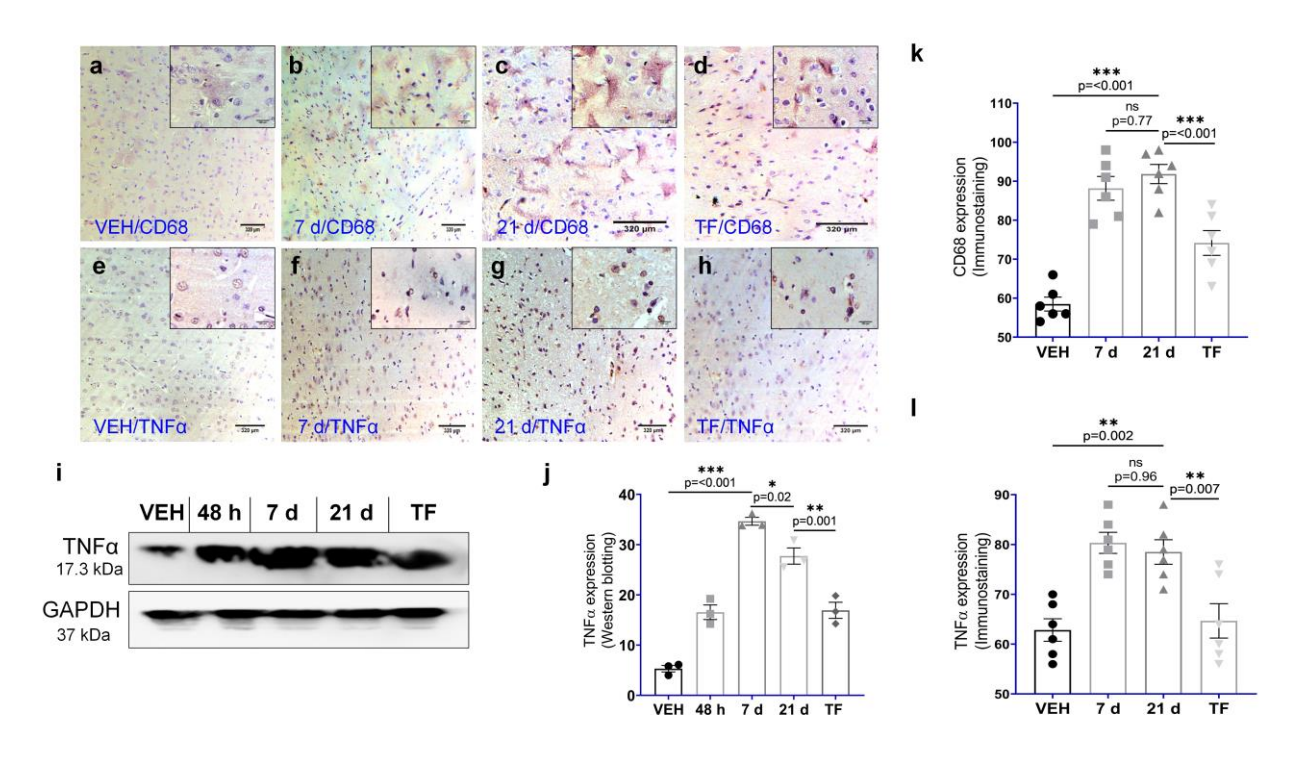
2. Advanced stage of pro-inflammation, ER stress, mitochondrial mediated cell death and demyelination in rat brain white matter lesions: Teriflunomide assisted recovery and remyelination

Pro-inflammation aggravated ER stress after 21 d p-TBI inhibited upon TF treatment.

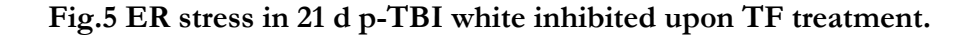
Rat brain white matter lesions cross sections immunostained with CD68 detected enhanced macrophages activation and TNFα detected slightly reduced cytokine secretion at 21 d after p-TBI shown in (Fig. 4c, g, k, l). However, Immunoblots of brain lysates with TNFα detected gradually enhanced expression from 48 h to 7 d after p-TBI with a reduced expression noted in 21 d p-TBI samples (Fig. 4i, j). TF treated p-TBI rat brain white matter lesions cross section samples immunostained for CD68 detected reduced labelling of macrophages and TNFα detected reduced labelling of cytokines in a comparison with the experimental rats (Fig. 4a-h, k, l). In contrast, Immunoblots of TF treated brain lysates with TNFα noted highly reduced expression among other experimental rats (Fig. 4i, j).

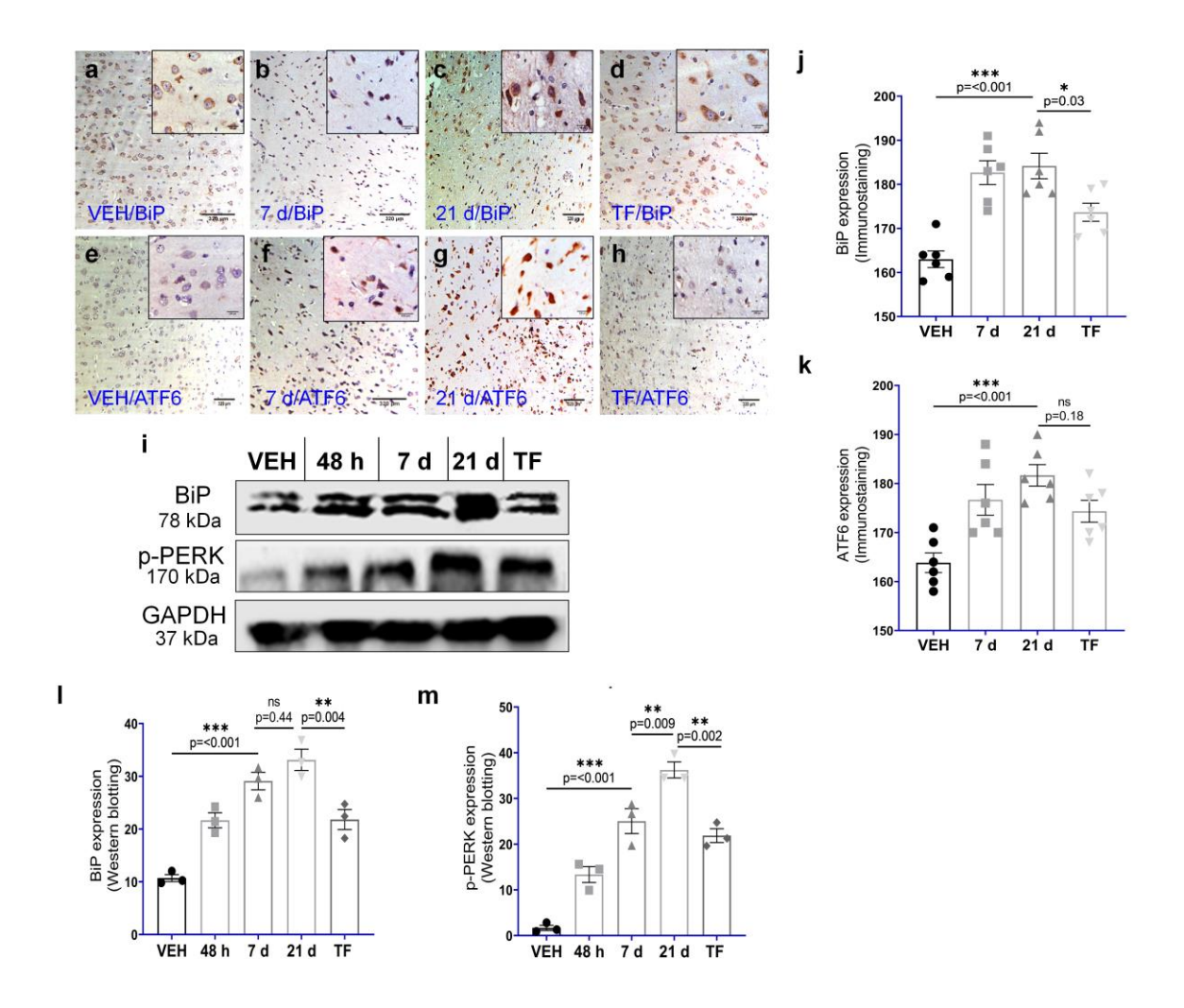
Immunostaining for BiP to detect ER chaperone binding protein and for ATF6 to detecte ER sensor activation revealed enhanced labelling of Immunostains in 21 d p-TBI rat brain white matter lesions cross section samples (Fig. 5c, d, j, k). However, TF treated p-TBI rat brain white matter sections revealed the reduced labelling of Immunostains for BiP and ATF6 (Fig. 5d, h, j, k). Immunoblots with BiP and p-PERK of brain lysates detected gradually elevated expression from 48 h to 21 d after post-TBI with a reduced expression noted in TF treated p-TBI rat brain lysates (Fig. 5i, l, m). According to these findings, even if macrophages are active, they lose their ability to secrete cytokines after 7 d p-TBI in rat brain white matter lesions. However, this time span is sufficient to induce and aggravate ER stress, which enhanced for more than 21 d following p-TBI. Interestingly, TF therapy decreased pro-inflammation while inhibiting ER stress.

Fig.4 Pro-inflammatory in 21 d p-TBI and TF treated rat brain samples being compared with 7 d p-TBI and vehicle groups.



Photomicrography of macrophages (a-d) and cytokines (e-h) in rat brain white matter lesions. Sham (a, e), 7 d p-TBI (b, f), 21 d p-TBI (c, g), and TF treatment (d, h). Cross section samples immunostained for CD68 to detect macrophages and TNF α to detect cytokines. Activated macrophages noted in **b** which further slightly enhanced in **c** and reduced in **d**. Secreted cytokines are detected **f** which reduced in **g** and noted high reduced labelling in **h**. Immunoblot of brain lysates from Vehicle, 48 h, 7 d, 21 d, and TF treatment with antibody to TNF α or GAPDH depicted in **i**. Graphical illustration of CD68 in **k** and TNF α in **l**. Quantitation of immunoblotted TNF α from brain lysates in **j**. n = 6/condition (immunostaining) and N = 3/condition (immunoblots). Statistical significance: (ns) P = 0.77, 0.96, *P = 0.02, **P = 0.001, **P = 0.002, **P = 0.007, ***P = 0.001. Scale bar = 320 μ m.





Photomicrography of BiP ER chaperone binding protein (a-d) and ATF6 ER sensors (e-h) in rat brain white matter lesions. Sham (a, e), 7 d p-TBI (b, f), 21 d p-TBI (c, g), and Teriflunomide TF treatment (d, h). Cross section samples immunostained for BiP to detect BiP ER chaperone binding protein and ATF6 to detect ATF6 ER sensor. BiP released or expression detected in b which enhanced in c and reduced in d. ATF6 activation detected in f which further enhanced in G and reduced labelling noted in h. Immunoblots of brain lysates from Vehicle, 48 h, 7 d, 21 d, and TF treatment with antibody to BiP, p-Perk or GAPDH depicted in i. Graphical representation of BiP in j and ATF6 in k. Quantification of immunoblot BiP from brain lysates in 1 and p-Perk in m. n = 6/condition (immunostaining) and n = 3/condition (immunoblots). Statistical significance: P = 0.18, P = 0.44 (ns), *P = 0.03, **P = 0.002, **P = 0.004, **P = 0.009, ***P = 0.001. Scale bar = 320µm.

Mitochondrial apoptotic pathway mediated cell death in p-TBI reversed upon TF therapy

Immunoblots with Bad and Bax, pro-apoptotic proteins show that the proteins receive stress signals and are gradually overexpressed from 48 h to 21 d after p-TBI brain lysates, that inhibited cell growth and induced cell death via a mitochondrial-dependent pathway (Fig. 6a-c). Bcl-xL, a transmembrane anti-apoptotic protein that was progressively overexpressed from 48 h to 21 d following p-TBI rat brain lysates to suppress apoptosis and Bax inhibition, was immunoblotted (Fig. 6a, d). Immunoblots of p-TBI rat brain lysates with caspase-3 and cleaved caspase-7 revealed gradual overexpression from 48 h to 7 d p-TBI, with reduced expression of caspase-3 and increased expression of cleaved caspase-7 identified in 21 d p-TBI rat brain lysates (Fig. 6a, e, f). Immunoblots of TF treatment p-TBI rat brain lysates revealed reduced expression of pro-apoptotic proteins bad, bax, and BclxL anti-apoptotic protein. Immunoblots of TF-treated p-TBI rat brain lysates with caspase-3 and cleaved caspase-7 revealed reduced expression in contrast to the experimental rats (Fig. 6a-f).

These findings highlight how ER stress signals received by pro-apoptotic and anti-apoptotic proteins suppressed cell development and triggered the mitochondrial apoptotic pathway in 21 d p-TBI rat brains. Furthermore, caspase-3 induced apoptosis by damaging cellular components such as DNA breakage and cytoskeleton protein degradation. Cleaved caspase-7, on the other hand, aids in the break down of cells. TF therapy inhibited ER stress signals and suppressed apoptosis by inhibiting pro and anti-apoptotic proteins.

Demyelination at 3 W p-TBI, followed by TF-assisted recovery and remyelination

Preliminary findings using hematoxylin and eosin staining demonstrated the cell morphological alterations in **Fig. 3a-c**, as well as evidence for progressively increased myelin loss from 48 h to 7 d p-TBI using MBP, CNPase, and S100 immunostains (**Fig. 3d-o**). Further, since the current study focuses on myelin loss or demyelination in late-stage p-TBI rats, immunostaining with MBP, CNPase, and S100 revealed accelerated myelin loss or breakdown in 21 d p-TBI rat brain white matter sections (**Fig. 7g, k, o, r-t**). Immunoblots of 21 d p-TBI brain lysates with MBP and CNPase revealed enhanced myelin loss in contrast to the other experimental rats (**Fig. 7q, u, v**).

Immunohistochemistry with MBP, CNPase, and S100, on the other hand, demonstrated remyelination or myelin restoration in TF-treated rat brain white matter cross-section samples following p-TBI (Fig. 7h, 1, p, r-t). Furthermore, immunoblots of brain lysates for MBP, CNPase, and S100 increased following TF treatment in p-TBI rats (Fig. 7q, u, v). These findings emphasize the significance of TF in healing and promoting myelin secretion at the injury site.

Fig.6 Mitochondrial apoptotic pathway associated cell death in p-TBI rat brain lysates which reversed following TF therapy.

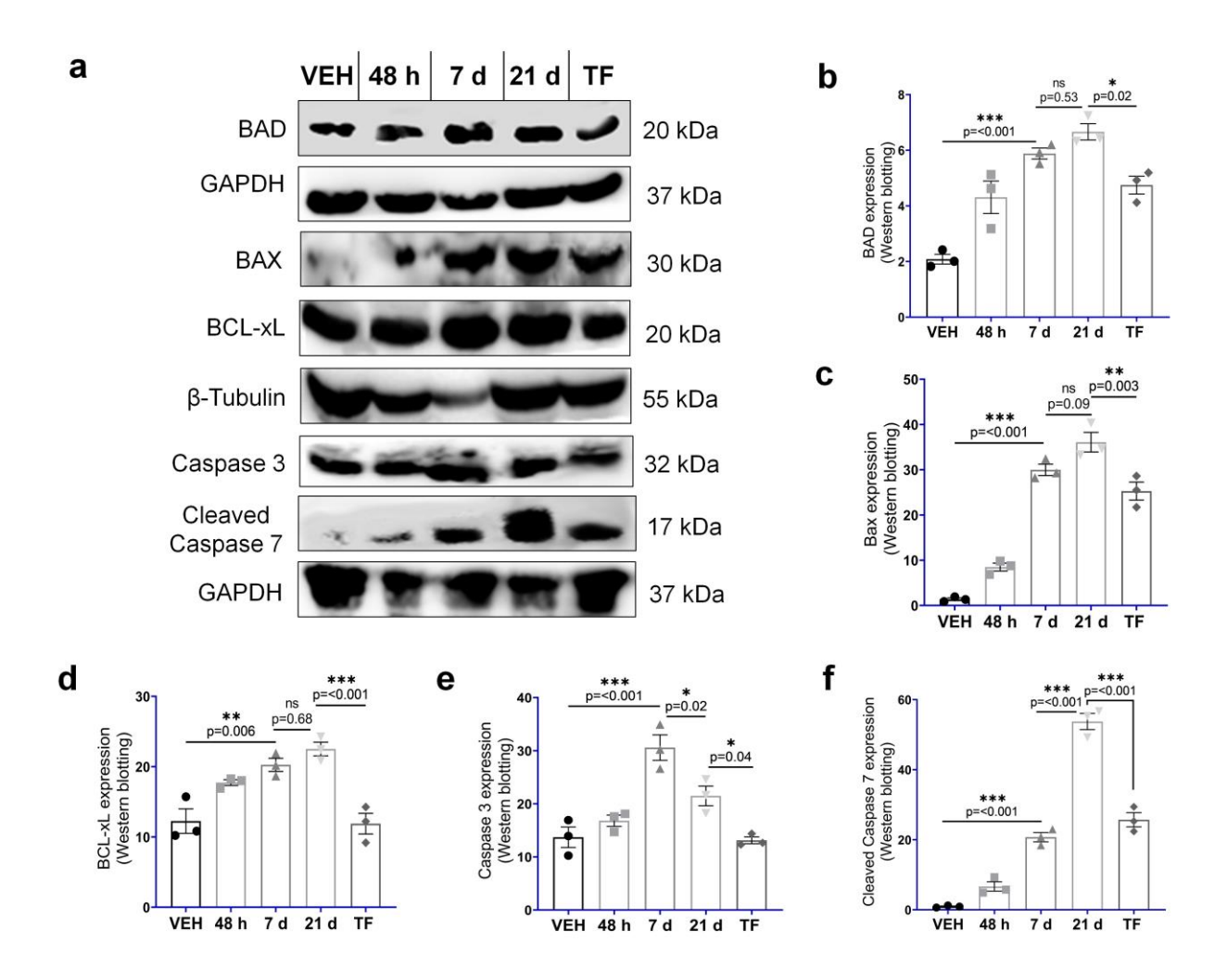
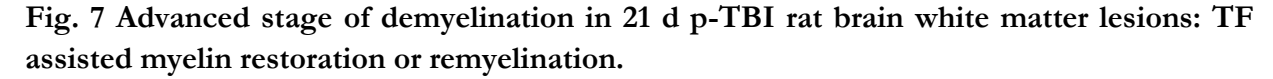


Fig. 6 Immunoblots of brain lysates from Vehicle, 48 h, 7 d, 21 d, and TF treatment with antibody to Bad, Bcl-xL, Bad, Caspase 3, Cleaved caspase 7 or β-Tubulin and GAPDH depicted in **a.** Quantification of immunoblots Bad in **b,** Bad in **c,** Bcl-xL in **d,** caspase 3 in **e,** and cleaved caspase 7 in **f.** n = 3/condition. Statistical significance: (ns) P = 0.09, 0.53, 0.68, *P = 0.02, 0.04, **P = 0.003, 0.006, and ***P = 0.001.



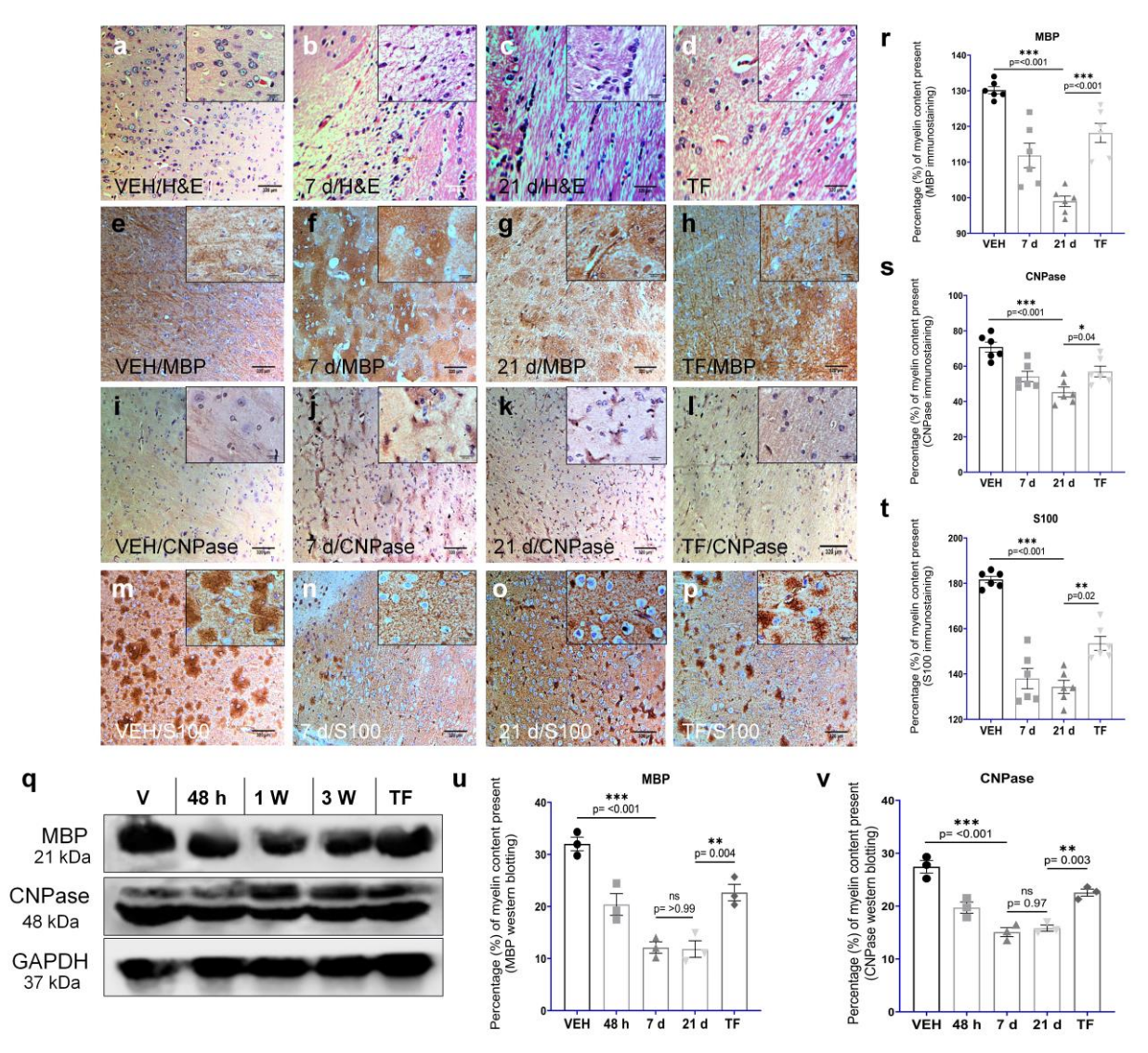
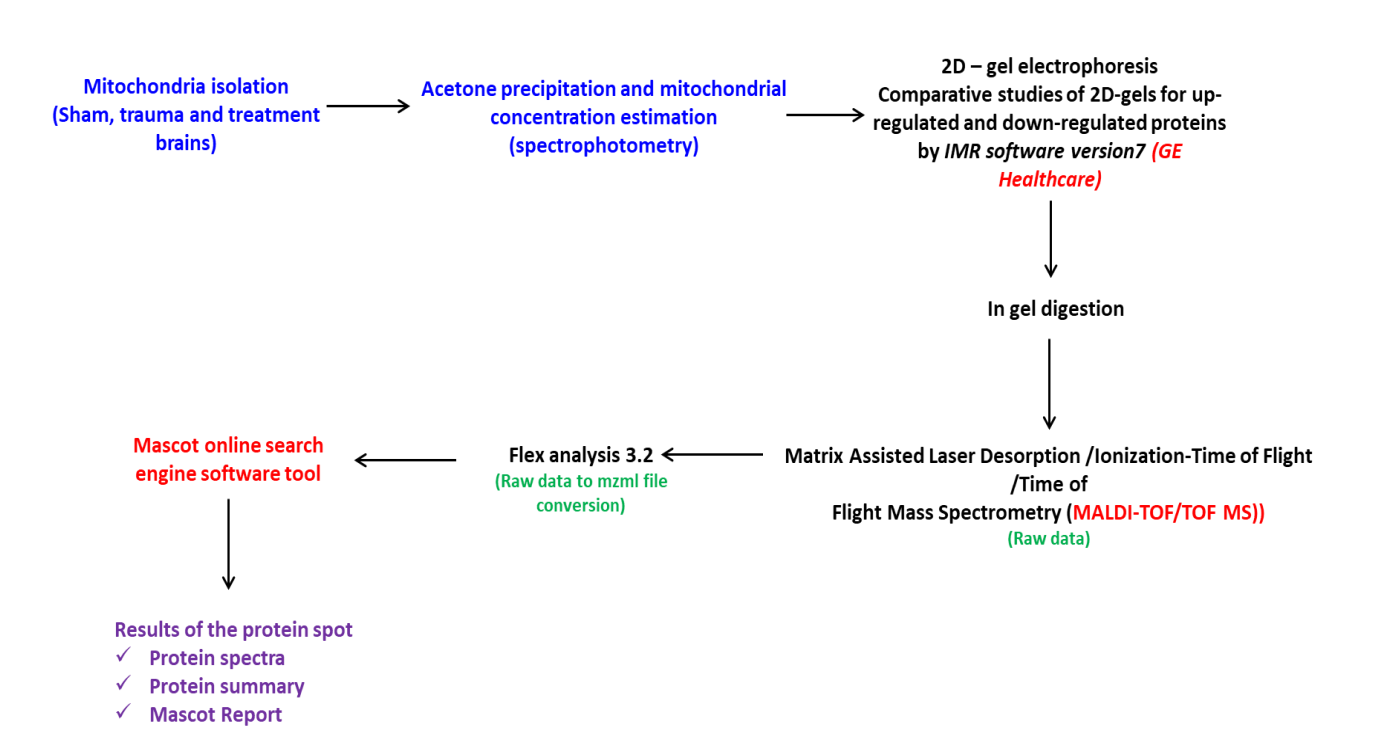


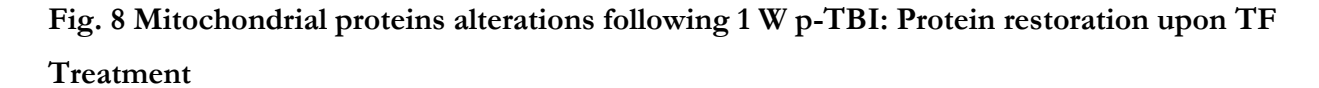
Fig.7 Photomicrographs of haematoxylin and eosin (a-d), myelin basic protein MBP (e-h), 2', 3'-cyclic nucleotide 3'-phosphodiesterase CNPase (i-l), and S100 (m-p) in rat brain. Sham (a, e, I, m), 7 d p-TBI (b, f, j, n), 21 d p-TBI (c, g, k, o), and TF (d, h, l, p) cross section samples were taken from white matter and immunostained for MBP, CNPase, and S100 to detect the percentage of myelin content. Noted cell morphological alterations in b which enhanced in c and recovery detected in d. Immunostain for MBP detected myelin loss in f which enhanced in g and myelin restoration in h. Immunostain for CNPase detected myelin loss in j which enhanced in k and myelin restoration in l. Immunostain for S100 detected myelin loss in n whereas increase myelin loss noted in O and remyelination detected in p. Graphical illustration of MBP in r, CNPase in s, and S100 in t. Immunoblots of brain lysates from Vehicle, 48 h, 7 d, 21 d, and TF treatment with antibody to MBP, CNPase, S100 or GAPDH depicted in q. Quantification of immunoblots MBP in u and CNPase in v. n = 6/condition (immunostaining) and n = 3/condition (immunoblots). Statistical significance: (ns) P = >0.99, 0.97, *P = 0.04, **P = 0.002, 0.003, 0.004, ***P = 0.001. Scale bar = 320μm.

3. Identification and characterization of mitochondrial protein alterations following one week p-TBI: Restoration upon TF treatment.

Schematic workflow

Proteomic studies





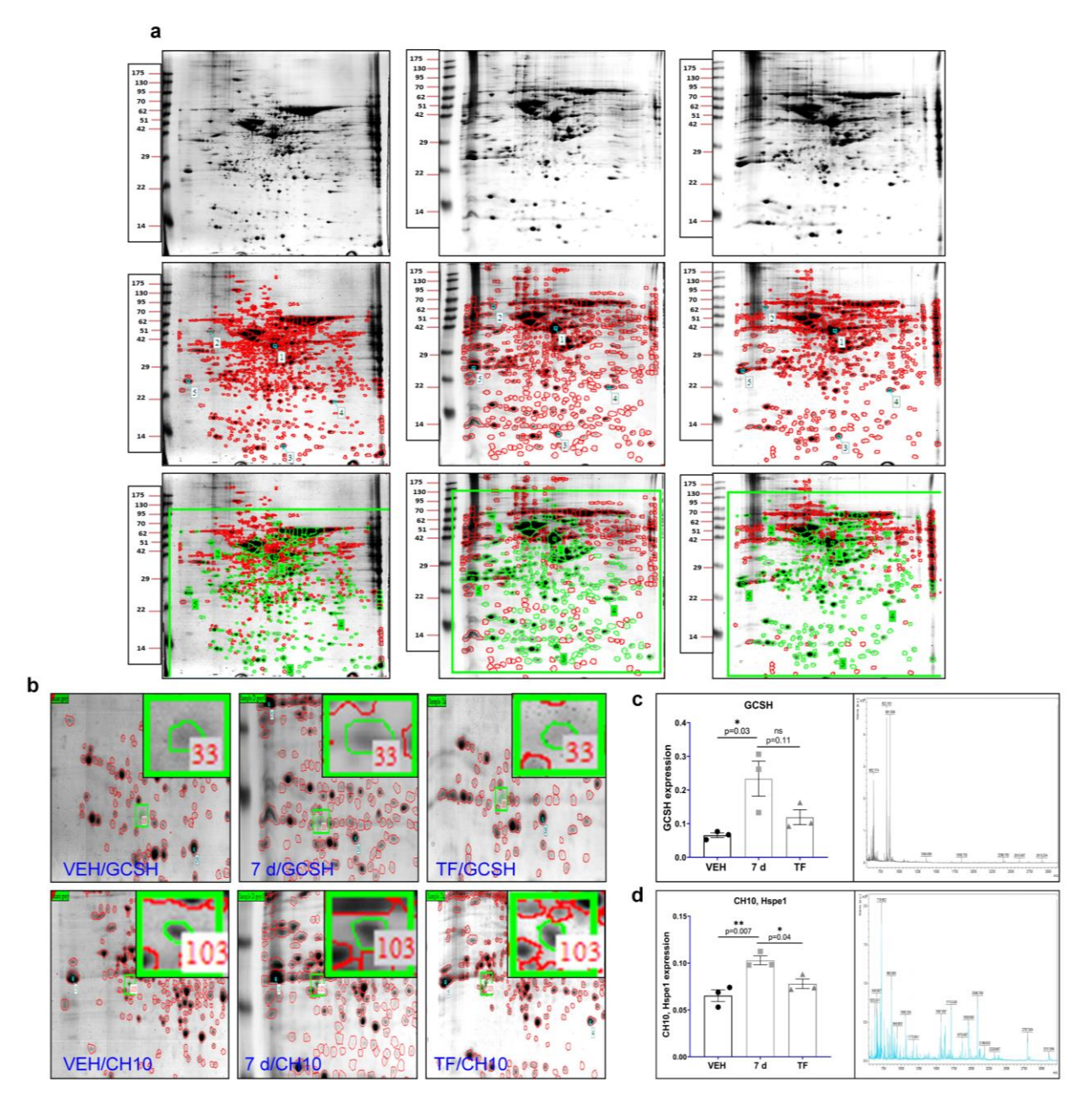
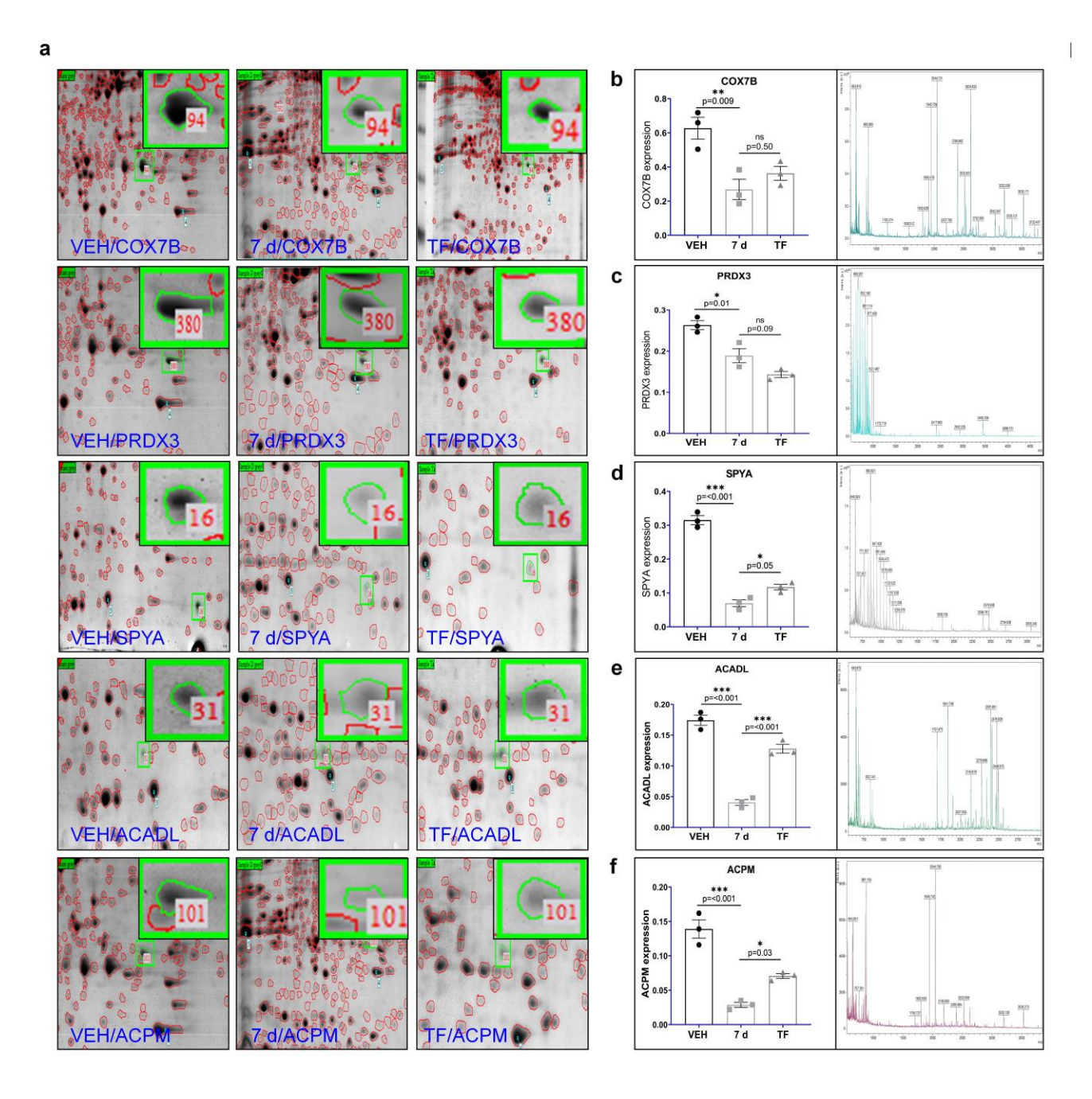


Fig.8 2D-gels of rat brain mitochondria from Vehicle, 7 d, and TF (3–10 pH, 17 cm size, GE Healthcare, gels were analysed by IMP software version 7 by GE Healthcare). Red spots in **a**, indicates matching proteins among VEH, 7 d, and TF. Green spots in **a**, indicates high intensity protein with alteration in comparison among VEH, 7 d, and TF. In **b** up-regulated mitochondrial proteins detected as GCSH and CH10, Hspe 1 using MALDI-MS flex analysis 3.2 and mascot search engine software tools. Quantification of mitochondrial protein spots along with protein spectra in **c** and **d**. n = 3/condition. Statistical significance: (ns) P = 0.11, *P = 0.03, 0.04, **P = 0.007.



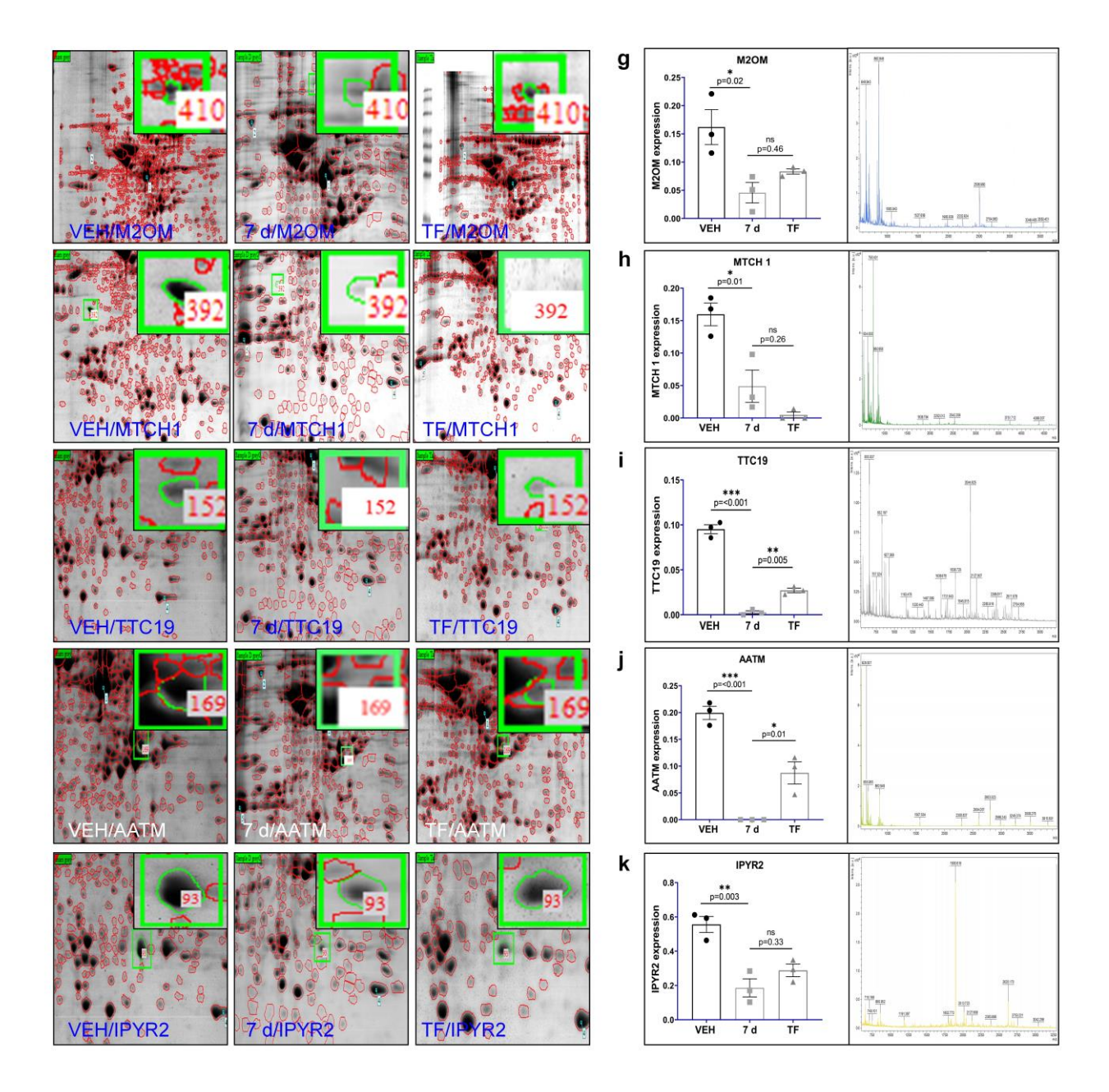


Fig.9 2D-gels of rat brain mitochondria from Vehicle, 7 d, and TF (3–10 pH, 17 cm size, GE Healthcare, gels were analysed by IMP software version 7 by GE Healthcare). In **(a)** down-regulated mitochondrial proteins detected as COX7B, PRDX3, SPYA, ACADL, ACPM, M2OM, MTCH1, TTC19, AATM, and IPYR2 using MALDI/TOF MS flex analysis 3.2 and mascot search engine software tools. Quantification of mitochondrial protein spots along with protein spectra in **b** and **k**. n = 3/condition. Statistical significance: (ns) P = 0.50, 0.46, 0.33, 0.26, *P = 0.05, 0.03, 0.02, 0.01, **P = 0.009, 0.005, 0.003, ***P = 0.0001.

Mitochondrial protein alterations following 7 d p-TBI which are restored upon TF administration

Mitochondrial proteins were separated using 2D-gel electrophoresis and identified by using MALDI MS. In comparison with VEH group, we found the differential expression of mitochondrial proteins in 7 d p-TBI rat brain mitochondria which are restored after TF treatment (Fig. 8a). Peptide sequences were identified decreased proteins in 7 d p-TBI rat brain mitochondria as COX7B- Cytochrome c oxidase subunit 7B, PRDX3- Thioredoxin-dependent peroxide reductase, SPYA- Serine--pyruvate aminotransferase, ACADL- long-chain specific acyl-CoA dehydrogenase, ACPM- Acyl carrier protein (Fig. 9a, c-d). Mitochondrial proteins, M2OM-mitochondrial 2-oxoglutarate/malate carrier protein, MTCH1- Mitochondrial carrier homolog 1, TTC19- Tetratricopeptide repeat protein 19, AATM- Aspartate aminotransferase, and IPYR2-Inorganic pyrophosphatase 2 which are restored upon TF treatment (Fig. 9b, h-l). Whereas, Peptide sequences were identified the increased proteins as GCSH-glycine cleavage system H protein and CH10, Hspe1- 10 kDa in 1 W p-TBI rat brain mitochondria (Fig. 8b-d). All these mitochondrial proteins restored or increased after TF treatment in comparison with VEH and experimental rats.

V. Discussion

This study aimed to demonstrates the active period of pro-inflammation that triggers ER stress in the rat brain white matter lesions based on prolonged time period of p-TBI. The studies explored how far ER stress can transmit signals that are received by pro-apoptotic and anti-apoptotic proteins, and how long these proteins can restrict cell growth and initiate the mitochondrial apoptotic pathway, promoting myelin-producing oligodendrocytic cell death and causing demyelination in p-TBI rat brain white matter lesions. New mitochondrial proteins involved in cell death, were identified which may enable the development of additional cell death indicators for the mitochondrial-mediated apoptotic pathways.

Myelin is maintained in the white matter by myelin-producing oligodendrocytes mostly populated in brain corpus callosum, which are required for neuronal connection and signal transmission [7]. Oligodendrocyte cell death causes myelin loss, which happens when cells lose their capacity to heal injured parts of the brain [14, 24].

Herein we demonstrate that TF has multifunctional properties in p-TBI rats via immunomodulation, cell death reversing mechanisms, and myelin secretion or remyelination at the injury site. However, TF is a well-known immunomodulatory medicine that is used to aid in the healing and repair of myelin in MS patients [19, 25, 26, 27].

Currently, many TBI animal models are used to induce neurodegeneration, which aids in the study of cell death mechanisms [28, 29]. In this work, we employed the weight-drop [30-32] approach to generate TBI in rats and demonstrate cell death processes in rat brain corpus callosum at different day intervals after p-TBI.

Preliminary findings of immunostains for CD68 to identify macrophages and TNFα to detect cytokines indicated early macrophagic activation at 48 h, which was amplified in 7 d p-TBI rat brain white matter lesion cross sections and exhibited elevated pro-inflammation. In female rats, increased macrophage expression and released cytokines were observed following localized traumatic brain damage [33-35]. Immunostains for BiP to identify ER chaperone binding protein and ATF6 to detect ER sensors expressed at 48 h and exhibited enhanced expression in 7 d p-TBI rat brain white matter cross sections. Pro-inflammatory cytokines cause ER stress, and ATF6 sensors in the ER stimulate the release of BiP chaperone binding protein, which subsequently translocates into the cytosol and initiates cell death by transmitting signals to pro-apoptotic proteins [11, 36, 37]. MBP, CNPase, and S100 immunostaining demonstrated significant early Myelin loss at 48 h, which accelerated following 7 d p-TBI. These myelin markers, which are expressed in myelin-producing oligodendrocytes in the central nervous system and Schwann cells

in the peripheral nervous system, have been used to identify myelin loss or demyelination in a wide range of neurological diseases [38-40].

In 21 d p-TBI rat brain white matter cross sections, immunostains for CD68 revealed increased macrophage activity and TNFα revealed decreased cytokine secretion. Immunoblots of rat brain lysates with TNFα, on the other hand, revealed a steadily increased expression from 48 h to 7 d after p-TBI, with a lower expression observed in 21 d p-TBI lysates. This is consistent with a previous study that found reduced TNFα expression in the cortex following TBI [41]. Immunostains for BiP and ATF6 increased progressively from 7 d to 21 d following p-TBI, which is consistent with the previously described endoplasmic reticulum stress to the inflammatory response [11, 37].

TF is an anti-inflammatory drug that stimulates macrophage deactivation and reduces cytokine secretion at the site of brain damage [25, 27]. Similarly, the current study sought to determine if TF therapy reduces pro-inflammation and inhibits ER stress following TBI. We employed TF as a therapeutic agent to treat pro-inflammation and to learn about the drug's ability to inhibit ER stress after TBI. Interestingly, immunostains for CD68 (macrophage) and TNFα (cytokines) in TF-treated p-TBI rat brain white matter samples revealed much lower expression of both markers in contrast to the experimental animal groups, suggesting that inhibiting macrophages limits cytokine release. BiP and ATF6 immunostain labeling, on the other hand, was much reduced when compared to experimental rats, demonstrating that TF inhibits ER stress following TBI.

To determine if ER stress signals activate the intrinsic apoptotic pathway after TBI in rats. Can TF prevent cell death in p-TBI conditions by inhibiting pro and anti-apoptotic proteins. Initially, immunoblots of brain lysates with pro-apoptotic proteins were performed. Bad and Bax demonstrate that the proteins receive ER stress signals and are gradually overexpressed from 48 h to 21 d after p-TBI, which suppressed cell growth and promoted cell death via a mitochondrial-dependent route [42]. Immunoblot for BclxL, a transmembrane anti-apoptotic protein gradually overexpressed following p-TBI from 48 h to 21 d to reduce apoptosis and Bax inhibition. This is comparable to a previous study on apoptosis after TBI [41]. These findings show how ER stress signals received by pro-apoptotic and anti-apoptotic proteins reduced cell growth and activated the mitochondrial apoptotic pathway in 21 d p-TBI rat brains. Interestingly, brain lysates from TF-treated p-TBI rats showed reduced expression of pro-apoptotic proteins Bad, Bax, and anti-apoptotic protein BclxL, indicating that TF can block pro-apoptotic proteins and rescue anti-apoptotic protein to improve cell survival.

Furthermore, Immunoblot with caspase-3 of p-TBI brain lysates detected progressively elevated expression from 48 h to 7 d and then reduced expression noted in 21 d p-TBI samples after execution of apoptosis by damaging cellular components such as DNA breakage and cytoskeleton protein degradation [41]. In contrast, immunoblots against cleaved caspase-7 indicated continuously increasing expression from 48 h to 21 d p-TBI, which is equivalent to that found in breast cancer cells [43]. Immunoblots of TF-treated p-TBI rat brain lysates with caspase-3 and cleaved caspase-7 exhibited lower expression in comparison to the experimental rats. These studies outline how TF treatment inhibited apoptosis by suppressing pro and anti-apoptotic proteins.

MBP, CNPase, and S100 immunostaining expression levels were shown to be lower in 21 d p-TBI rat brain white matter cross sections, in addition to other experimental animals. Immunoblots for MBP, CNPase, and S100 from 21 d p-TBI lysates revealed similarly reduced expressions, which are much lower than in any other experimental rat, indicating worsened demyelination during the late stages of TBI. Employing TF as a therapeutic medication resulted in modest myelin repair via increased expression of myelin markers MBP, CNPase, and S100 in both immunostaining and western blotting. A similar study found that TF stimulates oligodendrocyte precursor cell differentiation, which results in remyelination [19].

Mitochondrial dysfunction may be considered to be one of the early events that can cause cell death in the TBI. Though mitochondrial cell death has been reported in various pathological models the involvement of specific proteins is spar [44]. We observed considerable differences in mitochondrial functional proteins after 7 d p-TBI rat brain mitochondria. Proteomics studies came across mitochondrial carrier homolog 1 (MTCH1), decreased in the 7 d group and disappeared after TF treatment, has been detected. MTCH1 acts as the receptor for truncated BID (tBID) which is involved in apoptosis [12]. Mitochondrial 2-oxoglutarate/malate carrier protein (M2OM) which is a mitochondrial inner membrane protein decreased in 7 d p-TBI and slightly elevated following TF therapy. M2OM, a protein, is involved in the regulation of apoptosis [45]. This study found cytochrome c oxidase subunit 7B (COX7B) was decreased in 7 d p-TBI but marginally enhanced upon TF therapy. COX7B subunit contributes to the oligomerization of the apoptosis protease activating factor (APAF1) complex, which activates the caspase cascade and promotes apoptosis [16, 46]. This study predicts the activation of COX7B in the mitochondria as a result of TF therapy may diminish the activation of the apoptotic pathway, which is considered to play a crucial role in cell death.

This study detected decrease of thioredoxin-dependent peroxide reductase (PRDX3) in 7 d p-TBI, which slightly elevated after TF treatment. PRDX3 decrease enhances oxidative stress in the mitochondria, which is an important element of the cell's energy source [47]. Serine pyruvate aminotransferase (SPYA) decreased in 7 d p-TBI with an increase noted after TF treatment. Findings anticipated that decrease of SPYA affects the breakdown of metabolic processes and must have exacerbated cell death leading to demyelination in p-TBI, which is consistent with a publication claiming that SPYA protein is involved in gluconeogenesis and glyoxylate detoxification [48]. Data reveal that decrease of Long-chain specific acyl-CoA dehydrogenase (ACADL) noted in 7 d p-TBI which increased following TF therapy. Study predicts the restoration of ACADL protein after utilizing TF can increase cell cycle arrest and restrict cell proliferation and growth. According to one study, ACADL catalyses the initial stage of mitochondrial fatty acid beta-oxidation, which is an aerobic process [49]. Acyl carrier protein (ACPM) decreased in 7 d p-TBI rat brains, which enhanced by TF therapy. According to one research, ACPM can move electrons from NADH to the respiratory chain in the same way as ATP and CO2 are carried in the human body [50]. Tetratricopeptide repeat protein (TTC19) disappeared in 7 d p-TBI and reappeared after treatment with TF. TTC19 plays a crucial role in the preservation of the structural and functional integrity of mitochondrial respiratory complex III [51]. We expect that the absence of TTC19 will result in mitochondrial respiratory complex chain III deficit, and we propose that the TTC19 reappearance will aid in the restoration of complex III inadequacies. In our findings we came across increase of Heat shock protein (CH10 Hspe1) in 7 d p-TBI, whereas enhanced after TF therapy. Our prediction for this protein enhancing indicates the avoidance of protein denaturation and aggregation by refolding. Hspe1 avoids misfolding, promotes refolding, and ensures appropriate assembly of unfolded polypeptides synthesised under stress circumstances in the mitochondrial matrix [52]. We identified a total absence of aspartate aminotransferase (AATM), which reappeared after treatment with TF. AATM levels decreases soon after post-blast exposure TBI [53]. Findings demonstrated the decrease of inorganic pyrophosphatase 2 (IPYR2) in p-TBI and increase after TF treatment. IPYR2 affects mitochondrial membrane potential, as well as mitochondrial structure and function [54]. Proteomic analysis of mitochondria in experimental rats revealed substantial alterations following TF therapy, suggesting that mitochondrial proteins had been restored. Findings indicate significant alterations in proteins that are primarily involved in caspase cascade activation, cytochrome c release, apoptosis induction, detoxification, and the respiratory chain.

In summary the current findings provide evidence for the role of pro-inflammation in ER stress, which is followed by mitochondrial mediated cell death and exacerbate demyelination in rat brain white matter. Differential mitochondrial protein change in 7 d p-TBI rat brains may assist in the future development of novel cell death indicators. There has been no previous evidence of pro-inflammation, ER-mitochondrial mediated cell death at 21 d after p-TBI in rodent models. , TF therapy reduced inflammation via immunomodulation and reversed cell death mechanisms and promoted remyelination or myelin secretion. We believe TBI patients can benefit from TF as a remyelination treatment. Furthermore, comparing TBI progression in rats and humans should lead to a better knowledge of brain damage progression and therapy in general.

Chapter 2

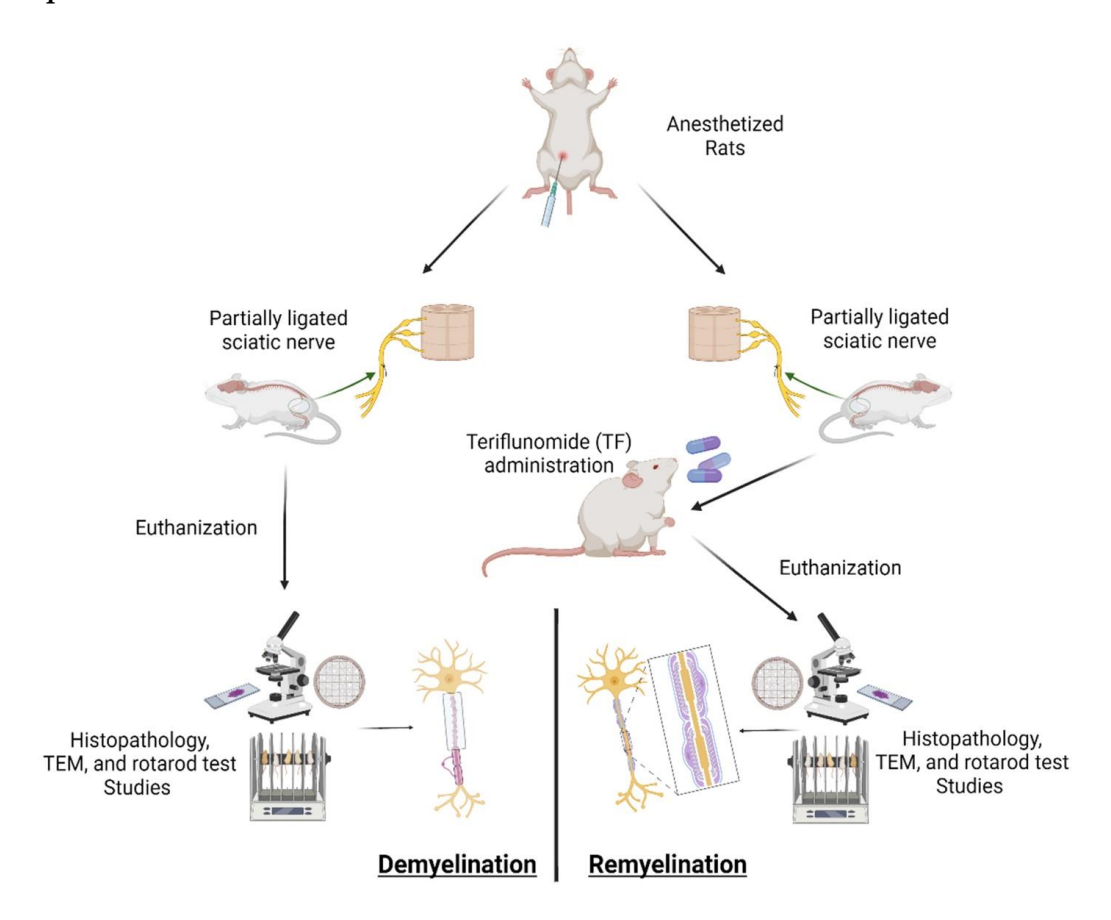
Surgically Induced Demyelination in the Rat Sciatic Nerve: Teriflunomide assisted Remyelination

I. Abstract

Demyelination is a common sign of peripheral nerve injuries (PNIs) caused by damage to the myelin sheath surrounding axons in the sciatic nerve. There are not many methods to induce demyelination in the peripheral nervous system (PNS) using animal models. This study de-scribes a surgical approach using a single partial sciatic nerve suture to induce demyelination in young male Sprague Dawley (SD) rats. After the post-sciatic nerve injury (p-SNI) to the sciatic nerve, histology and immunostaining show demyelination or myelin loss in early to severe phases with no self-recovery. The rotarod test confirms the loss of motor function in the nerve-damaged rats. Transmission electron microscopic (TEM) imaging of nerve-damaged rats reveals axonal atrophy and inter-axonal gaps. Further, administration of Teriflunomide (TF) to p-SNI rats resulted in the restoration of motor function, repair of axonal atrophies with inter-axonal spaces, and myelin secretion or remyelination. Taken together, our findings demonstrate a surgical procedure that can induce demyelination in the rat sciatic nerve which is then remyelinated after TF treatment.

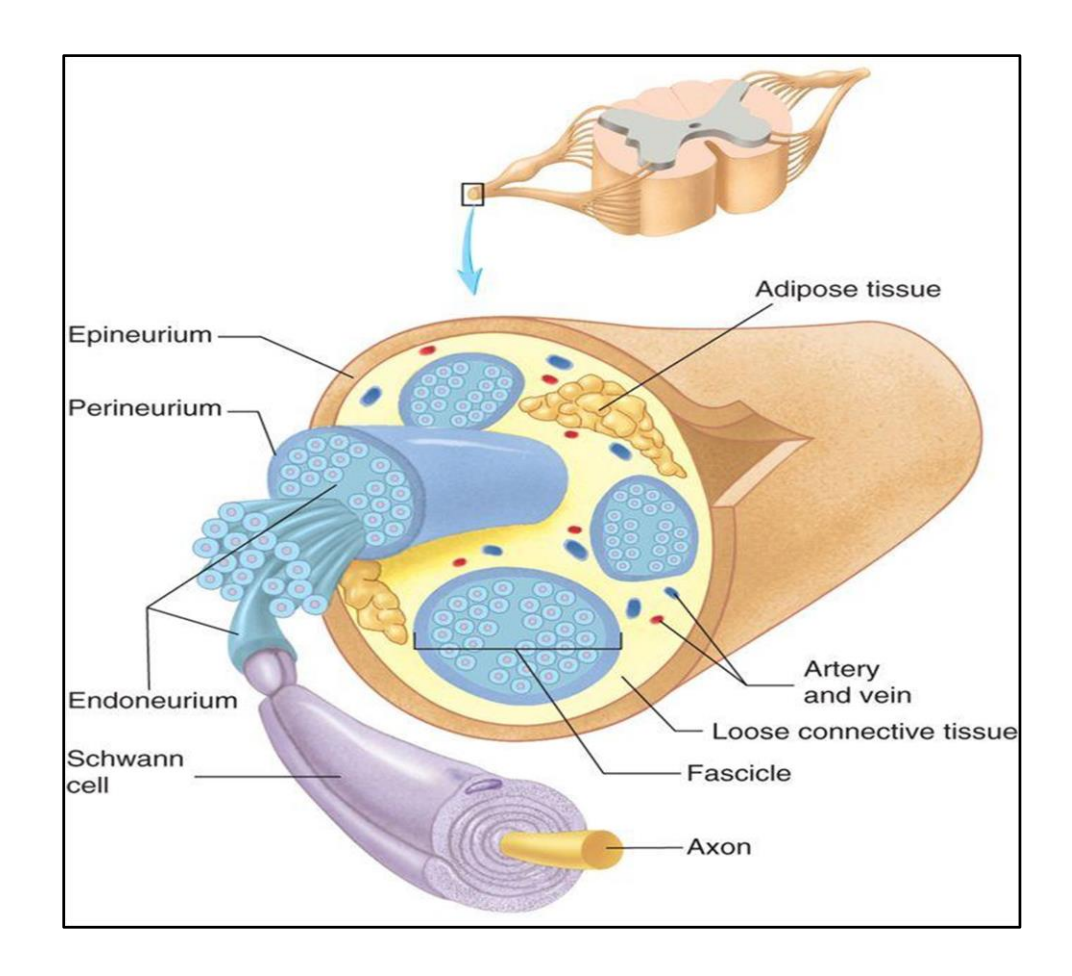
Keywords: Sciatic nerve injury · Demyelination · Teriflunomide · Remyelination

Graphical Abstract



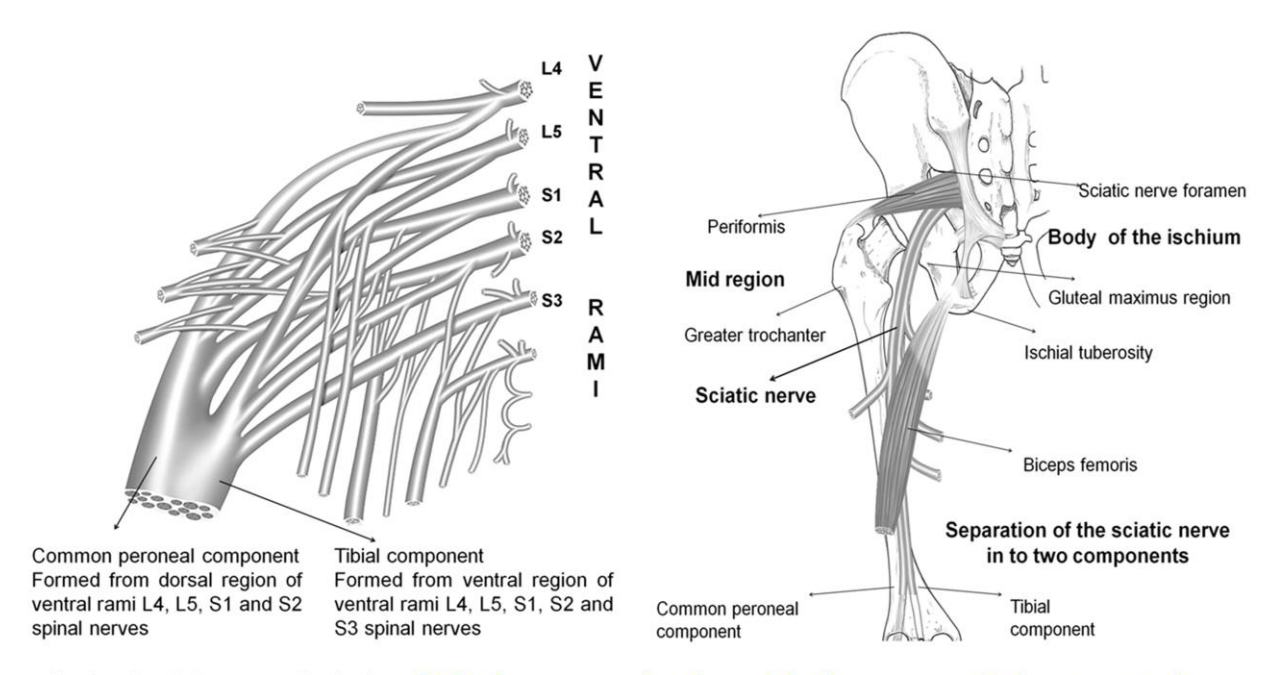
II. Introduction

Sciatic Nerve Anatomy



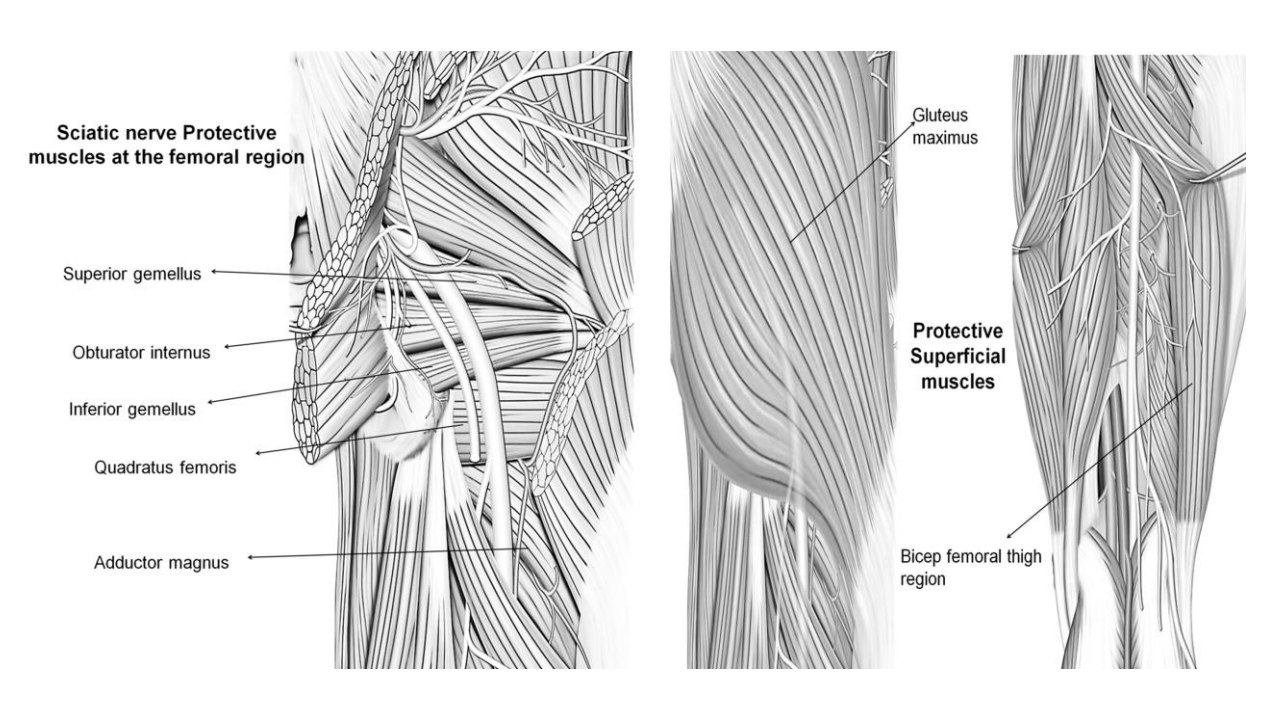
To date, many methods have been used to cause demyelination in the sciatic nerve mainly chemically induced demyelination such as cuprizone [55], Focal lysolecithin injections [56], tellurium – endoneurial injection to the tibial nerve [57], ethidium bromide – rat sciatic nerve [58], lysophosphatidylcholine – sciatic nerve. Virus triggered spinal cord demyelination and intracranially injected Theiler's encephalomyelitis virus [59]. Neuro-inflammatory animal models such as experimental autoimmune encephalomyelitis [60], intravitreal injection of the cytokines (TNF α , TNF/3, IL – 1, IL – 6, Interferon) [61], and chronic nerve compression model [62] are well known. The cuff model is reported to study the allodynia and neuropathic pain [63].

Origin of the Sciatic Nerve



<u>Sciatic Nerve Origin:</u> Sciatic nerve is the chief nerve of the posterior compartmental thigh and the largest branch of the sacral plexus and stood as the thickest nerve of the body

Protective and Superficial Muscles of Sciatic Nerve



Classification of nerve injuries

Table 1. Peripheral nerve injury classification					
Types of PNIs	Level of damage	Recovery			
Neurapraxia	Myelin loss. But good intact will perineurium, epineurium and endoneurium	High chances of recovery in days			
Axonotmesis	Axon loss. In rare cases loss of intact related to the perineurium and epineurium. But, strong intact with endoneurium				
Neurotmesis	Entire nerve damage. All the layers of the nerve perineurium, epineurium and endoneurium intact loss	Surgery compulsory. Less chances of maximum recovery			

Axonotmesis, neurotmesis, and neuropraxia are the three subtypes of peripheral nervous system injuries (PNIs). Level I neuropraxia, which is frequently observed in wrist drops and muscle twists, is a form of nerve damage or injury that doesn't include any nerve degeneration. In some rare instances, medication is necessary, but self-healing is generally evident. Neurotmesis is a third-level advanced injury that necessitates surgery yet shows inadequate healing because both the nerve and the nerve sheath are damaged. Axonotmesis, a form of Wallerian degeneration, that results in level II nerve injury. It is frequently observed in crash injuries and accident cases wherein axon and myelin sheath damage but endoneurium, perineurium, and epineurium are intact.

TF is an oral immunomodulatory approved drug for the treatment of relapsing-remitting CNS-based demyelinating illnesses such as multiple sclerosis [17, 18]. TF suppresses dihydroorotate dehydrogenase, which inhibits pyrimidine production and promotes oligodendroglial differentiation and myelination. A small dose of TF causes the cell cycle to exit, whereas a larger dose causes a reduction in cell survival [19].

In view of PNS, the current study designed a sciatic nerve injury rat model using a single partial nerve ligation or suture procedure and evaluated/examined the phases of demyelination, as well as axonal atrophies and inter axonal gaps, in experimental rats based on prolonged-time periods after p-SNI. In addition, we investigated motor functioning in experimental rats. Further, TF was repurposed to improve myelin restoration for p-SNI rats.

III. Materials and Methods

Ethics Statement: All the animal experiments were carried out after the approval of the institutional animal ethical UH/IAEC/PPB/2022/12, University of Hyderabad, India. Species-Sprague Dawley (SD) rats (3 months old, 220–250 g male) were purchased from the National Institute of Nutrition (NIN), Hyderabad. As per the experimental requirement, animals were acclimatized in the animal house facility, University of Hyderabad before 10 days of the experiments (Reg number: 151/1999/CPCSEA). The animals were housed in cages with an ambient temperature of 24 °C, constant and standard air humidity, natural day and night cycles, quality food, and water ad libitum.

Animals for PNS: SD-male rats aged (8-week-old) and weighing 220-250 g were purchased from the National Institute of Nutrition (NIN) in Hyderabad, Telangana State, India. The animals were housed in ventilated cages with an ambient temperature of 24 °C, consistent and standard air humidity-controlled (21 ± 3 °C, $50 \pm 10\%$), natural day/night cycles, and quality food and water ad libitum. All the rats used in this study are healthy and are not genetically modified. These have no prior research background. Every attempt was made to reduce the number of animals used and the suffering they endured. Table 1 contains a sample size list of the animals used in various experiments. To avoid surgical failures, all surgical procedures on rats were performed by a single expert. All the groups included in this study were first trained on Rotarod according to the procedure, and then the sciatic nerve was surgically injured. Afterward, motor functional was checked on Rotarod test, and timings were recorded. The same animals were slaughtered and sciatic nerves were utilized for pathological studies to prevent excessive animal use.

Estimation of sample size (PNS) by Power Analysis approach using G*Power 3.1 software

Cohen 1998 and Navarro 2015 proposed three categories of effect sizes:

- 1. 0.2 (small effect size), difference is unimportant between the groups
- 2. 0.5 (medium effect size), difference is important between the groups
- 3. 0.8 (larger effect size), difference is highly important between the groups

Based on the previous studies on inducing demyelination in the animal models and Teriflunomide (TF) treatment to mitigate inflammation and remyelination [20, 21] significant differences between the groups is highly important.

• To determine the sample size, in this study, we employed a larger effect size f (0.8), α-err prob (0.05), power (1 β-err prob) (0.8), number of groups (Experiment 1: 5 groups), as per the Cohen's standard effect size.

In Experiment 1, the sample size is n = 25/5 groups, therefore n = 5/group. Nonetheless, like in earlier literature, we utilized n = 6/group.

Table 1. Experiment 1. Histology, immunostaining, and rotarod test studies to evaluate the phases of demyelination along with motor functional ability (early to late phases) based on prolonged time periods after p-SNI to rats.

Animal group	Species, age, weight, and sex	Number of animals per group (n)
Sham	SD-male rats, 8-week-old, and weighing 220-250 g	6
4d p-SNI	SD-male rats, 8-week-old, and weighing 220-250 g	6
7 d p-SNI	SD-male rats, 8-week-old, and weighing 220-250 g	6
10 d p-SNI	SD-male rats, 8-week-old, and weighing 220-250 g	6
SR p-SNI	SD-male rats, 8-week-old, and weighing 220-250 g	6

• To determine the sample size, in this study, we employed a larger effect size f (0.8), α-err prob (0.05), power (1 β-err prob) (0.8), number of groups (**Experiment 2:** 2 groups), as per the Cohen's standard effect size.

In Experiment 2, the sample size is n = 16/2 groups, therefore n = 8/group. Nonetheless, we employed n = 6/group as per previous studies to maintain animal numbers consistency across all groups.

Experiment 2. Histology, immunostaining, and rotarod test to evaluate the myelin secretion and motor functionality after TF therapy to p-SNI rats.

Animal group	Species, age, weight, and sex	Number of animals per group (n)	Not
Vehicle	SD-male rats, 8-week-old, and weighing 220-250 g	6	Exp
10 d p-SNI	SD-male rats, 8-week-old, and weighing 220-250 g	-	eri
TF administered rats group	SD-male rats, 8-week-old, and weighing 220-250 g	6	me nt 2

utilizes the same 10 d p-SNI group aforementioned in Experiment 1 being compared to Vehicle and TF groups.

• To determine the sample size, in this study, we employed a larger effect size f (0.8), α-err prob (0.05), power (1 β-err prob) (0.8), number of groups (**Experiment 3:** 4 groups), as per the Cohen's standard effect size.

In Experiment 3, the sample size is n = 24/4 groups, therefore rat number was kept constant n = 6/ group).

Experiment 3. TEM imaging was employed to study the axonal alterations in the sciatic nerve following p-SNI and TF treatment.

Animal group	Species, age, weight, and sex	Number of animals per group (n)
Vehicle	SD-male rats, 8-week-old, and weighing 220-250 g	6
4 d p-SNI	SD-male rats, 8-week-old, and weighing 220-250 g	6
10 d p-SNI	SD-male rats, 8-week-old, and weighing 220-250 g	6
TF administered rats group	SD-male rats, 8-week-old, and weighing 220-250 g	6

We used a sample size of n = 6/condition since the entire experiment was conducted on SD-rats and n = 6 is the typical sample size for rat models.

Animal groups for PNS: Sham group (SH) that had surgery without damaging the sciatic nerve served as a control. The comparison of a sham group to experimental animal groups that underwent partial sciatic nerve ligation, euthanasia after post-sciatic nerve injury (p-SNI) at prolonged time periods i.e. experimental groups: rats euthanized at 4th day after p-SNI (4 d), euthanized at 7th day after p-SNI (7 d), euthanized at 10th day after p-SNI (10), and the selfrecovery group (SR), which had a partial ligation removed at 10th day after p-SNI and rats were maintained for 2 weeks or 14 days without treatment to evaluate self-healing. All of the animal groups included in this study were first trained on Rotarod according to the procedure, and then the sciatic nerve was surgically injured. Afterward, motor functional was studied using Rotarod test, and timings were recorded. The same were sacrificed and sciatic nerves were utilized for pathological studies to prevent excessive animal use. The vehicle group (VEH) represents the oral administration of carboxymethylcellulose prepared at a concentration of 0.06% (w/v) in water, to which Tween-80 was added to obtain a final dosage of 0.5% (v/v) to sham or control rats to rule out any deleterious effects. The vehicle group was compared to the previously mentioned 10 d p-SNI group, as well as Teriflunomide (TF) treated groups that had their partial ligation removed after 10 days of p-SNI and received their first dose of TF by oral administration, immediately after recovery from anaesthesia, which was continued for 2 weeks or 14 days on alternate days. After euthanasia, all the sciatic nerves were collected for further histology, immunostaining, and transmission electron microscopy imaging. For quantification and statistical analysis, each animal group used in this study contain n = 6/condition. i. e. n(SH) = 6, n(4 d) = 6, n(7 d) = 6, n(10 d) = 66, n(SR) = 6, n(VEH) = 6, n(TF) = 6.

Surgical procedure: All of the experimental rats were weighed and anaesthetized intraperitoneally using ketamine/xylazine as a sedative agent approximately 60mg/10mg per kg body weight of rat [64]. Antibiotics: Gentamycin 8 mg/250 g of SD-rat model (only single dose after performing the surgery). After sedation the hair at the femoral site was shaved with a surgical blade in the operated region. The rat was placed on the hot plate to keep warm, and the temperature was maintained at 37 °C. For sterile environment while performing the surgery, the rat's femoral region and the surrounding area were cleaned down with 70% ethanol. In order to locate the sciatic nerve, skin and gluteal muscle incisions were made. The sciatic nerve was exposed using forceps, and nerve injury was induced by inserting the 6-0 monofilament thread from the middle portion of the sciatic nerve for partial ligation to promote demyelination. Following injury, 3-0 surgical sutures were used to close the incisions made in the gluteal muscle and skin. For topical anaesthesia, Lignocaine hydrochloride gel (2%) was applied on the surface of operated region and shifted to the recovery chambers for acclimatization as per experimental schedules. The study included animals that underwent appropriate partial ligation of the rat sciatic nerve. If the suture was not correctly passed from the sciatic nerve for partial ligation, the animals were excluded. A few exclusions were made because of improper tissue processing, which might cause issues during pathological evaluations.

TF administration: After 10 d p-SNI, rats were sedated, and the partial ligation or suture was removed, and the rats were given their TF doses after recovery from anesthesia (TF provided by NATCO Pharma Limited, Hyderabad, T.S., India). TF was administered orally at a dos-age of 10mg/kg body weight through rat oral gavage for two weeks on alternate days [22]. TF was dissolved in the vehicle: carboxymethylcellulose made up to 0.06% (w/v) in water, to which Tween 80 was added to reach a final concentration of 0.5% (v/v). Rats were euthanized shortly after the therapy was completed, and sciatic nerves were severed and preserved in 10% formalin for pathological examinations.

Euthanasia followed by nerve harvesting procedure: All animals in this study were euthanized in accordance with the guidelines of the Institutional Animal Ethical Committee (approval number: UH/IAEC/PPB/2022/12). Euthanasia: Overdose of sodium pentobarbital (150 mg/kg) was delivered intraperitoneally to sacrifice the animals. All the experimental rats were euthanized and placed on the operation table. Skin and gluteal muscle incisions were performed to remove the operated sciatic nerve from the rats. The harvested nerves were then fixed in 10% formalin for pathological examinations.

Paraffin embedded tissue sections: Freshly obtained sciatic nerve samples were fixed for 48 h at room temperature in 10% formalin. After fixation, nerve samples were washed for 1 h under

running tap water, followed by dehydration phases of 30 min each with 70%, 80%, and 95% alcohol changes, and 3 changes of 100% alcohol each 1 hour. Tissue samples were cleaned in 1 change of xylene for 5 min, followed by another step of xylene and melted paraffin 1:1 ratio for 5 min, and the tissue was embedded in paraffin block. Tissue blocks were mounted to the microtome (LEICA RM2145), and 10 µm cross sections were cut and floated in a 40 °C maintained water bath containing clear distilled water. Sciatic nerve cross slices were then carefully transferred to glass slides for further pathological investigation.

Haematoxylin and eosin staining (H & E): Tissue cross sections were deparaffinized twice, for 2 min each, in xylene, and then rehydrated twice, for 3 min each, in 100%, 95%, 80%, and 70% alcohol. Slides were applied for 10 min water wash, had their nuclei stained with haematoxylin for 3 to 5 min, and then stained with eosin for the extracellular matrix and their cytoplasm for 2 min before being rinsed with tap water for 6 min. Sections underwent rehydration by being exposed to 30%, 50% alcohol for 6 min each, 70% alcohol for 10 min, 95% alcohol, and twice 100% alcohol for 3 min. After cleaning the tissue sections with two changes of xylene for 3 min each, the tissue sections were mounted on DPX slides for imaging under light microscopy.

Eriochrome (solo chrome) cyanine R myelin staining (EC): In EC myelin stain, the extracellular matrix and cytoplasm are grey and cream, whereas myelin is represented by a blue colour. Sections were deparaffinized in 2 changes of xylene for 3 min each, then rehydrated with 2 changes of 100% alcohol for 3 min each, then 3 changes of 95%, 80%, and 70% alcohol for 3 min each. After being rehydrated, slides were transferred for a 10 min water wash. Slides were then immersed in an eriochrome cyanine solution (eriochrome cyanine RS 0.2 g, H₂SO₄ 0.5 ml, distilled water 96 ml and 10% iron alum 4 ml for 100 ml solution) for 30 min at room temperature before being washed under running water. After being differentiated in 5% iron alum for 5-15 min, the tissue sample was washed with tap water. Borax ferricyanide separation was performed for 5-10 min (borax 1.0 g, potassium ferricyanide 1.25 g, and distilled water 100 ml protected from sunlight) before being washed with running tap water. The slides were then dehydrated with 2 changes of graded ethanol solutions (70%, 80%, 95%, and 100% alcohol) and cleaned with 3 changes of xylene before being DPX mounted for microscopy imaging.

Luxol fast blue myelin staining (LFB): Sciatic nerve cross sections were deparaffinized in two changes of xylene for 2 min each, then hydrated in 80% and 95% graded ethanol solutions for 3 min each. Slides were maintained in 0.1% luxol fast blue solution (catalogue no. L0294, SIGMA ALDRICH®) (luxol fast blue solution - 0.1 ml, ethyl alcohol 95% - 100 ml, glacial acetic acid - 0.5 ml) overnight at 56 °C in the oven. The excess stain was removed with 95% ethyl alcohol, followed by a distilled water wash. To differentiate the slides, a 0.05% lithium carbonate solution (catalog

no. 431559, 99.99% SIGA ALDRICH®) (lithium carbonate 0.05 g in 100 ml of distilled water) was used for 30-45 sec, followed by a 30 sec washing with 70% ethyl alcohol. This is followed by washing in distilled water and counterstained with 0.1% cresyl violet solution (cresyl fast violet -0.1 g in 100 ml of distilled water and 10 drops of glacial acetic acid added shortly before use and filtered) for 30-45 sec. Rinse in distilled water, then separate in 95% ethyl alcohol for 5 min, followed by 2 changes in 100% alcohol for 5 min. The tissue slices were then cleaned in two changes of xylene for 3 min each, followed by DPX mounting for microscope imaging.

Immunostaining for PNS: Slides were deparaffinized in 2 changes of xylene for 2 min each, then promptly transferred to a 1:1 xylene: 100% ethanol solution for 3 min. The slides were rehydrated in graded ethanol solutions of 100%, 95%, 70%, 50%, and 30% ethanol changes for 3 min each before being washed in tap water for 5 min. For antigen retrieval, tissue sections were immersed in antigen retrieval buffer (trypsin 0.05% in 100 ml PBS) for 15 min at 37 °C and then permeabilized (triton x - 100 0.2% in PBS) for 7-10 min, followed by 1 wash in PBS for 5 min. The slides were placed in a blocking solution (BSA 1%, NGS 5% in PBS) for 1 h at room temperature. Approximately 100 µl of diluted primary antibodies myelin basic protein MBP (AB clonal Catalog No: A1664, 86 Dr. Woburn, MA 01801, United States), S100 Beta EP 32 (PathnSitu Catalog No: CR070 – 0.1 ml Concentrated, USA-Registered Office 538, Selby Ln, Livermore, CA-94551 USA) and CD68 KP 1 (PathnSitu Catalog No: PM113 - 0.1 ml concentrated, USA-Registered Office 538, Selby Ln, Livermore, CA-94551 USA. (Dilution: 1:200 PBS with 0.02% sodium azide, 50% glycerol, pH 7.3) were applied to the tissue cross sections and incubated for 30 min at room temperature in a humidified environment. Sections were transferred for 2 wash steps with PBS for 5 min. Approximately 100 μl of diluted biotinylated secondary antibody was added to the sections on the slides (using the antibody dilution buffer) and incubated in a humidified chamber at room temperature for 30 min (covered from sunlight), followed by 5 min washes with PBS for 2 times. To show the colour of the antibody staining, a DAB substrate solution (freshly produced before use: 0.05% DAB, 0.015% H₂O₂ in PBS) was applied to the sections on the slides. The necessary colour intensity was achieved after less than 5 min of colour development, which was followed by three PBS changes that lasted 2 min each. Slides were submerged in haematoxylin for 2-3 min, depending on the thickness of the tissue sections, for counterstaining. This was followed by a 15-20 min water wash. In graded alcohol solutions of two changes of 95% and 100% alcohol, tissue slides were dehydrated for 5 min each. Coverslips were used to protect the mounted tissue sections after applying DPX mounting solution.

Transmission electron microscopic imaging (TEM): The nerve samples were first fixed in 2.5-3% glutaraldehyde in 0. 1 M phosphate buffer saline PBS (pH 7.2) for 24 h at 4 °C, and then

they were further fixed in 2% aqueous osmium tetroxide in the same buffer for 2 hour. Samples were dehydrated in a series of graded alcohols, penetrated with Araldite 6005 resin, or implanted in spur resin. A glass knife and an ultra-microtome (Leica Ultra cut UCT-GA-D/E-I/100) were used to slice material into extremely thin (50-70 nm) sections, which were then mounted on cop-per grids and stained with saturated aqueous acetate and Reynolds lead citrate. Samples were examined under TEM in a higher magnification and resolution (JEOL-JEM-F200 transmission electron microscopic imaging).

Rotarod test: All the animal groups (n = 6/condition) were trained for 1 week on the rotarod apparatus before surgical injury to the sciatic nerve (animal groups: SH, VEH, 4 d, 7 d, 10 d, SR, and TF). To ensure sterility, the device was wiped down with 70% alcohol after each trial. Rats were trained 4 times a day for 3 min each against a spinning rod at a speed of 5-25 rpm. The mean delay of the rat fall off the revolving rod was measured in sec (s) and recorded for each rat in the range of 120 sec above. Following the p-SNI, all the experimental rats were given the opportunity to undergo a rotarod test for motor functional examination at prolonged-time periods after p-SNI. **Statistical analysis:** All the statistical estimations were quantified as the mean percentage of expression by *ImageJ software*. In Sigma plot 11.0 software, a single group, one sample t-test is used to estimate the Mean \pm SEM from each individual experimental animal groups. *GraphPad Prism 8.0.2*, column analysis, one-way ANOVA test is used for the multiple comparisons (Tukey test) of the mean and significant *p-value*.

IV. Results

1. Sciatic Nerve Injury Model Development and Standardization.

The surgical approach for inducing demyelination in the rat sciatic nerve

Ketamine/Xylazine 60 mg/10 mg per kg body weight⁴¹ was used to anesthetize rats (Intraperitoneally). Fur was trimmed, skin and gluteal muscle incisions were made, and the sciatic nerve was exposed. A 6-0 monofilament thread was implanted from the middle of the sciatic nerve and partially ligated. Skin and gluteal muscle incisions was closed using 3-0 monofilament surgical thread (Fig.1).

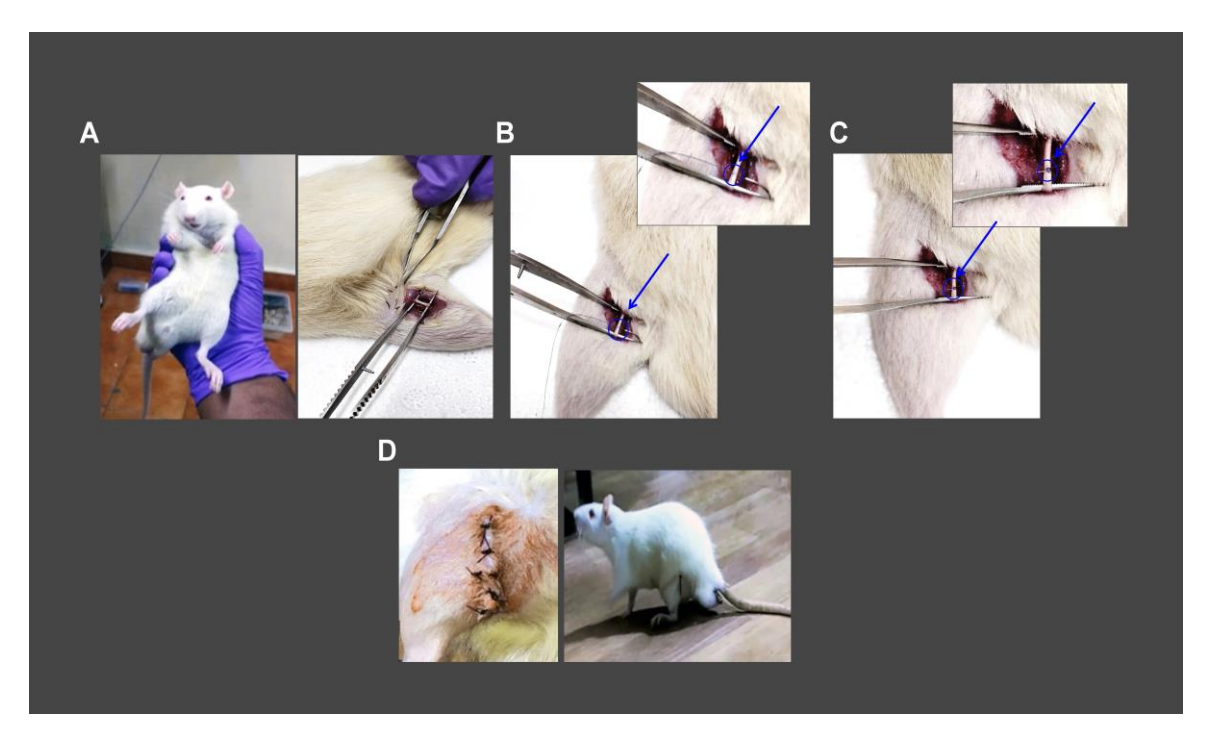
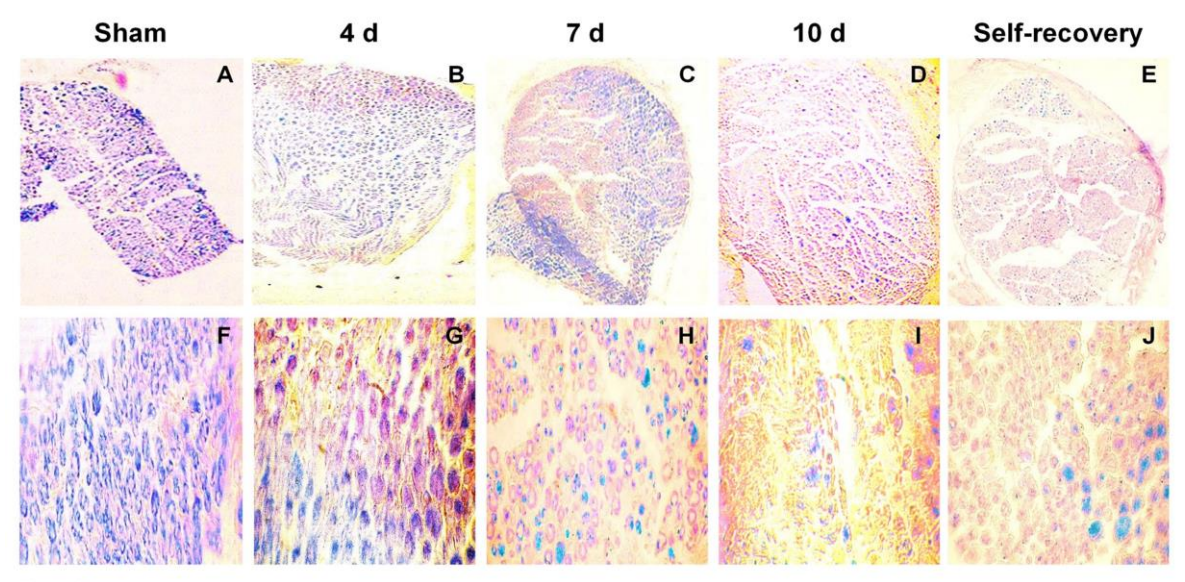


Fig.1 Depicts the surgical method used to injure the rat's sciatic nerve. **(A)** Rats were sedated, incisions were made in the skin and gluteal muscles, and the sciatic nerve was exposed. **(B)** Partial ligation with 6-0 monofilament suture thread placed from the centre of the sciatic nerve (blue arrow). **(C)** The sciatic nerve was partly ligated with a 6-0 monofilament thread (blue arrow) to induce myelin loss in rat's sciatic nerve. **(D)** Gluteal muscle and skin incisions were closed using a 3-0 polyamide black monofilament thread and rats recovered after anaesthesia. Rats N = 6/condition.

Model Standardization



Results:

Myelin: Blue, Nuclei: cream/white, Background: cream/white

Figure represents the standardization of partial sciatic nerve ligation model. **(A-E)** 4X magnification images of eriochrome (*solo chrome*) cyanine R (EC) staining depicts the sciatic nerve ligated partially or a portion of the sciatic nerve ligation by inserting 6-0 monofilament thread from the centre of the nerve. **(F-J)** 60X magnification images of EC staining represents the early myelin loss or demyelination began at 4 d which enhanced from 7 d to self-recovery based on the prolonged time-period following post-sciatic nerve damage. Rats N = 6/condition.

2. Stages of demyelination by the pathological studies

Pathological evaluation demonstrates the changes in cell morphology and demyelination phases at prolonged-time periods after p-SNI in rats

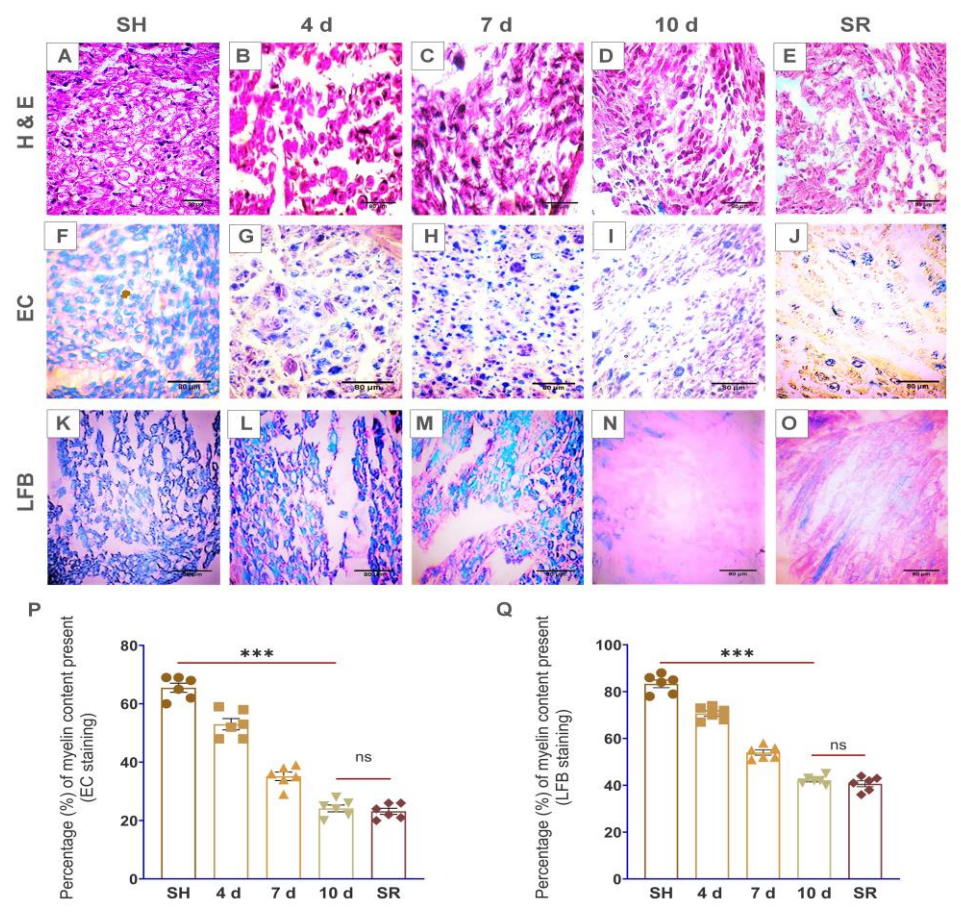


Fig.2 Photomicrographs demonstrate cell morphological changes and demyelination in the p-SNI rats sciatic nerve cross sections. (A-E) hematoxylin and eosin staining, which revealed cell morphological abnormalities, commenced on the N(4 d) = 6 and subsequently increased from N(7 d) = 6, N(10 d) = 6 up to N "self-recovery" (SR) = 6 p-SNI rats in contrast to the N "sham" (SH) = 6 rats. (F-J) EC stain (blue color: myelin; cream color: extracellular spaces) and (K-O) LFB stain (blue color: myelin; pink color: extracellular spaces) demonstrates steadily increasing myelin loss in nerve-damaged groups from the N(4 d) = 6, N(7 d) = 6, N(10 d) = 6 until N "self-recovery" (SR) = 6 in contrast to the N "sham" (SH) = 6 rats. Statistical information was visually represented in (P, Q). Olympus BX51 microscope was used to investigate stains and produce photographs. The results were all provided as Mean \pm SEM. Statistical significance: (ns) P = 0.988, 0.902, ***, P = <0.001. The scale bar in the images (A-O) is 80 µm. ImageJ software is used to quantify all of the photos by following measurement settings and analyze for the mean values. SigmaPlot 11.0 is used to produce statistical results, which are then examined using column analyses, one-way ANOVA, multiple comparisons, the Tukey test, and visually displayed using GraphPad Prism 8.

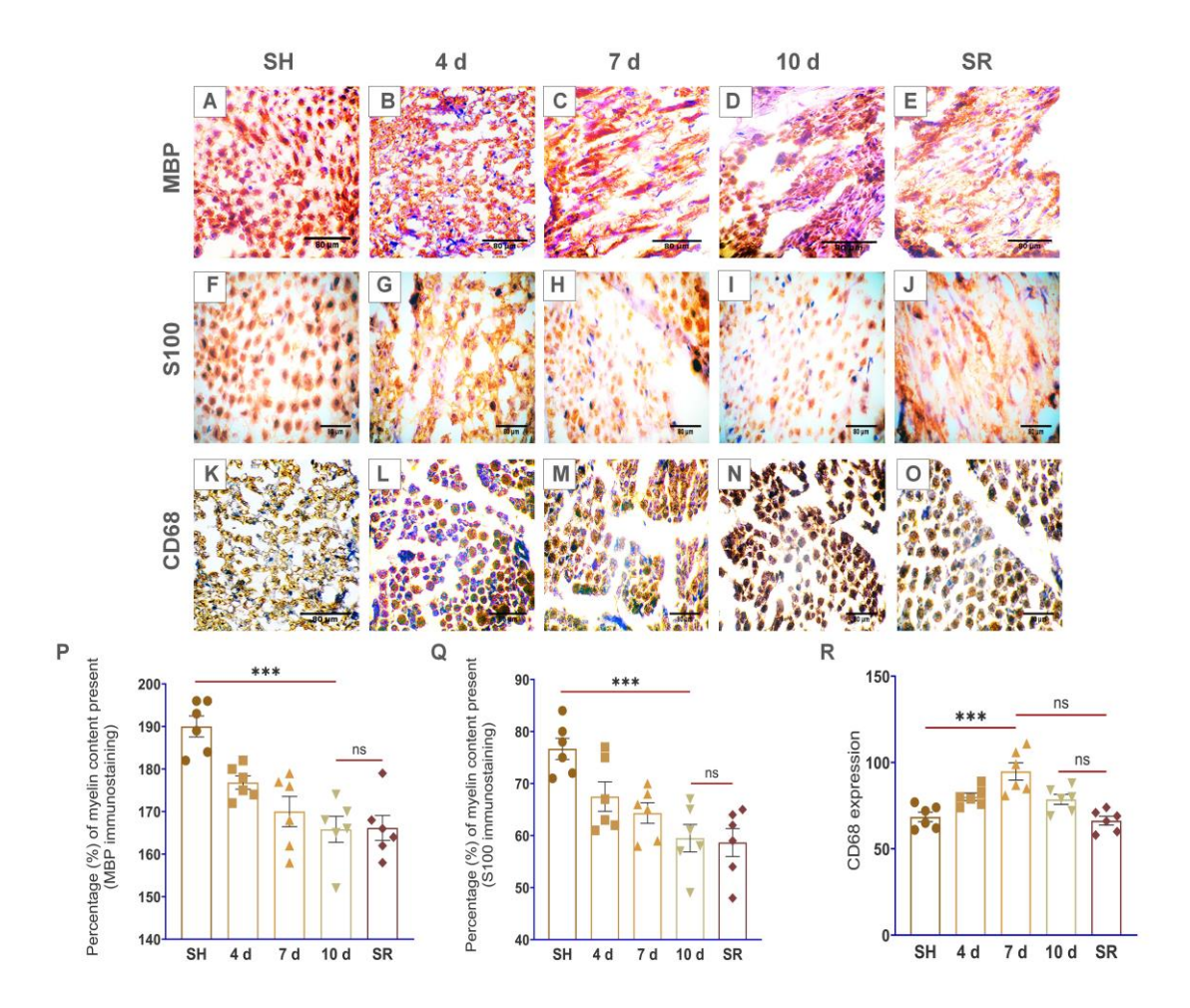


Fig. 3 Depicts demyelination phases after p-SNI at prolonged-time periods. Myelin basic protein (**A-E**) and S100 (**F-J**) were utilised as immunostaining indicators to designate the content of myelin present in nerves, revealing steadily increasing myelin loss in N(4 d) = 6, N(7 d) = 6, N(10 d) = 6, and N "self-recovery" (SR) = 6 p-SNI rats when compared to the N "sham" (SH) = 6 rats. (**K-O**) CD68 marker demonstrated an increase of macrophage accumulation on the N(4 d) = 6, which elevated in N(7 d) = 6, worsened at N(10 d) = 6, and reduced in N "self-recovery (SR) = 6 rats when compared to the N "sham" (SH) = 6. Statistical data was portrayed graphically in (**P-R**). Olympus BX51 microscope was used to examine the stains and produce photographs. The results were all provided as Mean ± SEM. Statistical significance: (ns) P = >0.999, 0.084 and ***, P = <0.001. The scale bar in the images (**A-O**) is 80 μm. *ImageJ software* is used to quantify all of the photos by following measurement settings and analyze for the mean values. *SigmaPlot 11.0* is used to produce statistical results, which are then examined using column analyses, one-way ANOVA, multiple comparisons, the *Tukey test*, and visually displayed using *GraphPad Prism 8*.

Haematoxylin and eosin (H & E) staining reveal cell morphological alterations in distinct day sites of the injured sciatic nerve. The cell morphological abnormalities in the sciatic nerve cross sections began promptly at 4 d p-SNI which progressively enhanced from 7 d to 10 d after p-SNI without displaying any SR even after 2 weeks after removing partial ligation from 10 d p-SNI rats shown in **Fig. 2A-E.** Myelin stains, EC and LFB verified demyelination commenced at 4 d and subsequently enhanced at 7 d and 10 d without demonstrating any SR even after 2 weeks after removing partial ligation from 10 d p-SNI rats (**Fig. 2**). Immunostaining with MBP and S100 myelin markers of p-SNI cross sections confirm early demyelination or myelin loss began at 4 d which progressively enhanced from 7 d to 10 d without any SR as represented and graphically in **Fig. 3**.

Monocyte-derived macrophages activation is critical and crucial in promoting successful regeneration or remyelination by releasing growth factors and crucial in clearing inhibitory myelin debris. We used the CD68 marker to label the macrophages and found spontaneous activation and accumulation of macrophages with a higher expression at 4 d p-SNI cross sections, which steadily increased from 7 d to 10 d after p-SNI in contrast to the SH group. Interestingly, data revealed a reduced expression of CD68 in SR, as illustrated in **Fig. 3**.

Pathological Findings confirm the remyelination upon TF

TF therapy helps p-SNI rats by suppressing macrophage activation and boosting myelin secretion or remyelination.

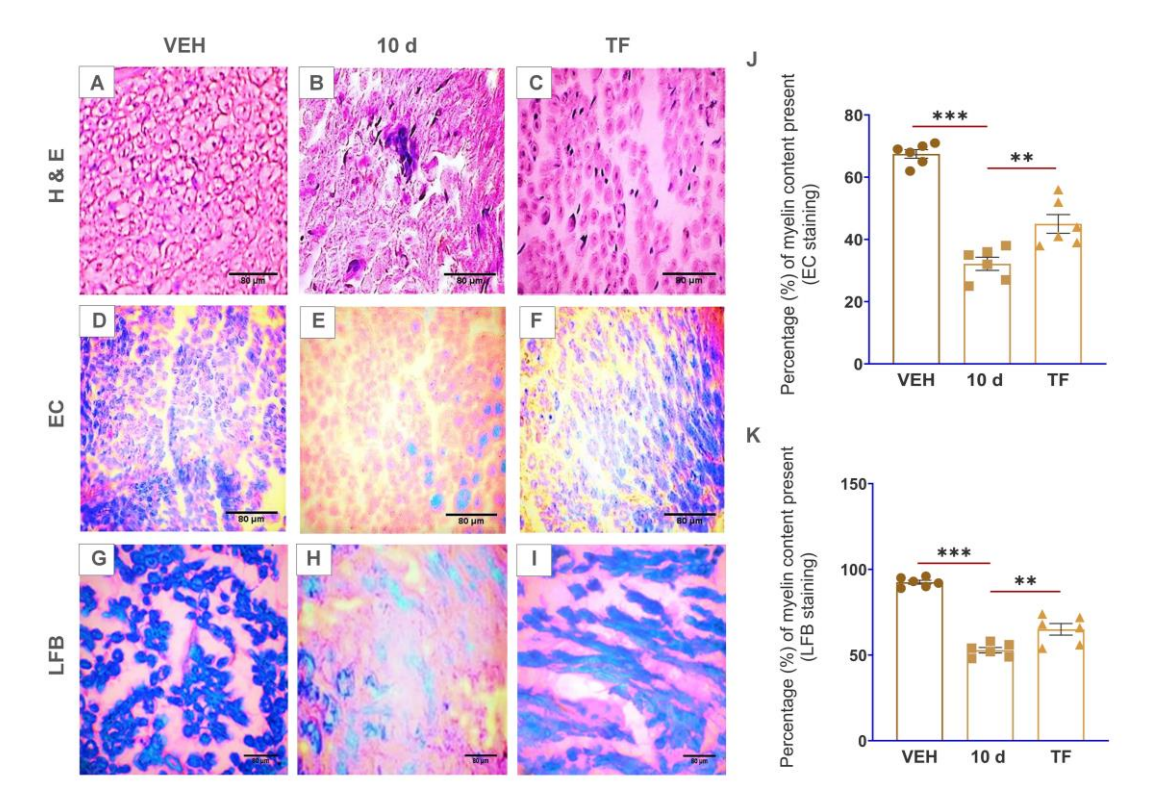


Fig.4 Photomicrographs demonstrates myelin restoration in TF-treated sciatic nerve cross sections after p-SNI. **(A-C)** Haematoxylin and eosin staining revealed the restoration of cell morphological features in N(TF) = 6 rats as compared to the N(10 d) = 6 and N "vehicle" (VEH) = 6. **(D-F)** EC stain (blue color: myelin; cream color: extracellular spaces) and **(G-I)** LFB stain (blue color: myelin; pink color: extracellular spaces) show remyelination or myelin secretion in N(TF) = 6 treated rats when compared to N(10 d) = 6 and N "vehicle" (VEH) = 6. Statistical data was represented visually in **(J, K)**. The Olympus BX51 microscope was used to study stains and take images. The results were all provided as Mean ± SEM. Statistical significance: **, P = 0.003, **, P = 0.004, and ***, P = <0.001. The scale bar in the images **(A-I)** is 80 μm. *ImageJ software* is used to quantify all of the photos by following measurement settings and analyze for the mean values. *SigmaPlot 11.0* is used to produce statistical results, which are then examined using column analyses, one-way ANOVA, multiple comparisons, the *Tukey test*, and visually displayed using *GraphPad Prism 8*.

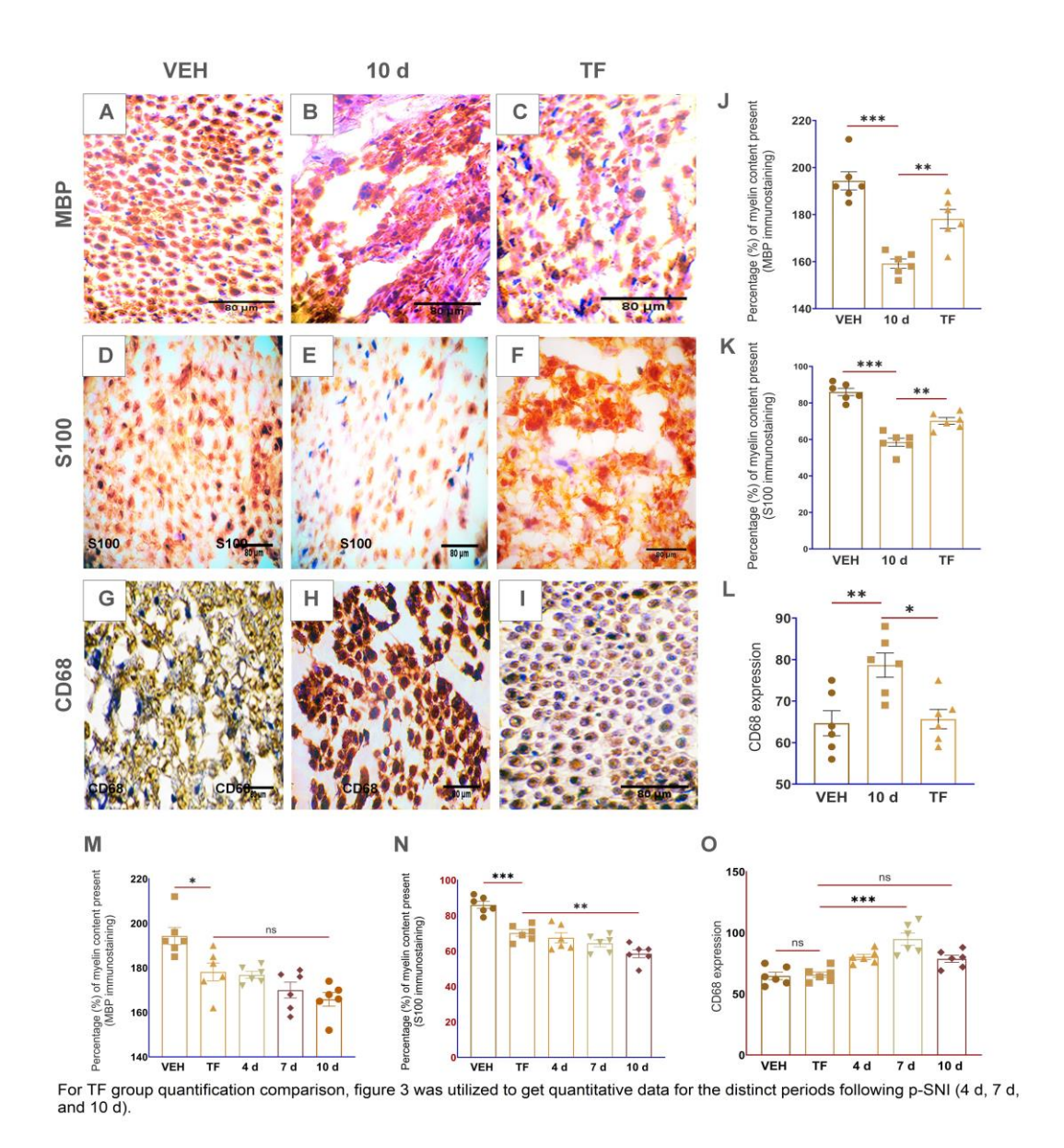


Fig.5 Immunostaining demonstrates myelin repair and macrophage inhibition in TF-treated rat sciatic nerves. When N(TF) = 6 rats were compared to N(10 d) = 6 and N "vehicle" (VEH) = 6 rats, (A-C) Myelin basic protein and (D-F) S100 myelin indicators revealed myelin restoration or remyelination in N(TF) = 6 rats. (G-I) CD68 demonstrated reduced macrophage accumulation in N(TF) = 6 rats when compared to the N(10 d) = 6. Statistical data was represented visually in (J-O). The Olympus BX51 microscope was used to study stains and take images. The results were all provided as Mean \pm SEM. Statistical significance: *, P = 0.12, **, P = 0.003, and ***, P = <0.001. The scale bar in the images (A-I) is $80 \mu m$. Image] software is used to quantify all of the photos by following measurement settings and analyze for the mean values. SigmaPlot 11.0 is used to produce statistical results, which are then examined using column analyses, one-way ANOVA, multiple comparisons, the Tukey test, and visually displayed using GraphPad Prism 8.

Early observations revealed active macrophages and demyelination at the site of the surgically injured rat sciatic nerve.

Following 10 d p-SNI, the rats were anesthetized, the partial ligation or suture was removed, and the animals were given their TF dosages once they recovered from anesthesia for 2 weeks alternate days (TF provided by NATCO Pharma Limited, Hyderabad, T.S., India). H&E staining of TF-treated rat sciatic nerve cross-sections shows the repair of cell morphological abnormalities, as illustrated in Fig. 4, as compared to the 10 d p-SNI and VEH groups. In contrast to p-SNI and VEH animals, EC and LFB myelin stains demonstrated myelin restoration in TF-treated rat sciatic nerve cross-sections (Fig. 4). Immunostaining with CD68 demonstrated reduced macrophages in TF-treated rats' sciatic nerve cross-sections compared to the experimental animal groups and VEH groups (Fig. 5). Immunohistochemistry for MBP and S100 indicated myelin repair or remyelination in TF-treated rat sciatic nerve cross-sections against experimental animal groups and VEH groups, graphically depicted in Fig. 5.

3. Transmission Electron Microscopy (TEM) Imaging Exhibits Axonal Atrophies and Inter Axonal Gaps in Injured Rat Sciatic Nerve Restored upon TF Treatment.

Inter axonal gaps were discovered using TEM imaging following p-SNI, which was repaired by TF treatment.

TEM analysis demonstrated distinct axonal morphology in VEH and 4 d after p-SNI. Atrophic axons with inter axonal gaps were seen in 10 d p-SNI cross-sections, coupled with myelin loss (Fig. 6).

In contrast, healing of inter axonal gaps and recovery from the axonal damage following 2 weeks of TF therapy on alternate days to the p-SNI rats depicted in **Fig. 6.**

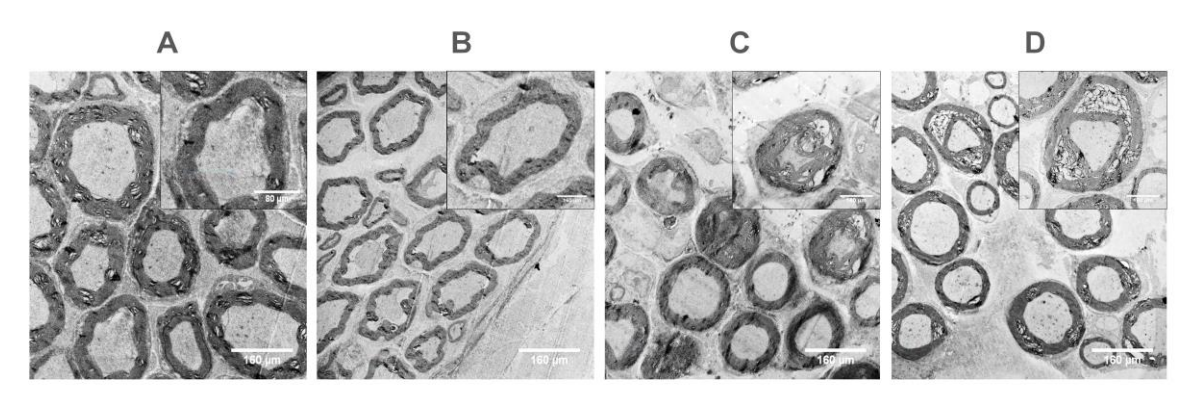


Fig.6 Indicate the restoration of axonal intactness and inter-axonal gaps after TF administration using transmission electron microscopy. **(A, B)** Shows clear axonal morphology in the N "vehicle" (VEH) = 6 and N(4 d) = 6 p-SNI rats. **(C)** Displays the alterations in axonal morphology and interaxonal gaps in the N(10 d) = 6 p-SNI rats. **(D)** Shows that the N(TF) = 6 rats axonal morphology and interaxonal spacing have been restored. *JEOL-JEM-F200* transmission electron microscopy (TEM) was used to collect all of the images. The scale bar in the images **(A-D)** is $160\mu m$.

4. Validation of Motor functional loss in damaged Rats: Motor Functional Restoration upon TF therapy

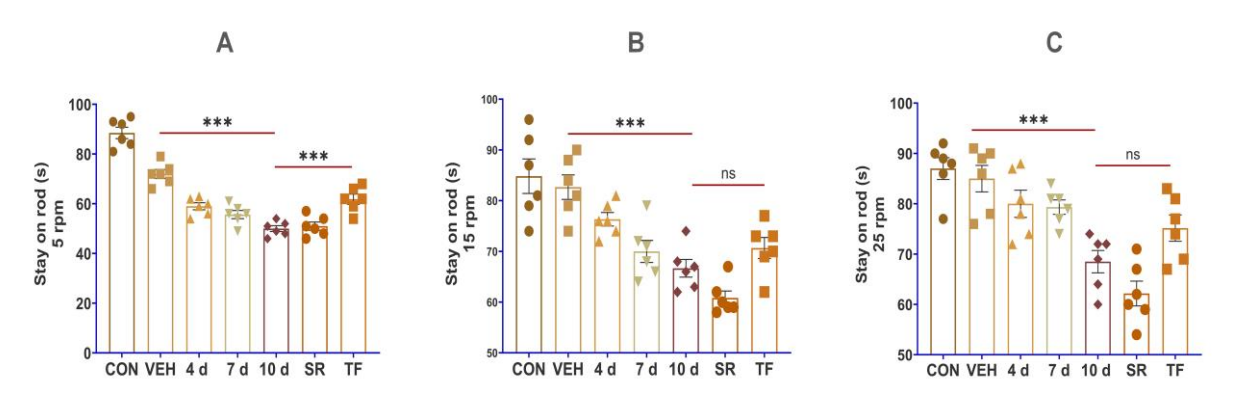


Fig.7 Depict that TF therapy restored motor function following surgical damage to the sciatic nerve. (A) 5 rpm, (B) 15 rpm, and (C) 25 rpm, graphical illustration of rotarod test statistical analyses demonstrates a progressive rise in motor functional loss from the N(4 d) = 6, N(7 d) = 6, N(10 d) = 6, to N "self-recovery" (SR) = 6 p-SNI rats when compared with N "control" (CON) = 6 and N "vehicle" (VEH) = 6 rats. In the N(TF) = 6 rats motor functioning was restored. The stay-on rod (s) seconds at 5-25 rpm were used for all statistical assessments. The results were all provided as Mean \pm SEM. Statistical significance: ns, P = 0.431, 0.847 and ***, P = <0.001. SigmaPlot 11.0 is used to produce statistical results, which are then examined using column analyses, one-way ANOVA, multiple comparisons, the Tukey test, and graphically displayed using GraphPad Prism 8. Rotarod test speed 5-25 rpm.

Rotarod test identified the motor functional deficit in p-SNI rats that was remedied by TF therapy

To assess the injured rats' motor functional loss, rotarod test was done and the findings revealed that the experimental animal groups lost motor function based on rod stay (s) from 5-25 rpm. Rotarod test detected progressively enhanced motor functional loss based on the prolonged-time period after p-SNI in rats. The experimental rats n(4 d, 7 d, and 10 d) = 6/condition were compared to the n(SH) = 6. Statistical data analysis identified variations of motor functionality depending on rod stay in seconds (s) from 5-25 rpm.

The TF therapy aided recovery and noted reversed motor dysfunction, as measured on the rotarod device using stay on rod (s) from 5-25 rpm which is compared to the experimental rats n(4 d, 7 d, and 10 d) = 6/condition and n(VEH) = 6 visually illustrated in **Fig. 7**.

V. Discussion

The current study describes a surgical method for peripheral nervous system (PNS) by inducing demyelination with a simple partial ligation to the rat sciatic nerve using a 6-0 monofilament thread. The study investigates how long macrophages will be active based on the prolonged-time period after p-SNI. The findings show that early myelin loss or demyelination progresses to greater demyelination with no evidence of self-recovery. Axonal atrophies and interaxonal gaps were found after varying periods of post-surgical sciatic nerve damage. Moreover, the rotarod test revealed that surgically nerve injured rats had lost motor functioning.

This research reveals that TF has multifunctional properties in sciatic nerve injured rats via immunomodulation and myelin secretion or remyelination at the injury site. However, TF is a well-known immunomodulatory medicine that aids in the healing and repair of myelin in multiple sclerosis (MS) patients [17, 18, 19, 22, 65].

There are now various animal models in use to induce demyelination in the rat sciatic nerve, each with its own set of limitations and downsides. Virus-induced demyelination [58, 59], Neuro-inflammatory animal models such as experimental autoimmune encephalomyelitis (EAE) [60], and intravitreal injection of the cytokines [61] are well-established to cause demyelination in animal models with certain limitations. The chronic nerve compression paradigm is widely established for inducing demyelination in animals. However, the disadvantage of this model is that the nerve is squeezed to generate demyelination. This makes remyelination research challenging [62]. The cuff model is used to study the allodynia and neuropathic pain [63].

Neurotoxins such as ethidium bromide, Lysolecithin, cuprizone, and tellurium are used to promote demyelination. However, this may result in indiscriminate demyelination [55-57]. The dose is based on an animal's susceptibility and tolerance depending on its body metabolism. But, not all animals respond to the same dosage in the same way, and some may develop resistance to the neurotoxins, making comparison studies and data interpretation within a given experiment challenging. Theiler's murine encephalomyelitis virus (TMEV) is a neuropathogenic virus that affects both susceptible and resistant B6 mouse models, causing persistent demyelination that starts 2-6 weeks after viral injection [58]. In contrast, demyelination begins shortly after the ligation on the 4 d in our model.

Experimental autoimmune encephalomyelitis (EAE) is commonly used to study the neuropathological features in inflammation, demyelination and axonal loss conditions. The counter-regulatory mechanisms in the EAE model involves in the resolution of inflammation along with the remyelination [60].

Previous animal model limitations prompted us to establish a model that could induce demyelination in rats immediately after injury. This study demonstrates a single partial sciatic nerve

ligation to induce demyelination or myelin loss in rats. Pathological investigations show early, moderate, and advanced stages of demyelination in prolonged-time periods following p-SNI in rats.

Our preliminary findings revealed abnormalities in the cell morphology on staining with H & E that began on 4 d after p-SNI and were steadily enhanced from 7 d to 10 d without any selfrecovery. This is in agreement with similar studies using H & E as basic stains to examine cell morphological changes [66, 67]. In our study, LFB and EC stains identified well-defined zones of demyelination began on the 4 d p-SNI and subsequently increased from 7 d to 10 d following p-SNI in rats and there was no evidence of self-recovery (SR). Previous research used similar dyes to analyse the myelin composition of tissues [68-73]. Immunostaining further confirms the activation of macrophages with CD68 marker and myelin loss or demyelination with MBP and S100 markers in varying time periods after p-SNI in rats. Immunostaining with CD68 detected active macrophages after peripheral nerve injury [74]. S100 is preferentially distributed in myelin forming Schwann cells [75]. S100A8 and S100A9 are the subunits initiate the early inflammation in injured peripheral nerve [76]. In a study, MBP detected the early myelination in the rat brain stem [77], MBP detected myelination in second trimester human foetal spinal cord [78]. MBP is a well-known marker to detect demyelination in multiple sclerosis, human auditory nerve and some other neurodegenerative diseases [79-82]. We found severe alterations in p-SNI rats, including neuroinflammation followed by monocyte-derived macrophage activation, as revealed by the CD68 marker.

Immunostaining verified the presence of activated macrophages using CD68 at 4 d p-SNI, which was subsequently elevated from 7 d to 10 d following p-SNI in rats and was reduced in self-recovery (SR) rats group. Interestingly, histology and immunostaining findings revealed that TF therapy reduced pro-inflammation by suppressing CD68 expression and improved healing and myelin regeneration or remyelination with enhanced expression of MBP and S100 markers in 10 d p-SNI rats with TF versus experimental animal groups. Similarly, CD68 is employed as a labeling stain to detect macrophage build-up, which aids in regeneration and cell debris clearance [83-85]. Findings are in consistent with other publication using TF to differentiate myelin-producing cells in the nervous system and to modulate immune response [19].

By using the rotarod test to analyse motor function, it was discovered that, in comparison to earlier studies [86, 87], all experimental rats in this research with p-SNI had little motor functional loss as measured by the length of time stay on the rod (s) at 5–25 rpm. Stay on rod (s) of rats on the rotarod device increased following TF therapy, indicating motor functional recovery. The rotarod test on all experimental rats presented data as per rod stay (s) and validates the present

model can produce motor functional loss that depends on the time frame length of surgical harm, which aids researchers in investigating motor functionalities in the PNS.

In comparison to the VEH and 4 d p-SNI rat groups, TEM data indicate atrophic axons; inter axonal space, and myelin loss in 10 d p-SNI rats. According to prior research, electron-microscopic alterations in a rat's sciatic nerve following differential traction damage were described [88-90]. Significant changes in axonal intactness and repair of inter-axonal gaps were observed in the TF-treated p-SNI rats, supporting our neuropathological findings on demyelination followed by recovery and remyelination after TF therapy.

In Summary the demyelination is accurate and reproducible, and the nerve damage is minimal since a single partial ligation is conducted to target just the portion of the sciatic nerve that contains axons. We observed identical demyelination throughout the whole batch and location, and the amount of ligation may be adjusted, making comparison studies easier. This model is appropriate for studying the molecular process behind demyelination and gives a chance to test possible therapeutics for demyelinating diseases. This rat model may be valuable to pharma, the biotech industry, and academic researchers in screening newly synthesized drugs.

Chapter 3

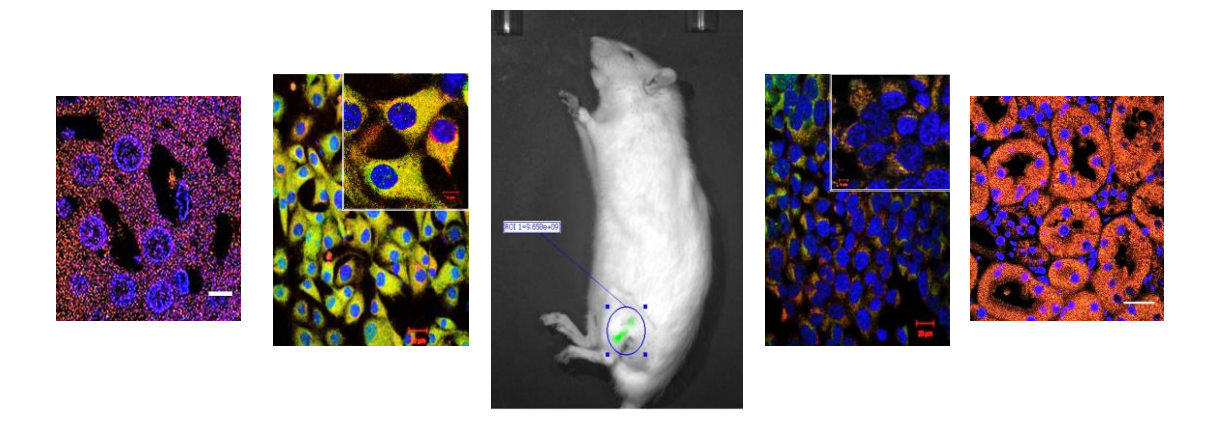
Application of the Developed Sciatic Nerve Injury Model

(Collaboration with Prof. Nagarajan, School of Chemistry, UOH)

I. Abstract

Fluorescent dyes or fluorophores have been used in a wide variety of *in vivo* and *in vitro* experiments by the researchers for decades. To validate our model we used a fluorescent compound which was synthesized by the collaborators in the School of Chemistry, University of Hyderabad. This compound is a derivative of indole alkaloid that emits fluorescence. To test the fluorescence activity *in vivo*, the compound was injected into the rat sciatic nerve and then processed *ex vivo* by euthanizing the rats and excising the sciatic nerve, followed by fluorescent investigations on sciatic nerve sections. To evaluate the compound's fluorescence, different *in vitro* established cultured cells was fixed and stained with the compound. Overall, our findings revealed that the compound excitation and emission values are similar to those found in commercially available mitotracker, making comparative studies easy. Perkin Elmer *in vivo* imaging confirmed the long-lasting fluorescent activity of the compound in the rat sciatic nerve, and sections of the sciatic nerve emitted fluorescence and co-localized with mitotracker which is a mitochondrial fluorescent dye. Furthermore, *in vitro* cell culture findings demonstrate the labelling of mitochondrion *in vivo*, *ex vivo*, and *in vitro* conditions.

Keywords: Fluorophores \cdot in vivo \cdot ex vivo \cdot in vitro



II. Introduction

Introduction

Fluorescent dyes or fluorophores are defined as the chemical substances used in biological samples which binds with fluorescent responsive proteins of a cell in an organism and emits fluorescence under laser based technologies [91]. The design or structure of the chemical compound, synthesis, brightness, contrast stability, and their role in non-invasive visualization, characterization, and quantification in biological processes of human and other living organisms made the fluorescent dyes unique and advanced tools in the field of biological sciences [92, 93].

Mitochondria are essential for cell survival and tissue function, since they meet high energy needs, regulate calcium, and control reactive oxygen species (ROS) generation [94, 95]. Morphological characteristics of mitochondria are directly connected to numerous activities of different cells found in diverse human tissues, and variations in morphology are also recognized in many diseases. Understanding the function of mitochondria in disease pathogenesis has been substantially increased by displaying these organelles [96-98].

We checked the efficacy of the model by injecting a fluorescent compound into the rat sciatic nerve and monitoring the fluorescence with a Perkin Elmer *in vivo* imaging technique. Nerve section imaging under confocal microscopy demonstrates the localization of that fluorescent dye in the rat sciatic nerve. Further, this study shows the fluorescent activity and localization of the fluorescent compound in several types of *in vitro* cell cultures.

III. Materials and Methods

Ethics Statement: All the animal experiments were carried out after the approval of the institutional animal ethical committee UH/IAEC/PPB/2022/12, University of Hyderabad, India. Species- Sprague Dawley (SD) rats (3 months old, 220–250 g male) were purchased from the National Institute of Nutrition (NIN), Hyderabad. As per the experimental requirement, animals were acclimatized in the animal house facility, University of Hyderabad before 10 days of the experiments (Reg number: 151/1999/CPCSEA). The animals were housed in cages with an ambient temperature of 24 °C, constant and standard air humidity, natural day and night cycles, quality food, and water ad libitum.

Animals for Fluorescent dye (BK2ME) experiments: Sprague Dawley (SD) male rats aged (8-week-old) and weighing 220-250 g were purchased from the National Institute of Nutrition (NIN) in Hyderabad, Telangana State, India. The animals were housed in ventilated cages with an ambient temperature of 24 °C, consistent and standard air humidity-controlled (21 \pm 3 °C, 50 \pm 10%), natural day/night cycles, and quality food and water *ad libitum*.

Estimation of sample size by Power Analysis (objective 3) approach using G*Power 3.1 software

Cohen 1998 and Navarro 2015 proposed three categories of effect sizes:

- 1. 0.2 (small effect size), difference is unimportant between the groups
- 2. 0.5 (medium effect size), difference is important between the groups
- 3. 0.8 (larger effect size), difference is highly important between the groups Based on the previous studies on inducing demyelination in the animal models and Teriflunomide (TF) treatment to promote anti-inflammation and remyelination^{37, 38} significant differences between the groups is highly important.
- To determine the sample size, in this study, we employed a larger effect size f (0.9), α-err prob (0.05), power (1 β-err prob) (0.8), number of groups (Experiment 1: 3 groups), as per the Cohen's standard effect size.

In Experiment 1, the sample size is n = 18/3 groups, therefore n = 6/group.

Experiment 1. Fluorescent activity of the compound in vivo using Perkin Elmer in vivo imaging

Animal group	Species, age, weight, and sex	Number of animals per group (n)
Vehicle	Sprague Dawley (SD) male rats, 8-week- old, and weighing 220-250 g	6
Sciatic nerve injured group + compound injected	Sprague Dawley (SD) male rats, 8-week- old, and weighing 220-250 g	6
Sciatic nerve without injure + compound injected	Sprague Dawley (SD) male rats, 8-week- old, and weighing 220-250 g	6

Animal groups: The vehicle group serves as the exposed sciatic nerve with an injected dimethyl sulphoxide (DMSO) without compound (n = 6). Injured group (n = 6) was injected with compound dissolved in DMSO through intra neural injection to the rat sciatic nerve and then sciatic nerve was partially ligated to create a damage. Without injure group (n = 6) was injected with compound dissolved in DMSO through intra neural injection to the rat sciatic nerve and muscle and skin incisions was sutured using 3-0 monofilament surgical thread.

Surgical procedure: All of the experimental rats were weighed and anaesthetized intraperitoneally using ketamine/xylazine as a sedative agent approximately 60mg/10mg per kg body weight of rat [64]. Antibiotics: Gentamycin 8 mg/250 g of SD-rat model (only single dose after performing the surgery). After sedation the hair at the femoral site was shaved with a surgical blade in the operated region. The rat was placed on the hot plate to keep warm, and the temperature was maintained at 37 °C. For sterile environment while performing the surgery, the rat's femoral region and the surrounding area were cleaned down with 70% ethanol. In order to locate the sciatic nerve, skin and gluteal muscle incisions were made. The sciatic nerve was exposed using forceps, and nerve injury was induced by inserting the 6-0 monofilament thread from the middle portion of the sciatic nerve for partial ligation to promote demyelination. Following injury, 3-0 surgical sutures were used to close the incisions made in the gluteal muscle and skin. For topical anaesthesia, Lignocaine hydrochloride gel (2%) was applied on the surface of operated region and shifted to the recovery chambers for acclimatization as per experimental schedules. The study included animals that underwent appropriate partial ligation of the rat sciatic nerve. If the suture was not correctly passed from the sciatic nerve for partial ligation, the animals were excluded. A few exclusions were made because of improper tissue processing, which might cause issues during pathological evaluations.

Administration of the fluorescent compound to the rat sciatic nerve for in vivo imaging:

Intraperitoneal injection of Avertin (anaesthetic) at concentration of 300 mg/kg body weight used to anaesthetize the rat to perform surgery. Femoral thigh region is trimmed and wiped with ethanol for sterilization of the operating area. Animal was placed under the table lamp on the heating pad to maintain the temperature around 37 °C. Right hind limb (upper region of the thigh) incision was made on the skin to expose the sciatic nerve and visualized by using surgical microscope. $100 \mu g/5 \mu l$ of Compound dissolved in dimethyl sulphoxide (DMSO) was injected to the rat sciatic nerve through intra neural injection to the rat sciatic nerve. After administration of the Compound, muscle and the skin incisions were stitched using surgical sutures and lignocaine local anaesthesia gel is applied for numbness at the sutured site. The bucker imaging analysis was used to check the fluorescence in the injected sciatic nerves in different day points.

Euthanasia followed by nerve harvesting procedure: All animals in this study were euthanized in accordance with the guidelines of the Institutional Animal Ethical Committee (approval number: UH/IAEC/PPB/2022/12). Euthanasia: Overdose of sodium pentobarbital (150 mg/kg) was delivered intraperitoneally to sacrifice the animals. All the experimental rats were euthanized and placed on the operation table. Skin and gluteal muscle incisions were performed to remove the operated sciatic nerve from the rats. The harvested nerves were then fixed in 10% formalin for pathological examinations.

Paraffin-embedded tissue sections: Freshly collected sciatic nerve samples were fixed with 10% paraformaldehyde or formalin for 48 h at room temperature. After fixation samples were washed under running tap water for 1 h followed by dehydration steps using 70%, 80%, 95% alcohol changes 30 min each and 3 changes of 100% alcohol for 1 h each. Sciatic nerve samples were cleared in 1 change of xylene for 5 min and another step of xylene + melted paraffin 1: 1 ratio for 5 min followed by immersing the samples in 3 changes of paraffin (Paraplast® - polyisobutylene mixture, catalogue no P3558 – SIGMA – ALDRICH®) 1 h each and embedded in a paraffin block. Sample blocks were fixed to the microtome (LEICA RM2145) and 10 μm sections were done and floated in a 40 °C maintained water bath containing clear distilled water. Tissue sections were transferred carefully to the glass slides for further pathological studies.

Mitotracker Red and DAPI (4',6-diamidino-2-phenylindole) staining: BK2ME injected rat sciatic nerve formalin fixed paraffin embedded tissue (FFPE) sections were firstly deparaffinised on the heating pad or heating plate and followed by tissue clearing for 2 min each in two xylene changes. Slides containing FFPE sections was rehydrated accordingly in two changes of 100% alcohol for 3 min each, thereafter 95%, 80%, and 70% alcohol for 3 min and followed by a 10 min water wash. Mitotracker Red was used for the localization with the injected fluorescent compound

sciatic nerve sections. Dissolve 50 μg of Mitotracker in 450 μL DMSO (200 μM stock), for working range 1:1000 of dissolved Mitotracker was diluted in phosphate buffer saline (PBS) maintained at 4 °C temperature and 150 μl of diluted Mitotracker was added on to the deparaffinized sections incubated for 30 min at 4 °C. 1-2 drops of DAPI was added to stain the nucleus for counter staining and mounted with DPX mounting covered with coverslips.

In vitro studies of fluorescent BK2ME on different types of cultured cells and colocalization with Mitotracker

SK – N – SH (neuroblastoma) cells, Thp – 1 (monocytic) cells, 293a cells (a clone of HEK – 293 cells), and HELA cells were individually grown in culture dishes with coverslips for seeding to 50-60% confluence. Medium from the cultured dishes were removed and washed with PBS for twice followed by 4% formalin fixation followed by PBS washes. 20 μ l of dimethyl sulfoxide (DMSO) used to dissolve 2mg (1 μ l = 100 μ g) compound for stock solution and diluted at 2:100 in DMSO for final working solution and stored at 4 °C. Add the adequate amount of solution to the fixed cultured cells and incubated for 30 min at 4 °C temperature for staining. Culture dishes with coverslips were washed with PBS twice. 200 μ M mitotracker was diluted for 1:1000 in PBS and added to the fixed coverslips, incubated for 30 min at 4 °C temperature followed by two washes with PBS for co-localization with the compound. 1-2 drops of DAPI was added to the washed coverslips and mounted on slides with DPX mounting for confocal microscopic imaging.

<u>Statistical analysis:</u> Statistical estimations were quantified and noted as the mean percentage of expression by ImageJ software. Sigma Plot 11.0 software single group one sample t-test is used to estimate the mean \pm SEM. GraphPad Prism 8.0.2, column analysis, and a one-way ANOVA test is used for the multiple comparisons (Tukey test) of the mean and significant P value.

IV. Results

1. Fluorescent compound activity in rat sciatic nerve *in vivo* and *ex vivo* followed by pathological studies to elucidate toxicity

Fluorescent compound activity in vivo using Perkin Elmer in vivo imaging

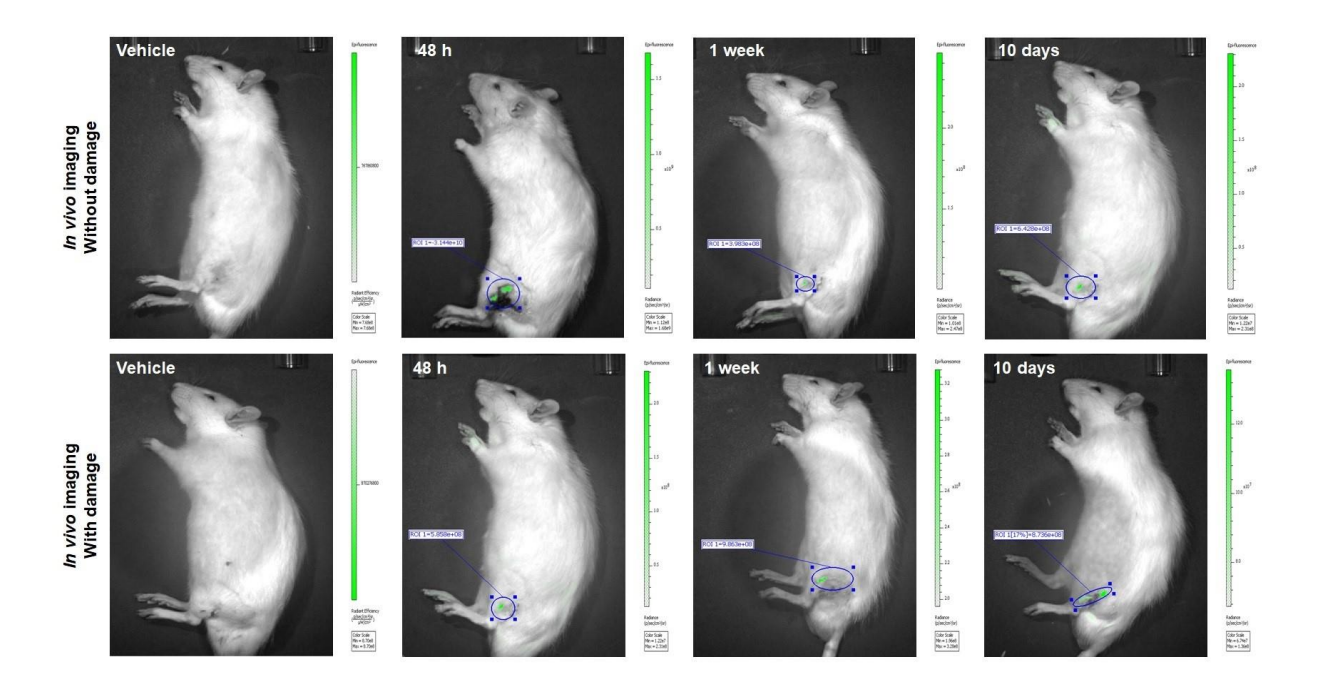
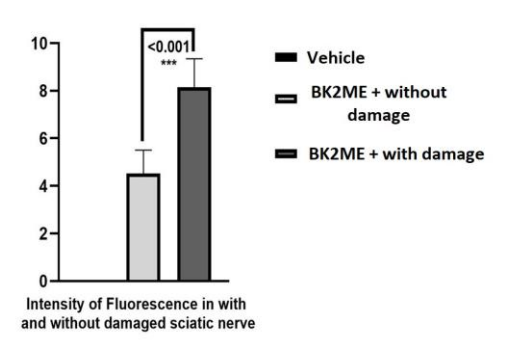


Fig.1 depicts *in vivo* imaging of rats with and without damage to the rat sciatic nerve after injecting BK2ME. First row of the figure shows the rats without damage to the rat sciatic and groups as sham and compound injected followed by Perkin Elmer *in vivo* imaging based on prolonged time period at 48 h, 1 week, and 10



days. Second row of the figure represents the rats with partially ligated sciatic nerve and groups as sham and compound injected followed by Perkin Elmer *in vivo* imaging based on prolonged time period at 48 h, 1 week, and 10 days. Fluorescence intensity values of compound injected in with and without sciatic nerve damaged groups along with the sham were all provided as Mean \pm SEM. Rats N = 6/condition. Statistical significance: ***, P = <0.001. SigmaPlot 11.0 is used to produce statistical results, which are then examined using column analyses, one-way ANOVA, multiple comparisons, the Tukey test, and graphically displayed using GraphPad Prism 8.

Ex vivo confocal microscopic imaging

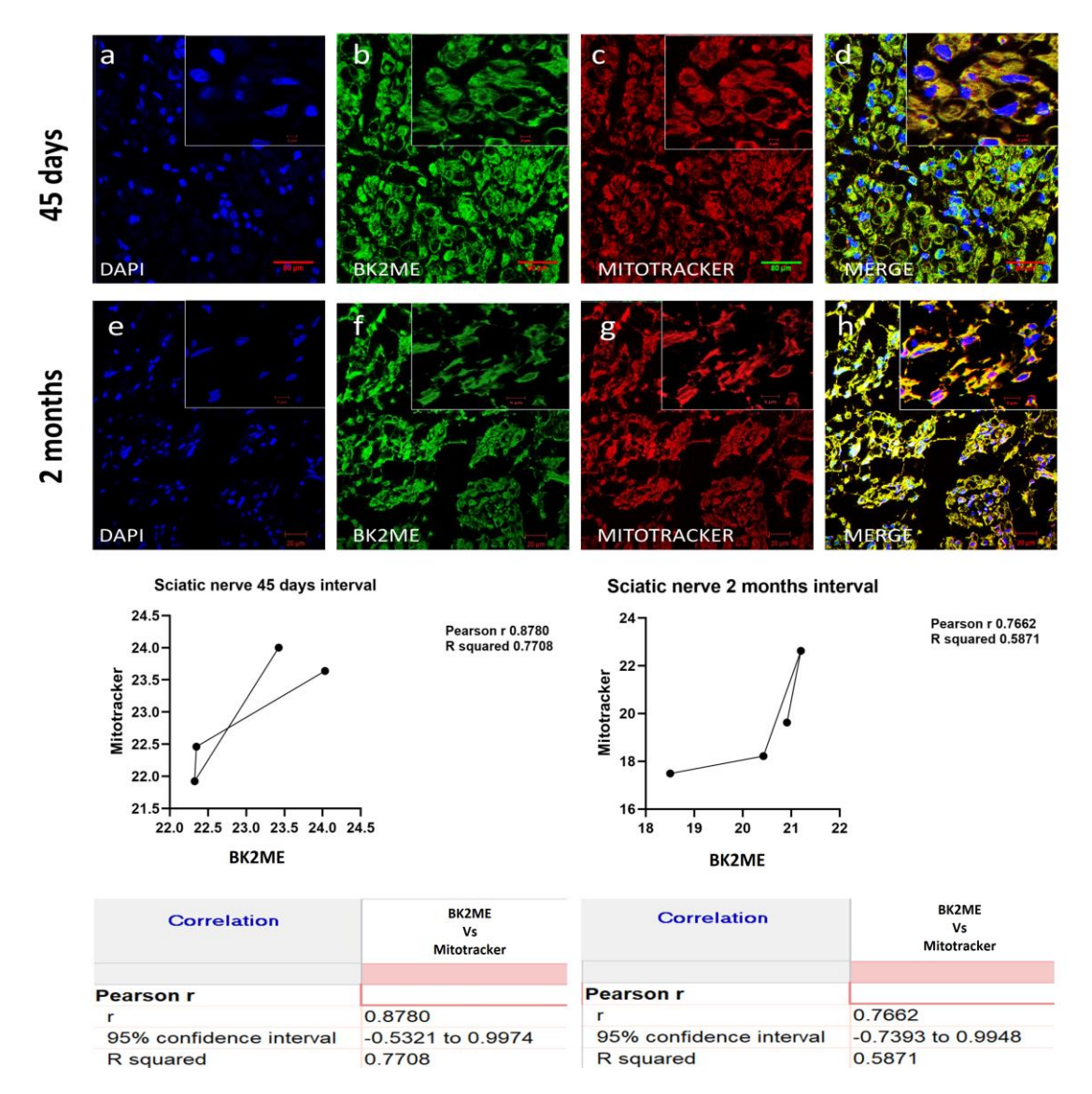


Fig.2 demonstrates confocal microscopic imaging of BK2ME injected rat sciatic nerve sections at 45 days and 2 months interval following euthanasia and formalin fixed paraffin embedding to examine the shelf life of BK2ME. (a, e) DAPI, (b, f) BK2ME, (c, g) Mitotracker, and (d, h) merged panels. (b-c) co-localization panels underwent Pearson coefficient correlation for efficiency of for 45 days shelf life (Pearson r 0.8780, R Squared 0.7708). (f-g) co-localization panels underwent Pearson coefficient correlation for efficiency of 2 months shelf life (Pearson r 0.7662, R Squared 0.5871). Rats N = 6/condition.

BK2ME injected rats were imaged under computerized Perkin Elmer *in vivo* imaging and the fluorescence was observed soon after post intra neural injection of the BK2ME in with and without injured rat sciatic nerve. Fluorescence was monitored based on prolonged time period at 48 h, 1 week, and 10 days point following BK2ME injecting to the rats sciatic nerve and noticed fluorescence remain constant. However, fluorescence in the injure group emitted more than in without damaged groups (Fig. 1).

Sciatic nerve FFPE sections with BK2ME emitted fluorescence under confocal microscopy considered as *ex vivo*. Fluorescence was noted in the sections of 45 days and 2 months after euthanasia and formalin fixed paraffin embedding to examine the shelf life of the compound. Pearson coefficient correlation values demonstrates the good efficiency of the BK2ME by colocalized with the Mitotracker which is a mitochondrial fluorescent stain which selectively accumulates in the mitochondrial matrix, covalently binds to mitochondrial matrix proteins by relating with free thiol groups of cysteine residue (**Fig. 2**). Counter stained with DAPI.

Toxicity studies of BK2ME injected rat sciatic nerve sections

BK2ME, we used our surgically injured rat sciatic nerve model [99] which was employed as a positive control. To evaluate the toxicity of BK2ME, three animal groups are maintained: vehicle-injected with DMSO alone, BK2ME injected with damaged rat sciatic nerve acts as a positive control, and BK2ME injected without generating an injury to the rat sciatic nerve.

Haematoxylin and eosin staining demonstrated cell morphological changes in the injured and BK2ME injected rats groups, which served as a positive control, as compared to the non-damaged and BK2ME injected rats groups, elucidating the non-toxic nature of the fluorescent dye BK2ME (Fig. 3a-c). Furthermore, specific myelin stains Eriochrome cyanine r (EC) and Luxol fast blue (LFB) demonstrate myelin loss in (Fig. 3e, h), with blue colour disappearance (myelin) functioning as a positive control group. The presence of normal myelin without any myelin loss in (Fig. 3f, i) validates the non-toxic nature of BK2ME *in vivo*.

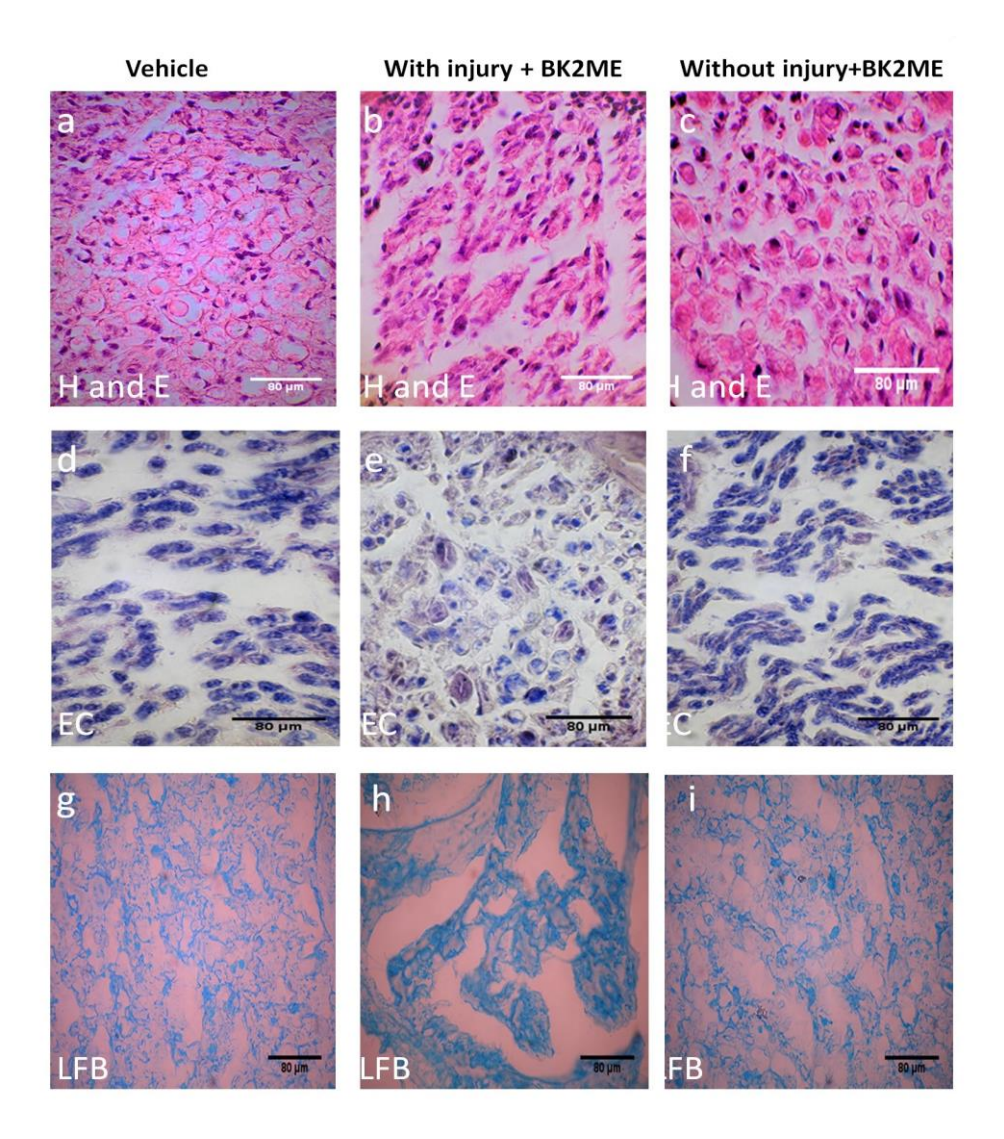


Fig.3 depicts the toxicity studies of BK2ME in the rat sciatic nerve cross sections using special myelin stains. (**a**, **d**, **g**) vehicle, (**b**, **e**, **h**) sciatic nerve injury and BK2ME injected, and (**c**, **f**, **i**) sciatic nerve without injury and BK2ME injected rat groups. (**a-c**) Haematoxylin and eosin H & E stain shows the clear cell morphology in **c**, cell morphological alterations in **b**, and no cell morphological changes in **a**. (**d-f**) eriochrome cyanine r EC stain demonstrates (**d**, **f**) with proper content of myelin present (blue colour) in the sciatic nerve cross sections whereas myelin loss noted in panel **e**. (**g-i**) luxol fast blue LFB stain represents (**g**, **i**) with proper content of myelin present (blue colour) in the sciatic nerve cross sections whereas myelin loss detected in **h**. Rats N = 6/condition.

2. Co-localization studies of BK2ME in vitro cultured cells

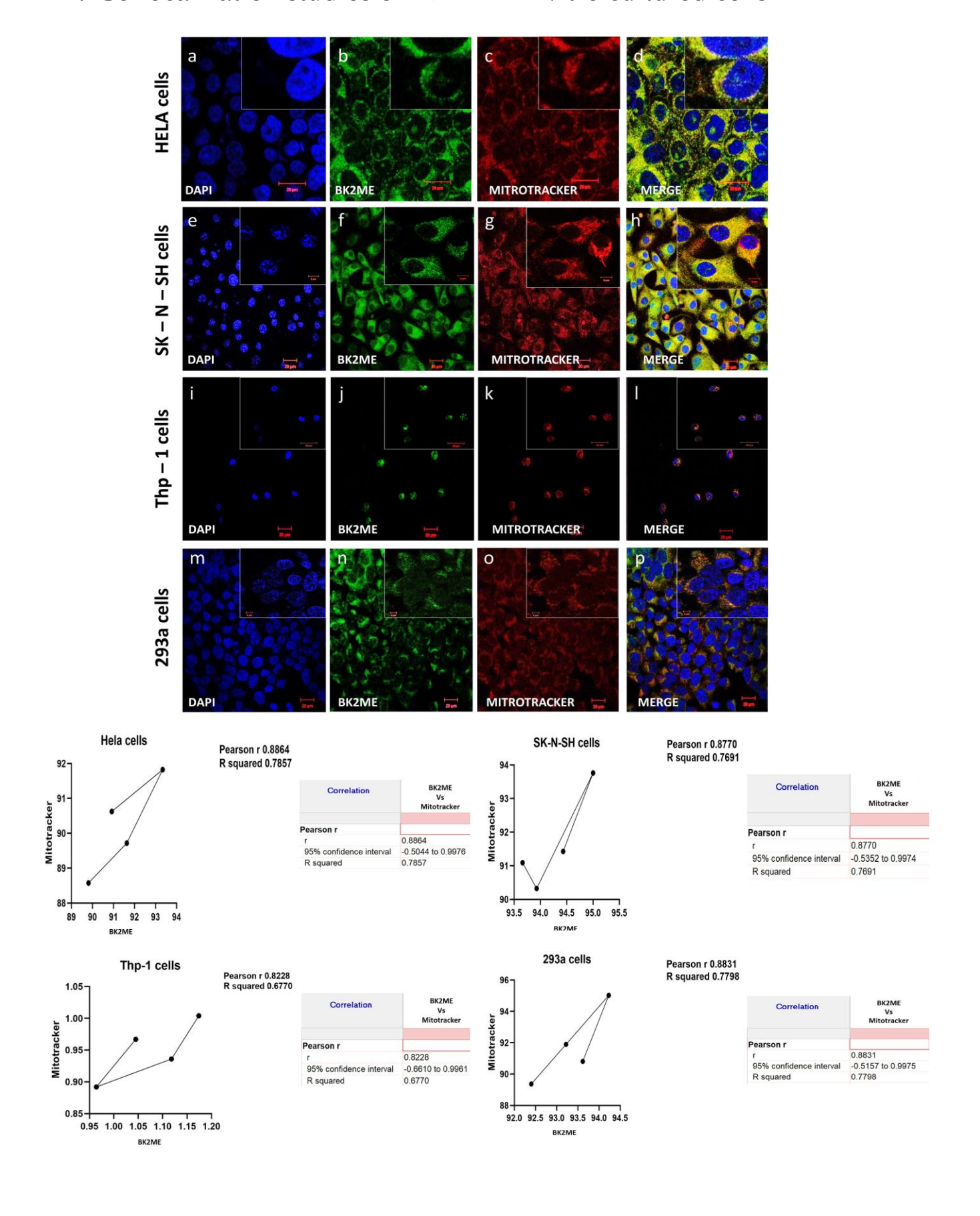


Fig.4 demonstrates the fluorescent activity of BK2ME *in vitro* cultured cells. **a,** DAPI; **b,** BK2ME; **c,** Mitotracker; and **d** as merged image. (**b, c**) co-localization represents fluorescence activity in Hela cells as mitochondrial stain disclosed in merged panel **d** and counter stained with **a** DAPI (Pearson r 0.8864, R squared 0.7857). **e,** DAPI; **F,** BK2ME; **g,** Mitotracker; and **h** merged image. (**f, g)** co-localization discloses the fluorescence activity of SK-N-SH cells as Mitotracker shown in **h** merged panel and counter stained with **e** DAPI (Pearson r 0.8770, R squared 0.7691). **i,** DAPI; **j,** BK2ME; **k,** Mitotracker; **1** merge image of Thp-1 cells. (**j, k)** co-localization uncovers the fluorescence activity of BK2ME in Thp-1 cells as mitochondrial stain in merged panel **1** which was counter stained with **i** DAPI (Pearson r 0.8228, R squared 0.6770). **m,** DAPI; **n,** BK2ME; **o,** Mitotracker; **p,** merged image represents 293a cells. (**n, o)** co-localization reveals fluorescence activity of BK2ME as mitochondrial stain shown in merged panel **p** by counter stain **m** DAPI (Pearson r 0.8831, R squared 0.7798).

HELA cells, SK - N - SH (neuroblastoma) cells, Thp -1 (monocytic) cells, 293a cells (a clone of HEK -293 cells) emitted efficient fluorescence under confocal microscopy after staining with BK2ME for 30 min. BK2ME counter stained with the DAPI and co-localised with Mitotracker mitochondrial fluorescent stain represented in **(Fig. 4)**.

V. Discussion

Fluorescent dyes are unique and advanced tools in the field of biological sciences due to their design or structure of the chemical compound, synthesis, brightness, contrast stability, and role in non-invasive visualization, characterization, and quantification in biological processes of humans and other living organisms [92, 93]. Additionally, to test the proof of the concept surgical sciatic nerve injury model, the study focused to screen a newly synthesized flurophore (BK2ME) *in vivo*.

Experiments on rats' sciatic nerve injected with BK2ME revealed fluorescence activity for 10 days *in vivo*. Displaying mitochondria sub-cellular organelles has significantly advanced understanding of mitochondrial activity in disease pathophysiology; nevertheless, the use of laser-based microscopes is still required [96-98]. *Ex vivo*, fluorescence experiments confirmed BK2ME localization with Mitotracker red and the significance of the newly synthesised fluorophore as a luminous or fluorescent mitochondrial dye. Pathological investigations demonstrated and confirmed BK2ME's non-toxicity when compared to the positive control and control rat groups. Furthermore, use of BK2ME on *in vitro* cultured cells stained the mitochondria by co-localizing with Mitotracker red validates the earlier *in vivo* and *ex vivo* findings and confirms the dye can be promoted as a fluorescent mitochondrial dye.

Summary

In summary, the current findings for CNS provide evidence for the role of proinflammation in ER stress, which is followed by mitochondrial mediated cell death and leading to demyelination in rat brain white matter lesions following p-TBI. Differential mitochondrial protein change in 1 W p-TBI rat brains may assist in the future development of novel cell death indicators. There has been no previous evidence of pro-inflammation, ER-mitochondrial mediated cell death at 21 d after p-TBI in animal models. TF therapy reduced inflammation via immunomodulation and reversed cell death mechanisms and promoted remyelination or myelin secretion. We believe TBI patients can benefit from TF as a remyelination treatment. Furthermore, comparing TBI progression in rats and humans should lead to a better knowledge of brain damage progression and therapy in general

Sciatic nerve injury model based demyelination is accurate and reproducible, and the nerve damage is minimal since a single partial ligation is conducted to target just the portion of sciatic nerve that contains axons. We observed identical demyelination throughout the whole batch and location, and the amount of ligation may be adjusted, making comparison studies easier. This model is appropriate for studying the molecular process behind demyelination and gives a chance to test possible novel therapeutics demyelinating illnesses. This rat model can also screen the fluorophore activity *in vivo* and helps in studying the toxicity of newly synthesised chemical substances by serving as a positive control which is more useful to Pharma, Biotech industry, and academic researchers.

Bibliography

- Bouçanova F., Chrast R. Metabolic Interaction Between Schwann Cells and Axons Under Physiological and Disease Conditions. Front. Cell. Neurosci. 2020;14:148. doi: 10.3389/fncel.2020.00148.
- Bryden D.W., Tilghman J.I., Hinds S.R. Blast-Related Traumatic Brain Injury: Current Concepts and Research Considerations. J. Exp. Neurosci. 2019;12;13:1179069519872213. https://doi.org/10.1177/1179069519872213
- 3. Cernak I. (2017) Understanding blast-induced neurotrauma: how far have we come? Concussion 2: 2017;CNC42. https://doi.org/10.2217/cnc-2017-0006
- 4. Semple B.D., Blomgren K., Gimlin K., Ferriero D.M., Noble-Haeusslein L.J. Brain development in rodents and humans: Identifying benchmarks of maturation and vulnerability to injury across species. *Prog. Neurobiol.* 2013;107: 1-16. https://doi.org/10.1016/j.pneurobio.2013.04.001
- 5. Williamson J.M., Lyons D.A. Myelin Dynamics Throughout Life: An Ever-Changing Landscape? Front. Cell. Neurosci. 2018;12:424. https://doi.org/10.3389/fncel.2018.00424
- Chung S., Fieremans E., Wang X., Kucukboyaci N.E., Morton C.J., Babb J., Amorapanth P., Foo F.A., Novikov D.S., Flanagan S.R., White Matter Tract Integrity: An Indicator of Axonal Pathology after Mild Traumatic Brain Injury. *J Neurotrauma*. 2018;35: 1015-1020. https://doi.org/10.1089/neu.2017.5320
- Marion C.M., Radomski K.L., Cramer N.P., Galdzicki Z., Armstrong R.C. Experimental Traumatic Brain Injury Identifies Distinct Early and Late Phase Axonal Conduction Deficits of White Matter Pathophysiology, and Reveals Intervening Recovery. J. Neurosci. 2018;38: 8723-8736. https://doi.org/10.1523/jneurosci.0819-18.2018
- 8. Sprenkle N.T., Sims S.G., Sánchez C.L., Meares G.P. Endoplasmic reticulum stress and inflammation in the central nervous system. *Molecular Neurodegeneration*. 2017;12: 42. https://doi.org/10.1186/s13024-017-0183-y
- 9. Logsdon A.F., Lucke-Wold B.P., Rosen C.L., Huber J.D. Disparity among neural injury models and the unfolded protein response. *J. Neurol. Disord. Stroke.* 2014;2: 21. http://www.ncbi.nlm.nih.gov/pmc/articles/pmc4896636/
- Hood K.N., Zhao J., Redell J.B., Hylin M.J., Harris B., Perez A., Moore A.N., Dash P.K. Endoplasmic Reticulum Stress Contributes to the Loss of Newborn Hippocampal Neurons after Traumatic Brain Injury. J. Neurosci. 2018;38: 2372-2384. https://doi.org/10.1523/jneurosci.1756-17.2018
- 11. Reverendo M., Mendes A., Argüello R.J., Gatti E., Pierre P. At the crossway of ER-stress and proinflammatory responses. *Febs. J.* 2019;286: 297-310. https://doi.org/10.1111/febs.14391

- 12. Cogliati S., Scorrano L. A BID on mitochondria with MTCH2. *Cell Research*. 2010;20: 863-865. https://doi.org/10.1038/cr.2010.100
- Zaltsman Y., Shachnai L., Yivgi-Ohana N., Schwarz M., Maryanovich M., Houtkooper RH, Vaz F.M., De Leonardis F., Fiermonte G., Palmieri F. MTCH2/MIMP is a major facilitator of tBID recruitment to mitochondria. *Nature Cell Biology*. 2010;12: 553-562. https://doi.org/10.1038/ncb2057
- 14. Korsmeyer S.J., Wei M.C., Saito M., Weiler S., Oh K.J., Schlesinger P.H. Pro-apoptotic cascade activates BID, which oligomerizes BAK or BAX into pores that result in the release of cytochrome c. *Cell Death & Differentiation*. 2000;7: 1166-1173. https://doi.org/10.1038/sj.cdd.4400783
- 15. Yang E., Zha J., Jockel J., Boise L.H., Thompson C.B., Korsmeyer S.J. Bad, a heterodimeric partner for Bcl-XL and Bcl-2, displaces Bax and promotes cell death. *Cell.* 1995;80: 285-291. https://doi.org/10.1016/0092-8674(95)90411-5
- 16. Shakeri R., Kheirollahi A., Davoodi J. Apaf-1: Regulation and function in cell death. Biochimie 2017;135: 111-125. https://doi.org/10.1016/j.biochi.2017.02.001
- 17. He D., Zhang C., Zhao X., Zhang Y., Dai Q., Li Y., Chu L. Teriflunomide for multiple sclerosis. *Cochrane Database Syst. Rev.* 2016;3:CD009882. doi: 10.1002/14651858.CD009882.pub3.
- Aly L., Hemmer B., Korn T. From Leflunomide to Teriflunomide: Drug Development and Immunosuppressive Oral Drugs in the Treatment of Multiple Sclerosis. Curr. Neuropharmacol. 2014;15:874

 –891. doi: 10.2174/1570159X14666161208151525.
- 19. Göttle P., Manousi A., Kremer D., Reiche L., Hartung H.P., Küry P. Teriflunomide promotes oligodendroglial differentiation and myelination. *J. Neuroinflamm.* 2018;15:018–1110. doi: 10.1186/s12974-018-1110-z.
- 20. Hozo, M. et al. Neurotropin accelerates the differentiation of Schwann cells and remyelination in a rat lysophosphatidylcholine-induced demyelination model. *Int. J. Mol. Sci.* 2018; 19(2), 516. https://doi.org/10.3390/ijms19020516
- Janos, G. et al. Teriflunomide attenuates Neuroinflammation-related neural damage in mice carrying human PLP1 mutations. *Journal of Neuroinflammation*. 2018;15, 194. https://doi.org/10.1186/s12974-018-1228-z
- 22. Ringheim G.E. Teriflunomide attenuates immunopathological changes in the dark agouti rat model of experimental autoimmune encephalomyelitis. *Front.* Neurol. 2013;4:169. doi: 10.3389/fneur.2013.00169.
- 23. Kwok C.S.N., Lai K.K.Y., Lam S.W., Chan K.K., Xu S.J.L., Lee F.W.F. Production of high-quality two-dimensional gel electrophoresis profile for marine medaka samples by using Trizol-based

- protein extraction approaches. *Proteome Science*. 2020;18: 5. https://doi.org/10.1186/s12953-020-00161-9
- 24. Kremer D., Akkermann R., Küry P., Dutta R. Current advancements in promoting remyelination in multiple sclerosis. *Mult. Scler.* 2019;25: 7-14. https://doi.org/10.1177/1352458518800827
- 25. Bar-Or A., Pachner A., Menguy V.F., Kaplan J., Wiendl H. Teriflunomide and its mechanism of action in multiple sclerosis. *Drugs.* 2014;74: 659-674. https://doi.org/10.1007/s40265-014-0212-x
- 26. Pol S., Sveinsson M., Sudyn M., Babek N., Siebert D., Bertolino N., Modica C.M., Preda M., Schweser F., Zivadinov R. Teriflunomide's Effect on Glia in Experimental Demyelinating Disease: A Neuroimaging and Histologic Study. *J. Neuroimaging*. 2019;29: 52-61. https://doi.org/10.1111/jon.12561
- 27. Rommer P.S., Milo R., Han M.H., Satyanarayan S., Sellner J., Hauer L., Illes Z., Warnke C., Laurent S., Weber M.S. Immunological Aspects of Approved MS Therapeutics. *Front. Immunol.* 2019;10:1564. https://doi.org/10.3389/fimmu.2019.01564
- 28. Rama R.K.V., Iring S., Younger D., Kuriakose M., Skotak M., Alay E., Gupta R.K., Chandra N. A Single Primary Blast-Induced Traumatic Brain Injury in a Rodent Model Causes Cell-Type Dependent Increase in Nicotinamide Adenine Dinucleotide Phosphate Oxidase Isoforms in Vulnerable Brain Regions. *Journal of Neurotrauma*. 2018;35: 2077-2090. https://doi.org/10.1089/neu.2017.5358
- 29. Xiong Y., Mahmood A., Chopp M. Animal models of traumatic brain injury. Nature Reviews Neuroscience 2013;14: 128-142. https://doi.org/10.1038/nrn3407
- 30. Chakraborty N., Hammamieh R., Gautam A., Miller S.A., Condlin M.L., Jett M., Scrimgeour A.G. TBI weight-drop model with variable impact heights differentially perturbs hippocampuscerebellum specific transcriptomic profile. *Experimental Neurology*. 2021;335: 113516. https://doi.org/10.1016/j.expneurol.2020.113516
- 31. Mychasiuk R., Farran A., Angoa P.M., Briggs D., Kuhn D., Esser M.J. A novel model of mild traumatic brain injury for juvenile rats. *J. Vis. Exp.* 2014;8: 51820. https://doi.org/10.3791/51820
- 32. Shishido H., Ueno M., Sato K., Matsumura M., Toyota Y., Kirino Y., Tamiya T., Kawai N., Kishimoto Y. Traumatic Brain Injury by Weight-Drop Method Causes Transient Amyloid-β Deposition and Acute Cognitive Deficits in Mice. Behav. Neurol. 2019;3248519. https://doi.org/10.1155/2019/3248519
- 33. Caprariello A.V., Mangla S., Miller R.H., Selkirk S.M. Apoptosis of oligodendrocytes in the central nervous system results in rapid focal demyelination. *Ann. Neurol.* 2012;72: 395-405. https://doi.org/10.1002/ana.23606

- 34. Taib T., Leconte C., Van Steenwinckel J., Cho A.H., Palmier B., Torsello E., Lai Kuen R., Onyeomah S., Ecomard K., Benedetto C. Neuroinflammation, myelin and behavior: Temporal patterns following mild traumatic brain injury in mice. *PLOS ONE*. 2017;12: e0184811. https://doi.org/10.1371/journal.pone.0184811
- 35. Turtzo L.C., Lescher J., Janes L., Dean D.D., Budde M.D., Frank J.A. Macrophagic and microglial responses after focal traumatic brain injury in the female rat. *Journal of Neuroinflammation*. 2014;11: 82. https://doi.org/10.1186/1742-2094-11-82
- 36. Bertolotti A., Zhang Y., Hendershot L.M., Harding H.P., Ron D. Dynamic interaction of BiP and ER stress transducers in the unfolded-protein response. *Nature Cell Biology*. 2000;2: 326-332. https://doi.org/10.1038/35014014
- 37. Zhang K., Kaufman R.J. From endoplasmic-reticulum stress to the inflammatory response. *Nature*. 2008;454: 455-462. https://doi.org/10.1038/nature07203
- 38. Frid K., Einstein O., Friedman L.Y., Binyamin O., Ben H.T., Gabizon R. Aggregation of MBP in chronic demyelination. *Ann. Clin. Transl. Neurol.* 2015;2: 711-721. https://doi.org/10.1002/acn3.207
- 39. Höftberger R., Guo Y., Flanagan E.P., Lopez-Chiriboga A.S., Endmayr V., Hochmeister S., Joldic D., Pittock S.J., Tillema J.M., Gorman M. et al. The pathology of central nervous system inflammatory demyelinating disease accompanying myelin oligodendrocyte glycoprotein autoantibody. *Acta. Neuropathol.* 2020;139: 875-892. https://doi.org/10.1007/s00401-020-02132-y
- 40. Santos G., Barateiro A., Brites D., Fernandes A. S100B Impairs Oligodendrogenesis and Myelin Repair Following Demyelination Through RAGE Engagement. *Front. Cell. Neurosci.* 2020;14:279. https://doi.org/10.3389/fncel.2020.00279
- 41. Yao J., Zheng K., Zhang X. (2015) Rosiglitazone exerts neuroprotective effects via the suppression of neuronal autophagy and apoptosis in the cortex following traumatic brain injury. Mol Med Rep 12: 6591-6597. https://doi.org/10.3892/mmr.2015.4292
- 42. Li Jiang, Man Luo, Dan Liu, Bojiang Chen, Wen Zhang, Lin Mai, Jing Zeng, Na Huang, Yi Huang, Xianming Mo & Weimin Li (2013) BAD overexpression inhibits cell growth and induces apoptosis via mitochondrial-dependent pathway in non-small cell lung cancer. Cancer Cell Int 13, 53. https://doi.org/10.1186/1475-2867-13-53
- 43. Simons M, Lyons DA (2013) Axonal selection and myelin sheath generation in the central nervous system. Current Opinion in Cell Biology 25: 512-519. https://doi.org/10.1016/j.ceb.2013.04.007
- 44. Kim S, Han SC, Gallan AJ, Hayes JP (2017) Neurometabolic indicators of mitochondrial dysfunction in repetitive mild traumatic brain injury. Concussion 2: 2017-0013. https://doi.org/10.2217/cnc-2017-0013

- 45. Xu F, Putt DA, Matherly LH, Lash LH (2006) Modulation of expression of rat mitochondrial 2-oxoglutarate carrier in NRK-52E cells alters mitochondrial transport and accumulation of glutathione and susceptibility to chemically induced apoptosis. J Pharmacol Exp Ther 316: 1175-1186. https://doi.org/10.1124/jpet.105.094599
- 46. Kim HE, Du F, Fang M, Wang X (2005) Formation of apoptosome is initiated by cytochrome c-induced dATP hydrolysis and subsequent nucleotide exchange on Apaf-1. Proc Natl Acad Sci U S A 102: 17545-17550. https://doi.org/10.1073/pnas.0507900102
- 47. Szeliga M (2020) Peroxiredoxins in Neurodegenerative Diseases. Antioxidants 9(12):1203. https://doi.org/10.3390/antiox9121203
- 48. Ichiyama A (2011) Studies on a unique organelle localization of a liver enzyme, serine:pyruvate (or alanine:glyoxylate) aminotransferase. Proc Jpn Acad Ser B Phys Biol Sci 87: 274-286. https://doi.org/10.2183/pjab.87.274
- 49. Zhao X, Qin W, Jiang Y, Yang Z, Yuan B, Dai R, Shen H, Chen Y, Fu J, Wang H (2020) ACADL plays a tumor-suppressor role by targeting Hippo/YAP signaling in hepatocellular carcinoma. npj Precision Oncology 4: 7. https://doi.org/10.1038/s41698-020-0111-4
- 50. Feng D, Witkowski A, Smith S (2009) Down-regulation of mitochondrial acyl carrier protein in mammalian cells compromises protein lipoylation and respiratory complex I and results in cell death. J Biol Chem 284: 11436-11445. https://doi.org/10.1074/jbc.m806991200
- 51. Habibzadeh P, Inaloo S, Silawi M, Dastsooz H, Farazi Fard MA, Sadeghipour F, Faghihi Z, Rezaeian M, Yavarian M, Böhm Jet al (2013) A Novel TTC19 Mutation in a Patient With Neurological, Psychological, and Gastrointestinal Impairment. Front Neurol 10:944. https://doi.org/10.3389/fneur.2019.00944
- 52. Kim JY, Kim JW, Yenari MA (2020) Heat shock protein signaling in brain ischemia and injury. Neurosci Lett 715: 20. https://doi.org/10.1016/j.neulet.2019.134642
- 53. Arun P, Abu-Taleb R, Oguntayo S, Wang Y, Valiyaveettil M, Long JB, Nambiar MP (2013) Acute mitochondrial dysfunction after blast exposure: potential role of mitochondrial glutamate oxaloacetate transaminase. J Neurotrauma 30: 1645-1651. https://doi.org/10.1089/neu.2012.2834
- 54. Kennedy H, Haack TB, Hartill V, Mataković L, Baumgartner ER, Potter H, Mackay R, Alston CL, O'Sullivan S, McFarland Ret al (2016) Sudden Cardiac Death Due to Deficiency of the Mitochondrial Inorganic Pyrophosphatase PPA2. Am J Hum Genet 99: 674-682. https://doi.org/10.1016/j.ajhg.2016.06.027
- 55. Johnson E.S., Ludwin S.K. The demonstration of recurrent demyelination and remyelination of axons in the central nervous system. *Acta Neuropathol.* 1981;53:93–98. doi: 10.1007/BF00689988.

- 56. Wallace V.C., Cottrell D.F., Brophy P.J., Fleetwood-Walker S.M. Focal lysolecithin-induced demyelination of peripheral afferents results in neuropathic pain behavior that is attenuated by cannabinoids. *J. Neurosci.* 2003;23:3221–3233. doi: 10.1523/JNEUROSCI.23-08-03221.2003.
- 57. Said G., Duckett S., Sauron B. Proliferation of schwann cells in tellurium-induced demyelination in young rats. *Acta Neuropathol.* 1981;53:173–179. doi: 10.1007/BF00688019.
- 58. Bondan E.F., Custódio P.R., Lallo M.A., Bentubo H.D.L., Graça D.L. Ethidium bromide-induced demyelination in the sciatic nerve of diabetic rats. *Arquivos de Neuro-Psiquiatria*. 2009;67:1066–1070. doi: 10.1590/S0004-282X2009000600020.
- Drescher K.M., Tracy S.M. Injection of the sciatic nerve with TMEV: A new model for peripheral nerve demyelination. *Virology*. 2007;359:233–242. doi: 10.1016/j.virol.2006.09.009.
- 60. Glatigny S., Bettelli E. Experimental Autoimmune Encephalomyelitis (EAE) as Animal Models of Multiple Sclerosis (MS) Cold. Spring. Harb. Perspect. Med. 2018;8:a028977. doi: 10.1101/cshperspect.a028977.
- 61. Shubayev V.I., Angert M., Dolkas J., Campana W.M., Palenscar K., Myers R.R. TNFalpha-induced MMP-9 promotes macrophage recruitment into injured peripheral nerve. *Mol. Cell. Neurosci.* 2006;31:407–415. doi: 10.1016/j.mcn.2005.10.011.
- 62. Gupta R., Nassiri N., Hazel A., Bathen M., Mozaffar T. Chronic nerve compression alters Schwann cell myelin architecture in a murine model. *Muscle Nerve*. 2012;45:231–241. doi: 10.1002/mus.22276.
- 63. Yalcin I., Megat S., Barthas F., Waltisperger E., Kremer M., Salvat E., Barrot M. The sciatic nerve cuffing model of neuropathic pain in mice. *J. Vis. Exp. JoVE*. 2014;89:51608. doi: 10.3791/51608.
- 64. Van Pelt L. Ketamine and for surgical anesthesia in rats. *J. Am. Vet. Med. Assoc.* 1977;171:842–844.
- 65. Gilli F., Li L., Royce D.B., DiSano K.D., Pachner A.R. Treatment of Theiler's virus-induced demyelinating disease with Teriflunomide. *J. Neurovirol.* 2017;23:825–838. doi: 10.1007/s13365-017-0570-8.
- 66. Cai M., Huang T., Hou B., Guo Y. Role of Demyelination Efficiency within Acellular Nerve Scaffolds during Nerve Regeneration across Peripheral Defects. *BioMed. Res. Int.* 2017;21:4606387. doi: 10.1155/2017/4606387.
- 67. Wang I.C., Chung C.Y., Liao F., Chen C.C., Lee C. H Peripheral sensory neuron injury contributes to neuropathic pain in experimental autoimmune encephalomyelitis. *Sci. Rep.* 2017;7:42304. doi: 10.1038/srep42304.

- 68. Clasen R.A., Simon R.G., Scott R., Pandolfi S., Laing I., Lesak A. The staining of the myelin sheath by luxol dye techniques. *J. Neuropathol. Exp. Neurol.* 1973;32:271–283. doi: 10.1097/00005072-197304000-00007.
- 69. Kiernan J.A. Histochemistry of Staining Methods for Normal and Degenerating Myelin in the Central and Peripheral Nervous Systems. *J. Histotechnol.* 2007;30:87–106. doi: 10.1179/his.2007.30.2.87.
- 70. Blackwell M.L., Farrar C.T., Fischl B., Rosen B.R. Target-specific contrast agents for magnetic resonance microscopy. *Neuroimage*. 2009;46:382–393. doi: 10.1016/j.neuroimage.2009.01.030.
- 71. Cloutier F., Sears-Kraxberger I., Keachie K., Keirstead H.S. Immunological demyelination triggers macrophage/microglial cells activation without inducing astrogliosis. *Clin. Dev. Immunol.* 2013;11:812456. doi: 10.1155/2013/812456.
- 72. Stefanović D., Stefanović M., Lalošević D. Use of eriochrome cyanine R in routine histology and histopathology: Is it time to say goodbye to hematoxylin? *Biotech. Histochem.* 2015;90:461–469. doi: 10.3109/10520295.2015.1057765.
- 73. Choi M.-H., Na J.E., Yoon Y.R., Lee H.J., Yoon S., Rhyu I.J., Baik J.-H. Role of Dopamine D2 Receptor in Stress-Induced Myelin Loss. *Sci. Rep.* 2015;7:11654. doi: 10.1038/s41598-017-10173-9.
- 74. Zigmond R.E., Echevarria F.D. Macrophage biology in the peripheral nervous system after injury. *Prog. Neurobiol.* 2019;173:102–121. doi: 10.1016/j.pneurobio.2018.12.001.
- 75. Mata M., Alessi D., Fink D.J. S100 is preferentially distributed in myelin-forming Schwann cells. *J. Neurocytol.* 1990;19:432–442. doi: 10.1007/BF01188409.
- 76. Chernov A.V., Dolkas J., Hoang K., Angert M., Srikrishna G., Vogl T., Baranovskaya S., Strongin A.Y., Shubayev V.I. The calcium-binding proteins S100A8 and S100A9 initiate the early inflammatory program in injured peripheral nerves. *J. Biol. Chem.* 2015;290:11771–11784. doi: 10.1074/jbc.M114.622316.
- 77. Rozeik C., Schulz-Harder B. Myelin basic protein immunohistochemistry: A study of the early stages of myelination in the brainstem of the rat. *Acta Histochem.* 1990;88:149–158. doi: 10.1016/S0065-1281(11)80127-3.
- Bodhireddy S.R., Lyman W.D., Rashbaum W.K., Weidenheim K.M. Immunohistochemical detection of myelin basic protein is a sensitive marker of myelination in second trimester human fetal spinal cord. *J. Neuropathol. Exp. Neurol.* 1994;53:144–149. doi: 10.1097/00005072-199403000-00005.
- 79. Vercellino M., Masera S., Lorenzatti M., Condello C., Merola A., Mattioda A., Tribolo A., Capello E., Mancardi G.L., Mutani R., et al. Demyelination, inflammation, and neurodegeneration in

- multiple sclerosis deep gray matter. *J. Neuropathol. Exp. Neurol.* 2009;68:489–502. doi: 10.1097/NEN.0b013e3181a19a5a.
- 80. Xing Y., Samuvel D.J., Stevens S.M., Dubno J.R., Schulte B.A., Lang H. Age-related changes of myelin basic protein in mouse and human auditory nerve. *PLoS ONE*. 2012;7:e34500. doi: 10.1371/journal.pone.0034500.
- 81. Frid K., Einstein O., Friedman-Levi Y., Binyamin O., Ben-Hur T., Gabizon R. Aggregation of MBP in chronic demyelination. *Ann. Clin. Transl. Neurol.* 2015;2:711–721. doi: 10.1002/acn3.207.
- 82. Kim H.S., Lee J., Lee D.Y., Kim Y.D., Kim J.Y., Lim H.J., Lim S., Cho Y.S. Schwann Cell Precursors from Human Pluripotent Stem Cells as a Potential Therapeutic Target for Myelin Repair. *Stem Cell Rep.* 2017;8:1714–1726. doi: 10.1016/j.stemcr.2017.04.011.
- 83. Lindborg J.A., Niemi J.P., Howarth M.A., Liu K.W., Moore C.Z., Mahajan D., Zigmond R.E. Molecular and cellular identification of the immune response in peripheral ganglia following nerve injury. *J. Neuroinflamm.* 2018;15:192. doi: 10.1186/s12974-018-1222-5.
- 84. Qian T., Wang P., Chen Q., Yi S., Liu Q., Wang H., Wang S., Geng W., Liu Z., Li S. The dynamic changes of main cell types in the microenvironment of sciatic nerves following sciatic nerve injury and the influence of let-7 on their distribution. *RSC Adv.* 2018;8:41181–41191. doi: 10.1039/C8RA08298G.
- 85. Stratton J.A., Holmes A., Rosin N.L., Sinha S., Vohra M., Burma N.E., Trang T., Midha R., Biernaskie J. Macrophages Regulate Schwann Cell Maturation after Nerve Injury. *Cell. Rep.* 2018;24:2561–2572. doi: 10.1016/j.celrep.2018.08.004.
- 86. Abada Y.S., Nguyen H.P., Schreiber R., Ellenbroek B. Assessment of motor function, sensory motor gating and recognition memory in a novel BACHD transgenic rat model for huntington disease. *PLoS ONE*. 2013;8:e68584. doi: 10.1371/journal.pone.0068584.
- 87. Tiwari V., He S.-Q., Huang Q., Liang L., Yang F., Chen Z., Tiwari V., Fujita W., Devi L.A., Dong X., et al. Activation of μ-δ opioid receptor heteromers inhibits neuropathic pain behavior in rodents. *Pain.* 2020;161:842–855. doi: 10.1097/j.pain.0000000000001768.
- 88. Shi X., Chen Y., Nadeem L., Xu G. Beneficial effect of TNF-α inhibition on diabetic peripheral neuropathy. *J. Neuroinflamm.* 2013;10:69. doi: 10.1186/1742-2094-10-69.
- 89. Byun S.-H., Ahn K.-M. Functional and electron-microscopic changes after differential traction injury in the sciatic nerve of a rat. *Maxillofac. Plast. Reconstr. Surg.* 2021;43:12. doi: 10.1186/s40902-021-00297-4.
- 90. Placheta-Györi E., Brandstetter L., Zemann-Schälss J., Wolf S., Radtke C. Myelination, axonal loss and Schwann cell characteristics in axonal polyneuropathy compared to controls. *PLoS ONE*. 2021;16:e0259654. doi: 10.1371/journal.pone.0259654.

- 91. Christie R.M. Fluorescent dyes, *Handbook of Textile and Industrial Dyeing*. 2011;1, 562-587. https://doi.org/10.1533/9780857093974.2.562.
- 92. Chen K., Chen X. Design and development of molecular imaging probes. *Curr Top Med Chem.* **10**, 1227–36 (2010).
- 93. Yap, M. L., McFadyen, J.D., Wang, X., Ziegler, M., Chen, Y.C., Willcox, A. Activated platelets in the tumor microenvironment for targeting of antibody-drug conjugates to tumors and metastases. *Theranostics.* **9,** 1154–69 (2019).
- 94. Rizzuto, R., De Stefani, D., Raffaello, A. & Mammucari, C. Mitochondria as sensors and regulators of calcium signalling. *Nat Rev Mol Cell Biol* **13**, 566–578 (2012).
- 95. Starkov, A. A. The role of mitochondria in reactive oxygen species metabolism and signaling. *Ann* NY Acad Sci 1147, 37–52 (2008).
- 96. Dorn, G. W. 2nd Mitochondrial dynamism and heart disease: changing shape and shaping change. *EMBO Mol Med* **7**, 865–877 (2015).
- 97. Miller, N., Shi, H., Zelikovich, A. S. & Ma, Y. C. Motor neuron mitochondrial dysfunction in spinal muscular atrophy. *Hum Mol Genet* **25**, 3395–3406 (2016).
- 98. Lopez-Crisos, C. et al. Sarcoplasmic reticulum-mitochondria communication in cardiovascular pathophysiology. Nat. Rev. Cardiol (2017).
- 99. Rayilla R.S.R., Naidu M., Babu P.P. Surgically Induced Demyelination in Rat Sciatic Nerve. Brain Sci. 2023;13(5):754. doi: 10.3390/brainsci13050754.

Central and Peripheral Nervous System Injuries: Evidence of Demyelination and Remyelination

by Rahul Shankar Rao Rayilla

Submission date: 26-Sep-2023 05:22PM (UTC+0530)

Submission ID: 2177414897

File name: Rahul_Shankar_Rao_Rayilla.docx (294.56K)

Word count: 18665 Character count: 100680

Librarian

Indira Gandhi Memorial Library UNIVERSITY OF HYDERABAD Central University P.O.

HYDERABAD-500 046.

Central and Peripheral Nervous System Injuries: Evidence of Demyelination and Remyelination

	NALITY REPORT	n and Remyelina	JCIOTT	
	2% ARITY INDEX	51% INTERNET SOURCES	50% PUBLICATIONS	3% STUDENT PAPERS
PRIMA	RY SOURCES			
1	WWW.M Internet Sour			35%
2	WWW.re	searchsquare.co	om	11%
3	Phanithi	nankar Rao Ray Prakash Babu. nation in Rat So s, 2023	"Surgically Inc	duced 4%
4	WWW.NC	bi.nlm.nih.gov		1 %
5	nrl.north	numbria.ac.uk		1 %
6	Phanithi Betweer Oligoder	nankar Rao Rayi . "Traumatic Bra n ER and Mitoch ndrocyte Cell De nation", Researd	ain Injury: Crossondria Contribeath and ch Square Plat	sstalk outes to

7	Roberta Ceci, Guglielmo Duranti, Alessia Leonetti, Stefano Pietropaoli et al. "Adaptive responses of heart and skeletal muscle to spermine oxidase overexpression: Evaluation of a new transgenic mouse model", Free Radical Biology and Medicine, 2017	<1%
8	libres.uncg.edu Internet Source	<1%
9	journals.biologists.com Internet Source	<1%
10	Submitted to Indian Institute of Science Education and Research Student Paper	<1%
11	Fawzi Bokhari. "siRNA screening of the kinome identified Aurora A kinase as a therapeutic target gene in cervical cancer", 'University of Queensland Library', 2014 Internet Source	<1%
12	www.oncotarget.com Internet Source	<1%
13	Presley, A.D "MitoTracker Green labeling of mitochondrial proteins and their subsequent analysis by capillary electrophoresis with laser-induced fluorescence detection", Journal of Chromatography B, 20030805	<1%
	Prof. P. Prake Department on Blotechnolo School of Life University of H Hyderabad-500	gy & Bioinformatics Sciences lyderabad 046. (T.S.)

14	Internet Source	<1%
15	Santi Rello-Varona, Miriam Fuentes-Guirado, Roser López-Alemany, Aida Contreras-Pérez et al. "Bcl-xL inhibition enhances Dinaciclib- induced cell death in soft-tissue sarcomas", Scientific Reports, 2019	<1%
16	Submitted to Institute of Graduate Studies, UiTM Student Paper	<1%
17	portlandpress.com Internet Source	<1%

Exclude quotes

On

On

Exclude bibliography On

Exclude matches

< 14 words

Prof. P. Prakash Babu

Prof. P. Prakash Babu

Department of Biotechnology & Bioinformatics
School of Life Sciences
School of Life Sciences
University of Hyderabad
University of Hyderabad
Hyderabad-500 046. (T.S.)